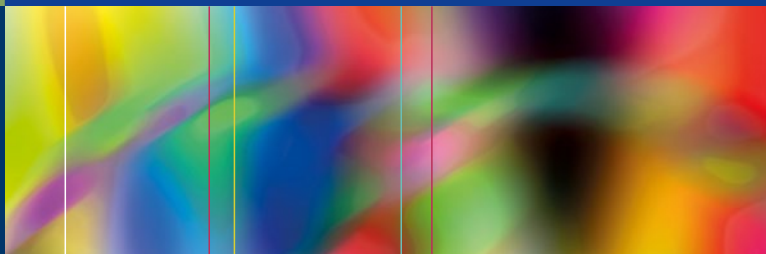Mary M. Salvatore
Ronaldo Collo Go
Monica A. Pernia M.

# Chest CT for Non-Radiologists

## A Practical Guide

# Chest CT for Non-Radiologists

Chest CT for the non-radiologist

Mary M. Salvatore
Ronaldo Collo Go
Monica A. Pernia M.

# Chest CT for Non-Radiologists

A Practical Guide

Springer

Mary M. Salvatore
Radiology
Icahn School of Medicine at
Mount Sinai
New York, NY
USA

Ronaldo Collo Go
Division of Pulmonary, Critical
Care, and Sleep Medicine
Crystal Run Health Care
Middletown, NY
USA

Monica A. Pernia M.
Internal Medicine
New York Medical College -
Metropolitan Hospital Program
New York, NY
USA

# Preface

"If you can't explain it simply, you don't understand it well enough."

—Albert Einstein

The purpose of this book is to teach an approach to chest CT scan review for those who deal with imaging exams on a regular basis but will not dedicate their career to radiology. It has been our goal to provide you with a foundation for viewing CT scans of the chest, with step-by-step instructions on how to systematically approach interpretation. This text will benefit medical students who do not have the opportunity to study radiology, health care professionals including residents and fellows who order chest CT scans and use the information provided to diagnose and treat patients, and scientists who are involved in studying pulmonary diseases. We feel confident that you will enjoy reading this hands-on text and utilize the information provided to ultimately benefit patients.

Overview of the approach to chest CT review

| Review | Series | Settings | Views | Specifics |
|--------|--------|----------|-------|-----------|
| 1. Dose | Dose | NA | NA | DLP<br>• 0–200 ok<br>• >200 Why? |
| 2. Scout | Scout | Window 400 Level 40 | AP Lateral | 1. Lines and tubes<br>2. Diaphragm<br>3. Scoliosis |

| Review | Series | Settings | Views | Specifics |
|---|---|---|---|---|
| 3. Airways | Lung windows | Window 1500 Level -650 | Axial | 1. Trachea<br>2. RUL bronchus<br>3. RML bronchus<br>4. RLL bronchus<br>5. LUL bronchus<br>6. LLL bronchus |
| 4. Lung parenchyma | Standard windows | Window 1500 Level -650 | Axial MIP | 1. RUL<br>2. RML<br>3. RLL<br>4. LUL<br>5. LLL<br>6. Pleura |
| 5. Mediastinum | Standard windows | Window 400 Level 40 | Axial | 1. Thyroid<br>2. Lymph nodes<br>3. Heart<br>4. Esophagus |
| 6. Upper abdomen | Standard windows | Window 400 Level 40 | Axial | 1. Liver<br>2. Spleen<br>3. Gallbladder<br>4. Pancreas<br>5. Adrenals<br>6. Kidneys<br>7. Bowel |
| 7. Soft tissue | Standard windows | Window 400 Level 40 | Axial | 1. Breast<br>2. Subcutaneous<br>3. Muscle |
| 8. Osseous structures | Standard windows | Window 2000 Level 300 | Axial Sagittal | 1. Spine<br>2. Sternum<br>3. Ribs<br>4. Shoulders |

New York, NY, USA                          Mary M. Salvatore
Middletown, NY, USA                        Ronaldo Collo Go
New York, NY, USA                       Monica A. Pernia M.

# Contents

# Chapter 1
# Radiation Dose and Imaging Protocols

- **Is the dose too high?**
- **Have I optimized ability to make diagnosis?**

## 1.1   Radiation Dose

It is appropriate that the first section of this text should address the radiation dose because the risk of radiation exposure is a stochastic risk that may be analyzed statistically but may not be predicted precisely. Therefore, every time a CT scan is ordered and performed, we must remember there is risk to the patient, and we should only perform CT when the risk-benefit ratio supports the exam. In the past CT looked to

obtain the most beautiful images with little regard for radiation dose. More recently the pendulum has swung in the opposite direction with radiologists looking to make the dose as low as possible to obtain diagnostic images. In 1984, the FDA described the *computed tomography dose index* (CTDI) which represented the dose from the primary beam plus scatter radiation [1].

CTDI = Dose from primary beam + Scatter radiation.

The *weighted CTDI* (CTDIw) is the sum of two thirds peripheral dose and one third central dose in acrylic phantoms in a 100 mm range [2].

CTDIw = 2/3 Peripheral dose + 1/3 Central dose.

The *volume CTDI* is the most common index and is derived by the CTDIw divided by the beam pitch factor.

CTDIvol = CTDIw / Beam pitch factor.

The *dose length product* (DLP) is the CTDIvol multiplied by the scan length (slice thickness × number of slices) [3].

CTDIvol × Scan length.

Many radiology CT reports include the dose of radiation to heighten awareness and gather data on acceptable norms. To make the DLP as low as possible, the radiologist must assure that only the requested parts of the body are imaged and that the milliampere second (mAs) is as low as possible. Ideally the DLP for a chest CT should be below 200 mGy. If the number is higher, we must question why.

## 1.2   Imaging Protocols

Surprisingly, imaging protocols are specific to each institution. In the following paragraphs, I will share with you our carefully considered protocols which have evolved over time.

(a) *Low-dose non-contrast CT scan of the chest*: The most common imaging protocol which can be used to evaluate everything from infection to neoplasm [4]. The benefit of a non-contrast exam is that it is quick and has little risk to the patient. Images include a scout film, axial images at 2.5 or 3 mm collimation using mediastinal window settings with a field of view that includes the entire breast, axial images at 2.5 or 3 mm collimation using lung window settings, axial images at 1.0 or 1.25 mm collimation using mediastinal window settings, sagittal reformatted images, coronal reformatted images, maximum intensity projection (MIP) images, and radiation dose [4, 5].

(b) *Contrast CT scan of the chest*: Less commonly used imaging protocol which may be indicated for the evaluation of mediastinal or hilar adenopathy [6]. The benefit of a contrast exam is that it enhances the pulmonary circulation [7]; however there is risk to the patient of allergic reaction. Images include a scout film, axial images at 2.5 or 3 mm collimation using mediastinal window settings with a field of view that includes the entire breast, axial images at 2.5 or 3 mm collimation using lung window settings, axial images at 1.0 or 1.25 mm collimation using mediastinal window settings, sagittal reformatted images, coronal reformatted images, MIP images, contrast dose, and radiation dose.

(c) *Pulmonary embolism CT*: Contrast-enhanced CT protocol which may be indicated for the evaluation of pulmonary emboli. The benefit of a contrast exam is that it

optimizes visualization of pulmonary circulation; however there is risk to the patient of allergic reaction. Timing of contrast injection is imperative. Approximately 80 cm$^3$ of contrast is injected at a rapid rate of 4 cm$^3$/s, and scanning begins when the amount of contrast in the pulmonary artery is optimal [8]. Images include a scout film, axial images at 2.5 or 3 mm collimation using mediastinal window settings with a field of view that includes the entire breast, axial images at 2.5 or 3 mm collimation using lung window settings, axial images at 1.0 or 1.25 mm collimation using mediastinal window settings, sagittal reformatted images, coronal reformatted images, MIP images, contrast dose, and radiation dose.

(d) *Interstitial lung disease non-contrast CT scan of the chest*: Indicated for the initial evaluation of interstitial lung disease [9]. The benefit of the exam is that it is quick and with little risk. Images include a scout film, axial images at 2.5 or 3 mm collimation using mediastinal window settings, axial images at 2.5 or 3 mm collimation using lung window settings, axial images at 1.0 or 1.25 mm collimation using mediastinal window settings, sagittal reformatted images, coronal reformatted images, MIP images, and radiation dose [10]. Expiratory images in end expiration are added to look for air trapping. Prone images can be used to differentiate dependent atelectasis from early fibrosis.

(e) *Tracheomalacia protocol*: Less commonly used imaging protocol which may be indicated for the evaluation of asthma that is resistant to treatment. The advantages include that it is rapid test with little risk to the patient. However, it can be difficult to perform, and the patient must be able to follow instructions [11]. Images include a scout film, axial images at 2.5 or 3 mm collimation using mediastinal window settings, axial images at 2.5 or 3 mm

collimation using lung window settings, axial images at 1.0 or 1.25 mm collimation using mediastinal window settings, sagittal reformatted images, coronal reformatted images, MIP images, and radiation dose. Expiratory images of the entire thorax are obtained, and dynamic expiratory images stationed just above the carina are obtained to look for airway collapse [12]. Dynamic images while coughing may be added as well.

## 1.3   ACR Appropriateness Criteria

In 1993, the ACR guidelines were presented to the US House Ways and Means Committee to provide recommendations for appropriate use of radiologic imaging. The ACR Appropriateness Criteria are guidelines designed to help clinicians make the most appropriate imaging choice to answer a clinical problem. The intent of the ACR guidelines is to recommend the study which will most effectively answer the clinical question. The guidelines are not static and contain frequent updates as new technology presents. Currently 221 topics are covered [13, 14].

There is a specific criterion for acute chest pain with suspicion for pulmonary embolus. Under this criterion there are three variants: intermediate probability with a negative D-dimer or low pretest probability, intermediate probability with a positive D-dimer or high pretest probability, and pregnant patient. In the first case, where the pretest probability is low, the ACR guidelines give highest recommendation for chest X-ray with a rating of 9; and a second highest rating for CTA of the chest with a rating of 5. V/Q scan has a rating of 2. When the pretest probability is high, a CTA of the chest receives the highest score of 9, while a VQ scan is rated 7. ACR recommends pregnant individuals have a Doppler of the legs (with recommendation level of 8) followed by CTA

and V/Q scan with level of 7 [15]. As you can see, the ACR guidelines are a valuable source to the clinician and can be used by the radiologist when consulted regarding clinical concerns.

# References

1. Department of Health and Human Services, Food and Drug Administration. 21 CFR Part 1020: diagnostic x-ray systems and their major components; amendments to performance standard; final rule. Fed Regist. 1984;49:171.
2. McNitt-Gray MF. AAPM/RSNA physics tutorial for residents: topics in CT. Radiation dose in CT. Radiographics. 2002;22(6):1541–53.
3. Coursey CA, Frush DP. CT and radiation: what radiologists should know. Appl Radiol. 2008;37(3):22–9.
4. Kubo T, Ohno Y, Nishino M, et al. Low dose chest CT protocol (50 mAs) as a routine protocol for comprehensive assessment of intrathoracic abnormality. Eur J Radiol. 2016;3:86–94. https://doi.org/10.1016/j.ejro.2016.04.001.
5. Kubo T, Ohno Y, Kauczor HU, Hatabu H. Radiation dose reduction in chest CT-review of available options. Eur J Radiol. 2014;83(10):1953–61.
6. Swensen SJ, Viggiano RW, Midthun DE, et al. Lung nodule enhancement at CT: multicenter study. Radiology. 2000;214(1):73–80.
7. Swensen SJ, Brown LR, Colby TV, Weaver AL. Pulmonary nodules: CT evaluation of enhancement with iodinated contrast material. Radiology. 1995;194(2):393–8.
8. Han D, Lee KS, Franquet T, Müller NL, Kim TS, Kim H, Kwon OJ, Byun HS. Thrombotic and nonthrombotic pulmonary arterial embolism: spectrum of imaging findings. Radiographics. 2003;23(6):1521–39.
9. Aziz ZA, Wells AU, Bateman ED, et al. Interstitial lung disease: effects of thin-section CT on clinical decision making. Radiology. 2006;238(2):725–33.
10. Mayo JR. CT evaluation of diffuse infiltrative lung disease: dose considerations and optimal technique. J Thorac Imaging. 2009;24(4):252–9.

11. Gilkeson RC, Ciancibello LM, Hejal RB, et al. Tracheobronchomalacia: dynamic airway evaluation with multi-detector CT. AJR Am J Roentgenol. 2001;176(1):205–10.
12. Baroni RH, Feller-Kopman D, Nishino M, et al. Tracheobronchomalacia: comparison between end-expiratory and dynamic expiratory CT for evaluation of central airway collapse. Radiology. 2005;235(2):635–41.
13. Cascade PN. Setting appropriateness guidelines for radiology. Radiology. 1994;192(1):50A–4A.
14. Cascade PN. The American College of Radiology. ACR Appropriateness Criteria project. Radiology. 2000;214(Suppl):3–46.
15. www.acr.org/ac.

# Chapter 2
# The Scout Film

- **_Is there anything that the patient wasn't born with on the image?_**
  - **_Is the diaphragm elevated?_**

Six to eleven percent of important findings are excluded in the CT FOV, and 2% of these can be seen on the scout film, thus highlighting its importance [1]. Leonard Berlin's article, reviewing the CT scout view: medicolegal and ethical considerations, admits that the scout film is unlikely to demonstrate a significant abnormality; however, because 85 million CT scans are performed a year, the scout film could help to identify nearly 2.5 million abnormalities not included on the CT scan FOV [2]. The value of the scout film cannot be overstated; it provides an overview of the patient's condition. Review of the scout film helps you to identify lines and tubes that you may otherwise have ignored. Orthopedic hardware assessment is facilitated on the scout film as is foreign body recognition. Scoliosis can be measured on the scout film [3]. Diaphragmatic elevation can be quantified on this view. Let's review some examples.

## 2.1   Lines and Tubes Visible on the Scout Film

Endotracheal tubes are ideally positioned 2.5 cm above the carina. This is difficult because when we look at the endotracheal tube, we do not know the position of the head which may cause the endotracheal tube position to change. There is an expression, "as goes the nose, so goes the hose." When the neck is flexed, the ET tube moves inferiorly, and when the neck is extended, the tube moves superiorly [4]. When judging the location of the tube, it should not project above the clavicles or at the level of the carina (Fig. 2.1).

Feeding tube needs to be positioned with its tip below the diaphragm to assure that it is not in the lung, ideally, 10 cm beyond the gastroesophageal junction [5]. The distal tip of the tube does not need to be included on the film to say that it is well-positioned to use (Fig. 2.2). If a feeding tube does not extend below the diaphragm, one cannot be sure if it is in the esophagus and it needs to be repositioned.
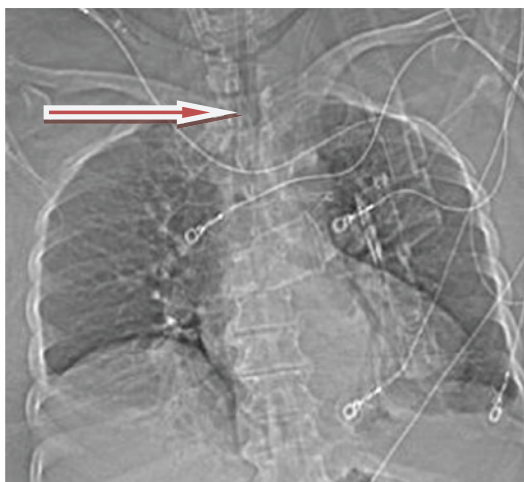


Fig. 2.1  Endotracheal tube in correct position on scout film
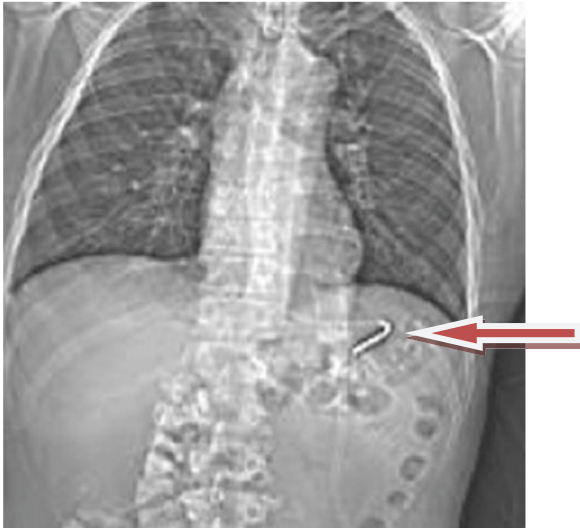
FIG. 2.2  Feeding tube in correct position on scout film

Central lines are either subclavian or internal jugular lines. The important thing to remember is that all right-sided catheters should stay on the right and left-sided catheters should cross to the right. If the catheter does not, it may be located in an artery, and a blood gas should be obtained from catheter blood to ensure location in a vein and not an artery. Ideally most catheters should terminate at SVC/right atrial junction [6] unless they are being used for high flow and then they may be situated in the right atrium (Figs. 2.3 and 2.4).

Chest tubes have a discontinuous line that identifies the last side hole. This area of discontinuity must project over the hemithorax, or there will be an air leak. Typically the tip of a chest tube is placed superiorly in a pneumothorax in an upright patient and anteriorly in a supine patient. A chest tube is ideally placed inferiorly to treat a pleural effusion in an upright patient and posteriorly in a supine patient [7] (Fig. 2.5).

Sternotomy wires can be circular or in a figure eight configuration depending on the surgeon's preference.
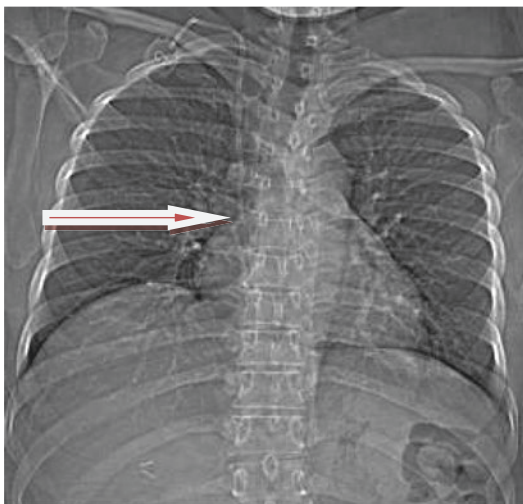
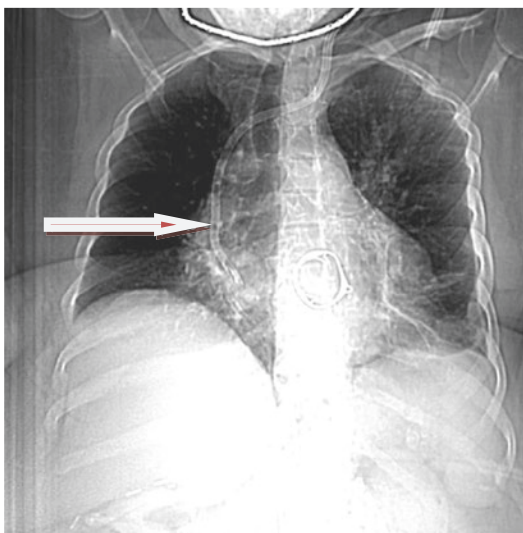Fig. 2.3  Right IJ catheter with tip in SVC/right atrial junction



Fig. 2.4  Left internal jugular catheter with tip in right atrium. Mitral valve prosthesis and partially imaged IVC filter
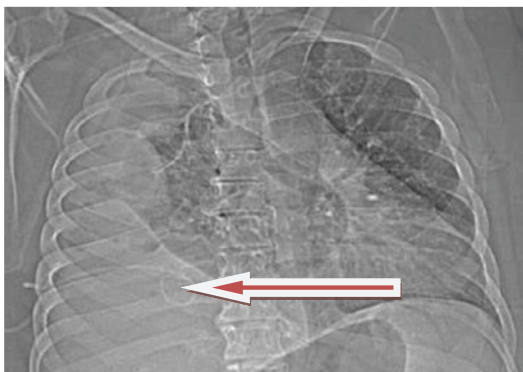
Fɪɢ. 2.5  Right chest tube for pleural effusion



Fɪɢ. 2.6  Dehiscent sternal wires in patient with sternal infection

Discontinuous wires suggest the possibility of sternal infection and should be noted [8] (Fig. 2.6).

Pacemakers are common and can stop working if wires are fractured which happens when people "twiddle" with the device under their skin. One can suspect "Twiddler's syndrome" if the wires appear stretched and redundant [9] (Fig. 2.7).

Fig. 2.7 Intact left-sided pacemaker



Fig. 2.8 Right shoulder prosthesis

## 2.2  Orthopedic Hardware Assessment

Shoulder prosthesis can be readily identified on the scout film. Evaluation of prosthesis on axial images is limited by beam-hardening artifact [10] (Fig. 2.8).

Spinal fixation devices are frequent, and alignment can often be better judged on the scout film than on the axial images because of beam-hardening artifacts (Fig. 2.9).
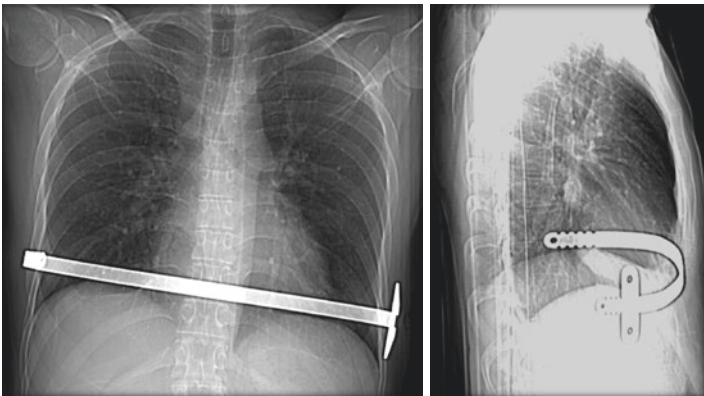
FIG. 2.9 Cervical spine fixation



FIG. 2.10 Pectus correction device

Pectus correction apparatus is used when patients have a Haller index of greater than 2.5. Haller index is a measure of transverse diameter over narrowest AP diameter. The larger the number, the greater the deformity [11] (Fig. 2.10).

FIG. 2.11  Shrapnel

## 2.3    Foreign Body

Retained catheter fragments can be difficult to appreciate on the axial images especially if contrast is used, so the scout film allows an opportunity to identify the object. Shrapnel can occur anywhere in the chest, and recognizing the appearance of shrapnel is important so as not to confuse it for other diseases (Fig. 2.11).

## 2.4    Spine Deformity

Scoliosis is quantified on X-ray by measuring the Cobb angle at the location of most severe curvature [12] (Fig. 2.12).

Kyphosis is common with aging. It is often accelerated when a patient develops a wedge-shaped anterior compression fracture
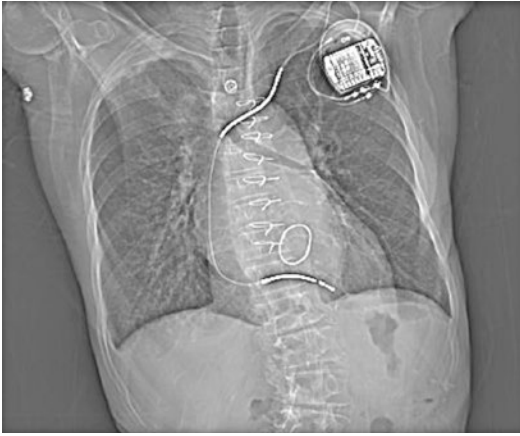
Fig. 2.12  Scoliosis



Fig. 2.13  Vertebroplasty for treatment of compression fracture

[13]. Compression fractures are often treated with vertebroplasty in order to regain the normal alignment of the spine (Fig. 2.13).

## 2.5    Diaphragm

Apparent elevation of the diaphragm can occur when there is a tear in the diagram and the abdominal organs herniate through the tear (Fig. 2.14). Injuries to the right hemidiaphragm are three times more common than injuries to the left hemidiaphragm following blunt injury. Injuries to the left hemidiaphragm are more frequently missed than injuries to the right hemidiaphragm. The "collar sign" is a waist-like constriction of the herniating hollow viscous at the site of the diaphragmatic tear [14].

Phrenic nerve paralysis can happen because of mediastinal cancer invading the nerve or secondary to surgery where the nerve is injured. Preoperative chest X-rays where the diaphragm is normal followed by postoperative chest X-ray where it is elevated will suggest the later diagnosis [15] (Fig. 2.15).
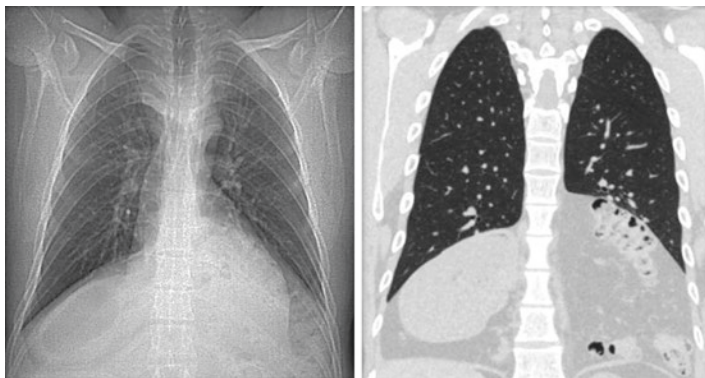


Fig. 2.14  Herniated bowel above the diaphragm
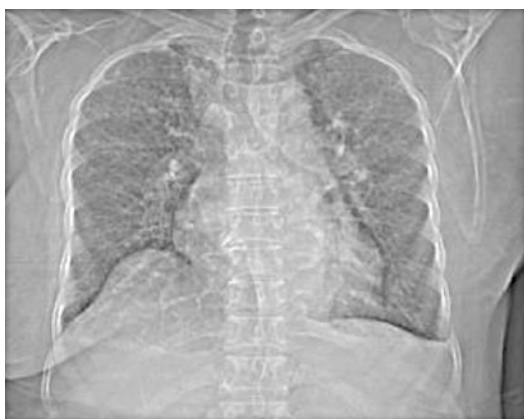
Fig. 2.15  Phrenic nerve paralysis



Fig. 2.16  Diaphragmatic eventration

Eventration or mammillation of the hemidiaphragm is common and caused by focal weakness allowing abdominal contents to bulge superiorly [16] (Fig. 2.16).

# References

1. Johnson PT, Scott WW, Gayler BW, Lewin JS, Fishman EK. The CT scout view: does it need to be routinely reviewed as part of the CT interpretation? AJR Am J Roentgenol. 2014;202:1256–63.
2. Berlin L. Reviewing the CT scout view: medicolegal and ethical considerations. AJR Am J Roentgenol. 2014;202(6):1264–6.
3. Ho EK, Upadhyay SS, Ferris L, Chan FL, Bacon-Shone J, Hsu LC, Leong JC. A comparative study of computed tomographic and plain radiographic methods to measure vertebral rotation in adolescent idiopathic scoliosis. Spine (Phila PA 1976). 1992;17(7):771–4.
4. Goodman LR, Conrardy PA, Laing F, Singer MM. Radiographic evaluation of endotracheal tube position. AJR Am J Roentgenol. 1976;127(3):433–4.
5. Pillai JB, Vegas A, Brister S. Thoracic complications of nasogastric tube: review of safe practice. Interact Cardiovasc Thorac Surg. 2005;4(5):429–33.
6. Funaki B. Central venous access: a primer for the diagnostic radiologist. AJR Am J Roentgenol. 2002;179(2):309–18.
7. Godoy MC, Leitman BS, de Groot PM, Vlahos I, Naidich DP. Chest radiography in the ICU: part 1, evaluation of airway, enteric, and pleural tubes. AJR Am J Roentgenol. 2012;198(3):563–71.
8. Schimmer C, Reents W, Elert O. Primary closure of median sternotomy: a survey of all German surgical heart centers and a review of the literature concerning sternal closure technique. Thorac Cardiovasc Surg. 2006;54(6):408–13.
9. Sharifi M, Inbar S, Neckels B, Shook H. Twiddling to the extreme: development of twiddler syndrome in an implanted cardioverter-defibrillator. J Invasive Cardiol. 2005;17(3):195–6.
10. Yian EH, Werner CM, Nyffeler RW, Pfirrmann CW, Ramappa A, Sukthankar A, Gerber C. Radiographic and computed tomography analysis of cemented pegged polyethylene glenoid components in total shoulder replacement. J Bone Joint Surg Am. 2005;87(9):1928–36.

11. Rao AG. Haller index in patients with pectus excavatum. AJR Am J Roentgenol. 2012;199(5):W665. author reply W666.
12. Langensiepen S, Semler O, Sobottke R, Fricke O, Franklin J, Schönau E, Eysel P. Measuring procedures to determine the Cobb angle in idiopathic scoliosis: a systematic review. Eur Spine J. 2013;22(11):2360–71.
13. Katzman WB, Wanek L, Shepherd JA, Sellmeyer DE. Age-related hyperkyphosis: its causes, consequences, and management. J Orthop Sports Phys Ther. 2010;40(6):352–60.
14. Iochum S, Ludig T, Walter F, Sebbag H, Grosdidier G, Blum AG. Imaging of diaphragmatic injury: a diagnostic challenge. Radiographics. 2002;22:S103–16.
15. Gaissert H, Wilcox SR. Diaphragmatic dysfunction after thoracic operations. Thorac Cardiovasc Surg. 2016;64(8):621–30.
16. Verhey PT, Gosselin MV, Primack SL, Kraemer AC. Differentiating diaphragmatic paralysis and eventration. Acad Radiol. 2007;14(4):420–5.

# Chapter 3
# The Trachea and Bronchi

- *Is it dilated?*
- *Is it narrowed?*
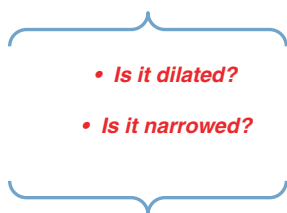
## 3.1 Normal Anatomy of Airways

The airways should be reviewed on axial images, lung window settings (Window 1500, Level −500). First, scroll through the trachea and then the right upper lobe bronchus with its three divisions, anterior, posterior, and apical. The right upper lobe bronchus resembles a gold fish cracker (Fig. 3.1).

The right middle lobe bronchus has medial and lateral branches [1] which can be remembered because the initials of middle lobe are M and L (medial, lateral) (Fig. 3.2).

The right lower lobe bronchus has five divisions [1] which are anterior, posterior, medial, and lateral like a compass and then superior (Fig. 3.3).

The left upper lobe has four branches [1]. There is the anterior and apical posterior and the superior and inferior (Fig. 3.4).

Fig. 3.1  Right upper lobe bronchus and divisions

Fig. 3.2  Right middle lobe bronchus and divisions

The left lower bronchus also has four divisions [1]. They are the same as the right lower lobe but the anterior and medial are combined (Fig. 3.5). Remember this by thinking about a clock and AM are the initials of anterior and medial combined.

Fig. 3.3  Right lower lobe bronchus and divisions

A tracheal bronchus or bronchus suis is a right upper lobe bronchus that emerges directly from the trachea [2]. It is important to know about because if a patient with a tracheal bronchus is intubated, they can develop right upper lobe atelectasis if the endotracheal tube projects below the opening [3]. A cardiac bronchus is a supernumerary bronchus which comes off the medial aspect of the bronchus intermedius [4].
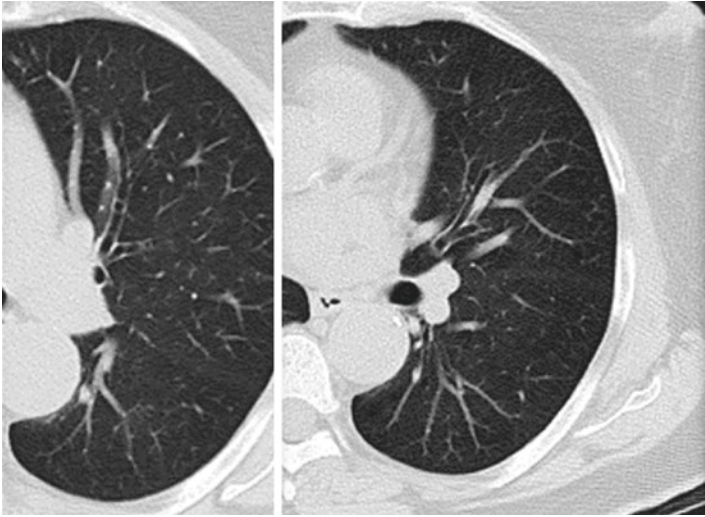
Fig. 3.4 Left upper lobe bronchus and divisions

A rare congenital abnormality called isomerism or heterotaxic syndrome involves bilateral right sidedness or bilateral left sidedness [5]. In bilateral right sidedness, also known as Ivemark's syndrome, the lung on the right has three lobes as does the lung on the left, and it is associated with asplenia [5, 6]. In contrast, in bilateral left sidedness or polysplenia syndrome, there are two lobes on the left and two lobes on the right. It is associated with polysplenia, dextrocardia, and midline liver and cardiac abnormalities [7] (Fig. 3.6).

In summary the right lung typically has ten bronchial branches and is separated into three lobes, and the left lung has eight branches and is separated into two lobes. There are variations of normal branching patterns [2].

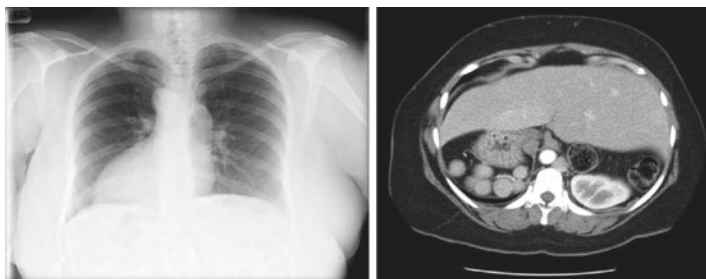FIG. 3.5  Left lower lobe bronchus and divisions



FIG. 3.6  Polysplenia. Bilateral left sidedness, dextrocardia, midline liver, and multiple spleens

## 3.2   Diseases of the Trachea

Tracheal dilatation is also called tracheomegaly. This term can be used when the trachea measures greater than 3 cm in size. Tracheomegaly is associated with Mounier-Kuhn disease which is also called tracheobronchomegaly (Fig. 3.7). It is associated with tracheal diverticula and bronchiectasis [8].

Tracheomalacia can also cause the trachea to dilate. In these patients the transverse diameter of the trachea is enlarged compared to the anterior-posterior dimension giving the trachea the appearance of a lemon. On expiration, patients with tracheomalacia have significant, greater than 70%, collapse of the posterior membrane of the trachea [9] (Figs. 3.8 and 3.9).

Circumferential thickening of the trachea can be caused by granulation tissue formation from prolonged intubation. It is important for an endotracheal tube to be replaced by trache-
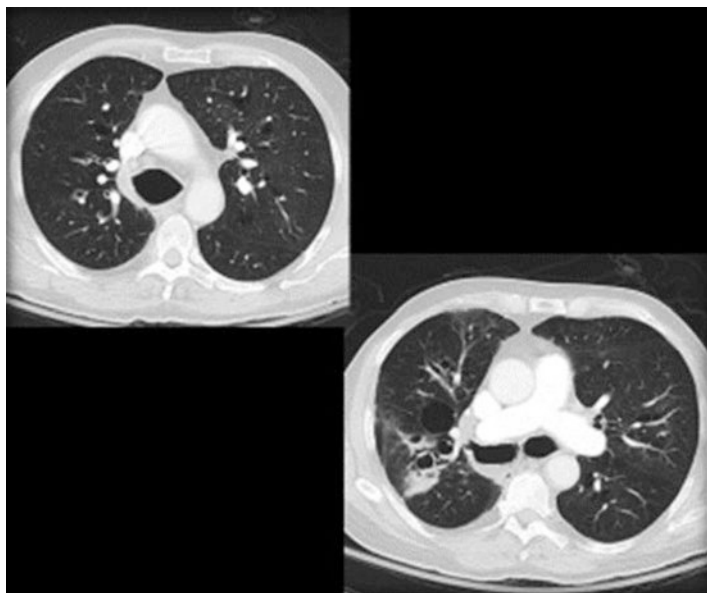


Fig. 3.7  Mounier-Kuhn disease or tracheobronchomegaly

Fig. 3.8 Tracheomalacia on inspiration giving a "lemon-shaped" trachea



Fig. 3.9 Tracheomalacia on expiration with total collapse of the airways

ostomy tube if greater than 10 days of intubation is required [10] (Fig. 3.10).

The trachea can become diffusely thickened by diseases such as Wegener's granulomatosis, sarcoidosis, amyloidosis, and Crohn's disease [11–14].

The trachea can thicken anteriorly and spare the posterior membrane with relapsing polychondritis and tracheobronchopathia osteochondroplastica [15, 16] (Fig. 3.11).
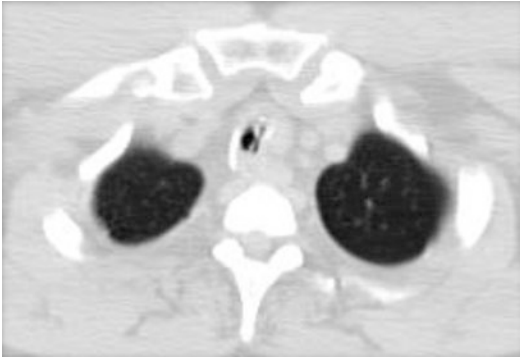
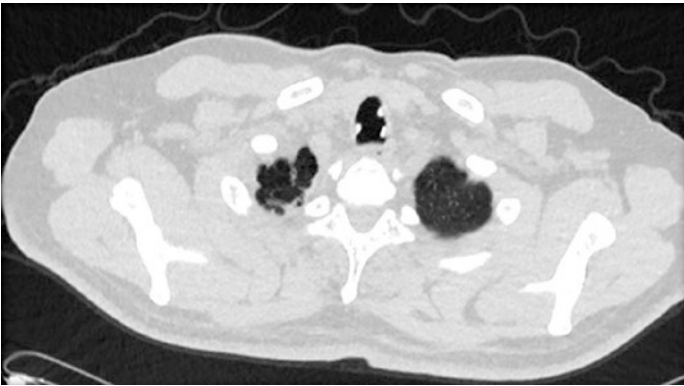Fɪɢ. 3.ɪo Circumferential tracheal narrowing due to stricture



Fɪɢ. 3.ɪɪ Tracheobronchopathia osteochondroplastica

Cancer affects the trachea. In smokers the typical cancer is squamous cell carcinoma, and in nonsmokers, adenoid cystic carcinoma [17]. Polyps can occur within the trachea and are typically pedunculated (Fig. 3.12).

Mucous is commonly seen within the trachea [18]. It characteristically is in the dependent portion and may contain air bubbles (Fig. 3.13). If the tracheal soft tissue is nondependent, it still may represent adherent secretions, and a follow-up CT scan of the chest should be obtained in 1 month
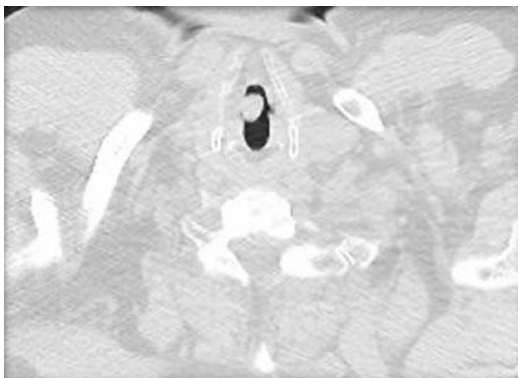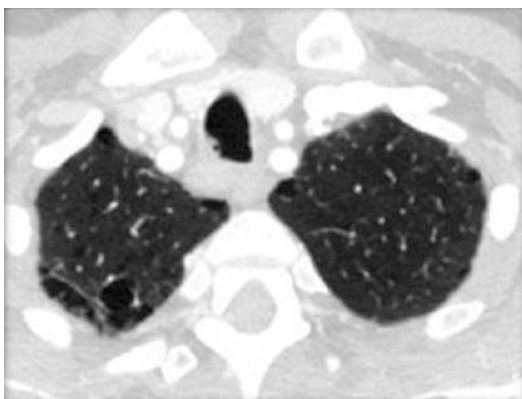
Fig. 3.12  Tracheal polyp



Fig. 3.13  Mucous along the right lateral wall of the trachea

following pulmonary toilet. It is a good practice in general to instruct patients to cough prior to a CT scan of the chest so that any tracheal mucous will be removed thus avoiding unnecessary repeat scanning.

## 3.3   Diseases of the Bronchi

Bronchiectasis affects the center of the secondary pulmonary lobule, and by definition the bronchus becomes irreversibly larger in cross section than its accompanying artery [19]. In the 1950s Lynne Reid described three types of bronchiectasis based on her cadaver dissections, cylindrical, varicoid, and cystic [20] (Fig. 3.14).

Dr. Reid noted that in the healthy individual, there were 11 bronchial subdivisions from the trachea to the peripheral bronchus. In cylindrical bronchiectasis, where the bronchus is just slightly larger than its derived bronchus, the normal branching pattern is maintained. In varicoid bronchiectasis, however, pruning of the bronchi alters the branching pattern, and only seven subdivisions can be observed. This bronchial pruning reaches a maximum level in cystic bronchiectasis, where it is possible to identify only four remaining branches.
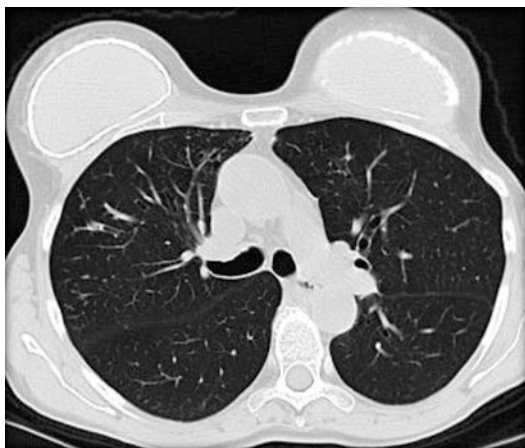


FIG. 3.14  Cylindrical bronchiectasis

The lung parenchyma that surrounds cystic bronchus is devoid of vascular supply when evaluated with V/Q scan [20, 21]. We continue to use Dr. Reid's classification system today.

Bronchiectasis has multiple causes [19]. For this reason, the extent and distribution of the disease must be considered to limit the differential diagnosis. Focal bronchiectasis occurs with bronchial atresia and is seen with surrounded by air trapping, a typical finding of this entity (Fig. 3.15) [22].

Focal bronchiectasis can be seen distal to an obstructing lesion such as a broncholith or a bronchial tumor such as a carcinoid tumor [23, 24] (Fig. 3.16).
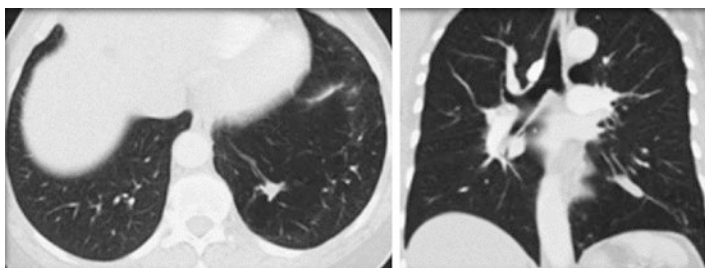


Fig. 3.15  Bronchial atresia



Fig. 3.16  Endobronchial carcinoid

Diffuse bronchiectasis can be central or peripheral. Allergic bronchopulmonary aspergillosis is characterized by central bronchiectasis with mucoid impaction affecting the first to the fourth division of bronchi (Fig. 3.17). It is associated with asthma. The appearance has been described as a finger in a glove with the glove representing the dilated bronchus and the mucous representing the finger [8, 25] [10].

Williams-Campbell disease is a rare cause of bronchiectasis that affects the fourth to the eighth level of bronchi [26]. Notice how the central and peripheral bronchi are not involved in this disease [11].

Diffuse bronchiectasis that can affect peripheral airways can be divided into upper lung and lower lung diseases. Upper lobe posterior bronchiectasis is seen in stage 4 sarcoidosis (S4). On chest X-ray, the fibrosis observed in this case appears to pull outward from the hilum giving the appearance of a swag curtain [27] (Fig. 3.18).

Radiation treatment causes fibrosis and bronchiectasis to areas of the lung which receive greater than 20 Gy dose [28]. It is included in the upper lobe fibrosis because cancer of the lung is more common in the upper lobes (Fig. 3.19). In this example a right upper lobe cancer is treated with external
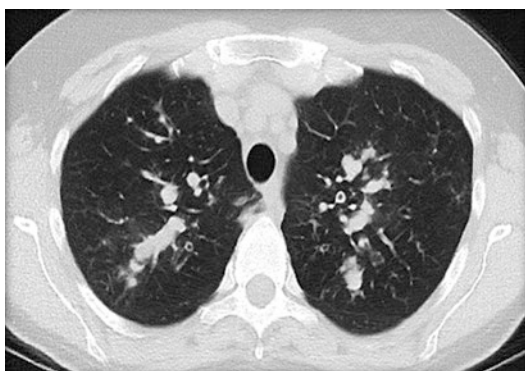


Fig. 3.17 Patient with asthma-related allergic bronchopulmonary aspergillosis (ABPA) with "finger in glove" appearance
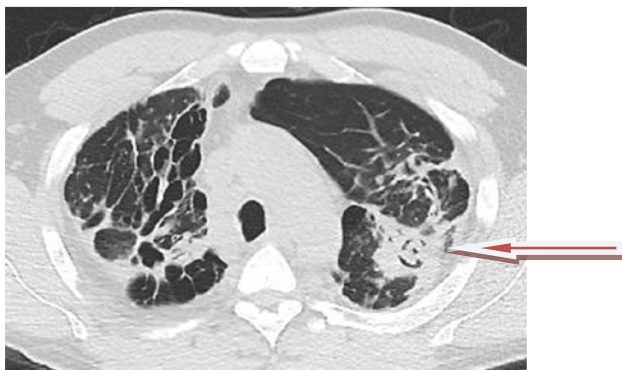
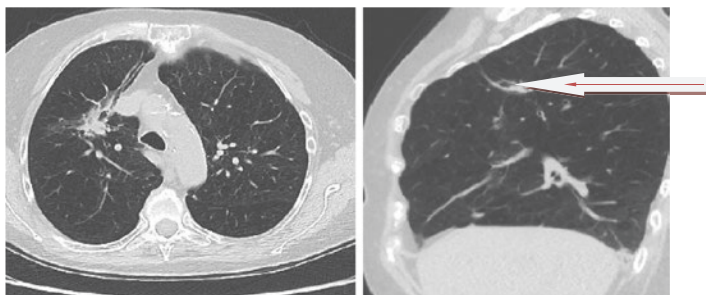FIG. 3.18  Stage 4 sarcoidosis with left upper lobe mycetoma



FIG. 3.19  Radiation fibrosis

beam radiation with resulting bronchiectasis. On lateral projection, the fibrosis is appreciated as linear. Radiation-induced fibrosis can evolve over a 2-year period, and focal recurrence is relatively uncommon [29]. Recurrence is suspected when there is opacification of a previously dilated bronchus.

Mycobacterium avium-intracellulare (MAI) infection is a frequent cause of right middle lobe and lingular bronchiectasis, predominantly, in older women who suppress their cough, and the constellation of findings is called Lady Windermere syndrome [30] (Fig. 3.20).
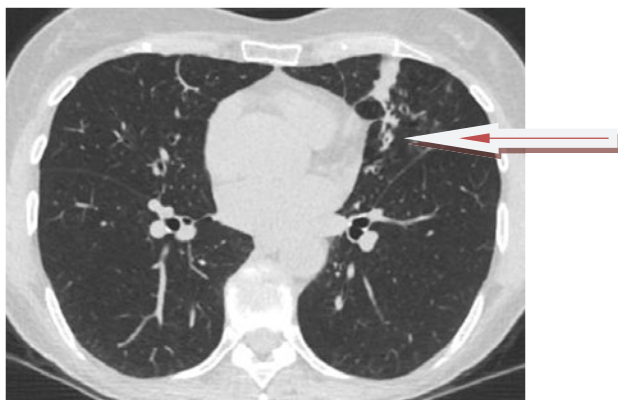
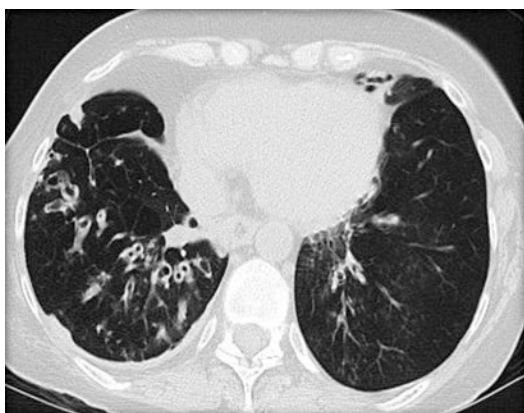Fɪɢ. 3.20  Lady Windermere syndrome involving predominantly the lingula



Fɪɢ. 3.21  Ciliary dyskinesia

Ciliary dyskinesia presents as lower lobe bronchiectasis with recurrent pulmonary infections. When ciliary dyskinesia occurs in association with situs inversus and chronic sinusitis, it is called Kartagener's syndrome [31] (Fig. 3.21). If concomitant yellow nails are present, it is called yellow nail syndrome [32]. Finally, if there is azoospermia, the condition is termed Young's syndrome [33] [15, 16].

Bronchiectasis can also be a result of recurrent pneumonia. When there is evidence of bronchiectasis in the lower lobe, suspect aspiration pneumonia as the causative agent (Fig. 3.22).

*Minimum intensity projection images* (MINIPS) accentuate structures with low HU such as the trachea and bronchi and obscure vessels (Fig. 3.23). They can enhance our ability to recognize bronchiectasis, cysts, and honeycombing as in the patient below with bronchiectasis [34].
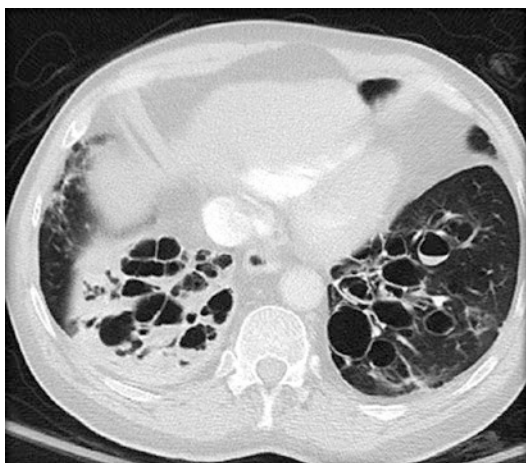


FIG. 3.22  Recurrent pneumonia



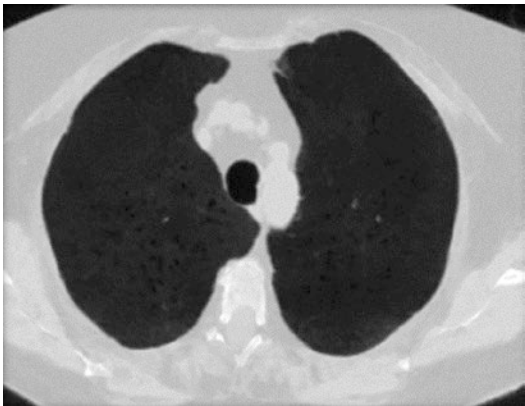FIG. 3.23  MINIPs demonstrating left lower lobe bronchiectasis

FIG. 3.24 MINIPS demonstrating central lucency in a patient with centrilobular emphysema

MINIPS also accentuate hypodense lung parenchyma and help make the correct diagnosis of centrilobular emphysema (Fig. 3.24).

SUMMARY TABLE: PATTERNS OF BRONCHIECTASIS

| Focal | Central | Peripheral Upper lobe | Peripheral Middle lobe | Peripheral Lower lobe |
|-------|---------|-----------------------|------------------------|-----------------------|
| – Bronchial atresia | – Mounier-Kuhn | – Sarcoid | – MAI | – Ciliary dyskinesia |
| – Broncholithiasis | – ABPA | – Cystic fibrosis | | – Recurrent pneumonia |
| – Bronchial tumor | – Williams-Campbell | – Radiation fibrosis | | |

# References

1. Minnich DJ, Mathisen DJ. Anatomy of the trachea, carina, and bronchi. ThoracSurgClin. 2007;17(4):571–85.
2. Doolittle AM, Mair EA. Tracheal bronchus: classification, endoscopic analysis, and airway management. Otolaryngol Head Neck Surg. 2002;126(3):240–3.

3. Berrocal T, Madrid C, Novo S, Gutiérrez J, Arjonilla A, Gómez-León N. Congenital anomalies of the tracheobronchial tree, lung, and mediastinum: embryology, radiology, and pathology. Radiographics. 2004;24(1):e17.

4. McGuinness G, Naidich DP, Garay SM, Davis AL, Boyd AD, Mizrachi HH. Accessory cardiac bronchus: CT features and clinical significance. Radiology. 1993;189(2):563.

5. Ghosh S, Yarmish G, Godelman A, et al. Anomalies of viscero-atrial situs. AJR Am J Roentgenol. 2009;193(4):1107–17.

6. Ivemark BI. Implications of agenesis of the spleen on the pathogenesis of conotruncus anomalies in childhood; an analysis of the heart malformations in the splenic agenesis syndrome, with fourteen new cases. ActaPaediatr. 1955;44(Suppl 104):7–110.

7. Winer-Muram HT, Tonkin ILD, Gold RE. Polysplenia syndrome in the asymptomatic adult: computed tomography evaluation. J Thorac Imaging. 1991;6:69–71.

8. Laroia AT, Thompson BH, Laroia ST, van Beek EJ. Modern imaging of the trachea-bronchial tree. World J Radiol. 2010;2(7):237–48.

9. Carden KA, Boiselle PM, Waltz DA, Ernst A. Tracheomalacia and tracheobronchomalacia in children and adults: an in-depth review. Chest. 2005;127:984–1005.

10. Ridge CA, O'Donnell CR, Lee EY, Majid A, Boiselle PM. Tracheobronchomalacia: current concepts and controversies. J Thorac Imaging. 2011;26(4):278–89.

11. Daum TE, Specks U, Colby TV, Edell ES, Brutinel MW, Prakash UB, DeRemee RA. Tracheobronchial involvement in Wegener's granulomatosis. Am J Respir Crit Care Med. 1995;151(2 Pt 1):522–6.

12. Soares MT, Sousa C, Garanito L, Freire F. Extensive upper respiratory tract sarcoidosis. BMJ Case Rep. 2016. https://doi.org/10.1136/bcr-2015-213325.

13. O'Regan A, Fenlon HM, Beamis JF Jr, Steele MP, Skinner M, Berk JL. Tracheobronchial amyloidosis. The Boston University experience from 1984 to 1999. Medicine (Baltimore). 2000;79(2):69–79.

14. Lu DG, Ji XQ, Zhao Q, Zhang CQ, Li ZF. Tracheobronchial nodules and pulmonary infiltrates in a patient with Crohn's disease. World J Gastroenterol. 2012;18(39):5653–7.

15. Schina M, Karsaliakos P, Apostolou T, Mousoulis G. Relapsing polychondritis as a secondary phenomenon of primary systemic vasculitis. ClinNephrol. 2008;70(5):446–9.

16. Wang N, Long F, Jiang S. Tracheobronchopathia osteochondro-plastica: two cases reports and review of literature. Medicine. 2016;95(19):e3396.

17. Urdaneta AI, Yu JB, Wilson LD. Population based cancer reg-istry analysis of primary tracheal carcinoma. Am J Clin Oncol. 2011;34:32–7.

18. Heidinger BH, Occhipinti M, Eisenberg RL, Bankier AA. Imaging of large airways disorders. AJR Am J Roentgenol. 2015;205(1):41–56.

19. Maselli DJ, Amalakuhan B, Keyt H, Diaz AA. Suspecting non-cystic fibrosis bronchiectasis: what the busy primary care clinician needs to know. Int J ClinPract. 2017;71(2). https://doi.org/10.1111/ijcp.12924.

20. Reid LM. Reduction in bronchial subdivision in bronchiectasis. Thorax. 1950;5(3):233–47.

21. Ashour M. Hemodynamic alterations in bronchiectasis: a base for a new subclassification of the disease. J Thorac Cardiovasc Surg. 1996;112:328–34.

22. Traibi A, Seguin-Givelet A, Grigoroiu M, Brian E, Gossot D. Congenital bronchial atresia in adults: thoracoscopic resec-tion. J Visc Surg. 2017;30(3):174.

23. Dakkak M, Siddiqi F, Cury JD. Broncholithiasis presenting as bronchiectasis and recurrent pneumonias. BMJ Case Rep. 2015;23:2015.

24. Meisinger QC, Klein JS, Butnor KJ, Gentchos G, Leavitt BJ. CT features of peripheral pulmonary carcinoid tumors. AJR Am J Roentgenol. 2011;197(5):1073–80.

25. Agarwal R. Allergic bronchopulmonary aspergillosis: lessons for the busy radiologist. World J Radiol. 2011;3(7):178–81.

26. Noriega Aldave AP, William Saliski D. The clinical mani-festations, diagnosis, and management of Williams-Campbell Syndrome. N Am J Med Sci. 2014;6(9):429–32.

27. Abehsera M, Valeyre D, Grenier P, Jaillet H, Battesti JP, Brauner MW. Sarcoidosis with pulmonary fibrosis: CT patterns and correlation with pulmonary function. AJR Am J Roentgenol. 2000;174(6):1751–7.

28. Jennings FLAA. Development of radiation pneumonitis: time and dose factor. Arch Pathol. 1962;74:351–60.

29. Benveniste MFK, Welsh J, Godoy MCB, Betancourt SL, Mawlawi OR, Munden RF. New era of radiotherapy: an update in radiation-induced lung disease. Clin Radiol. 2013;68(6):e275–90.

30. Reich JM, Johnson RE. Mycobacterium avium complex pulmonary disease presenting as an isolated lingular or middle lobe pattern. The lady Windermere syndrome. Chest. 1992;101(6):1605–9.
31. Skeik N, Fl J. Kartagener Syndrome. International Journal of General Medicine. 2011;4:41–3.
32. Vignes S, Baran R. Yellow nail syndrome: a review. Orphanet J Rare Dis. 2017;12:42.
33. De longh R, Ing A, Rutland J. Mucociliary function, ciliary ultrastructure, and ciliary orientation in Young's syndrome. Thorax. 1992;47(43):184–7.
34. Perandini S, Faccioli N, Zaccarella A, Re TJ, Mucelli RP. The diagnostic contribution of CT volumetric rendering techniques in routine practice. Indian J Radiol Imaging. 2010;20(2):92–7.

# Chapter 4
# The Lung Parenchyma

- *Is it in the alveoli?*
- *Is it in the interstitium?*
- *Is it related to pulmonary artery?*
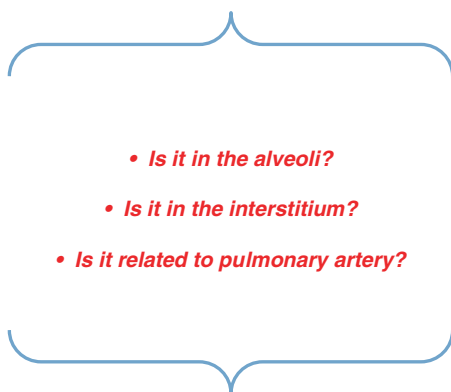
## 4.1 Introduction

The lung parenchyma should be evaluated on axial images using lung window settings (window 1500, level −500) which are recorded on the computer image. Scroll using the mouse through the right lung beginning at the apex and moving toward the lung bases evaluating the lung parenchyma in front of the right major fissure which will include the right upper and middle lobes of the lung. Next scroll from the bases of the lung to the apex reviewing the lung posterior to

the right major fissure, the right lower lobe. Repeat this process reviewing the left lung parenchyma. In front of the left major fissure is the left upper lobe which includes the lingual and posterior is the left lower lobe (Fig. 4.1).

An azygous lobe is formed when the azygous vein invaginates the pleura and is located lateral to the mediastinum [1] (Fig. 4.2). This is a common congenital anomaly reported to occur in about 1% of the population [2].

The lung is composed of secondary pulmonary lobules (SPLs) which are the smallest unit of the lung entirely outlined by connective tissue septa [3]. SPLs are irregularly shaped hexagons measuring on average 11–17 mm in size and thus visible on CT [4] particularly in the periphery of the lung and at the lung bases (Fig. 4.3).

The periphery of the secondary pulmonary lobule is outlined by the interlobular septa which are extensions from the peripheral pleura. The interlobular septa were described by Weibel as part of the peripheral interstitial fiber system [5]. This peripheral interstitium covers the surface of the lung and penetrates into the lung parenchyma as the interlobular
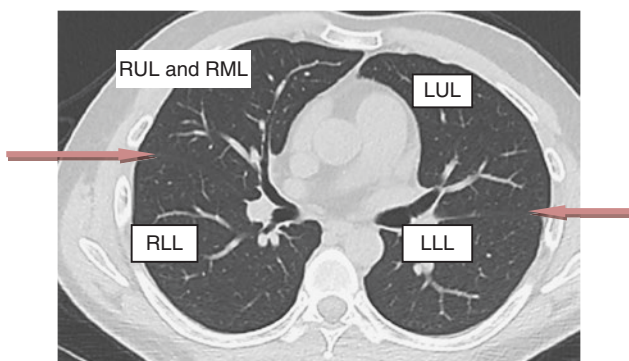


FIG. 4.1 The right lung is separated into right upper and middle lobes (RUL, RML) and right lower lobe (RLL) by the right major fissure. The right upper and middle lobes are separated by the minor fissure. The left upper lobe (LUL) and lower lobe (LLL) are separated by the left major fissure
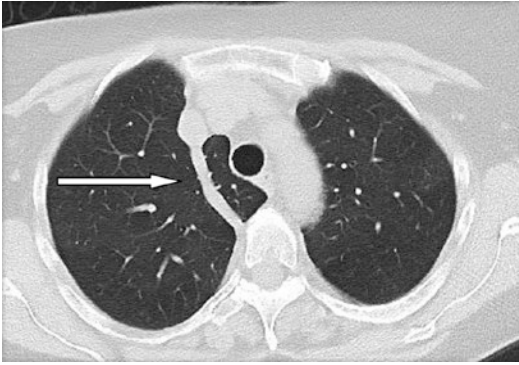
Fɪɢ. 4.2 Laterally displaced azygous vein (arrow) creating an azygous lobe



Interlobular septae
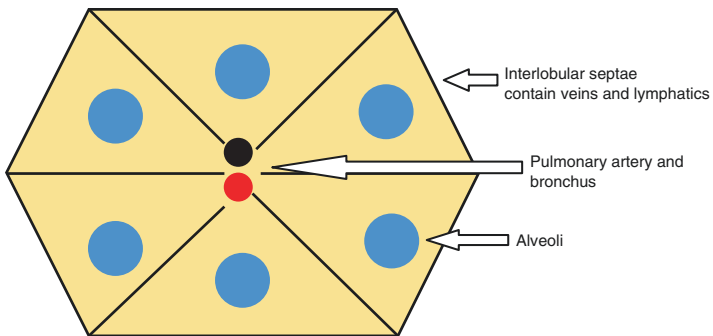contain veins and lymphatics

Pulmonary artery and
bronchus

Alveoli

Fɪɢ. 4.3 Anatomy of the secondary pulmonary lobule; diagrammatic representation

septa. The pulmonary veins and lymphatics travel within the interlobular septa. Diseases that affect the veins such as congestive heart failure or the lymphatics such as lymphangitic spread of cancer will cause thickening of the interlobular septa (Fig. 4.4).
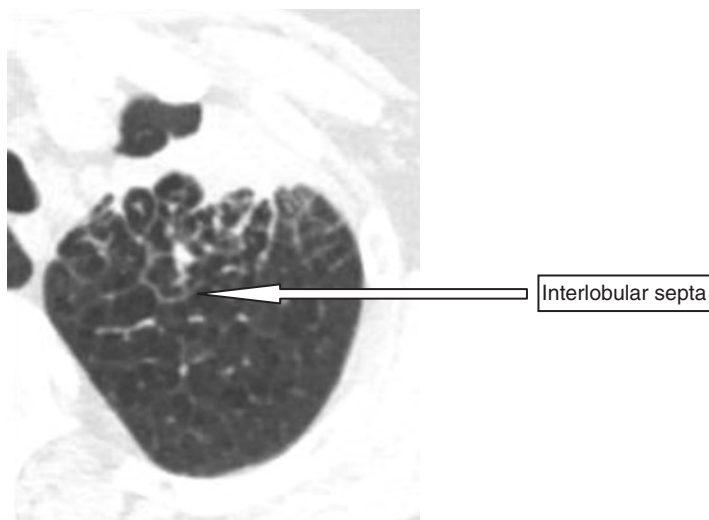
FIG. 4.4 Thickened interlobular septa caused by lymphangitic spread of lung cancer

In the center of the secondary pulmonary lobule are the pulmonary artery and its accompanying bronchiole [6]. The bronchiole is not normally identified on CT scan in the periphery of the lung but can be seen when it becomes dilated due to lung fibrosis. Disease that affects the pulmonary artery will be located in the center of the SPL such as metastases and miliary tuberculosis.

The pulmonary artery and bronchus are surrounded by alveoli and their closely associated capillaries. The pulmonary acinus which is 6–10 mm is the largest lung unit in which all airways participate in gas exchange [4–7]. Secondary pulmonary lobules are composed of 3–24 acini [8].

## 4.2   The Alveoli

The average human lung contains 480 million alveoli, and an individual alveolus has an average diameter of $4.2 \times 10(6)$ microm$^3$ [9, 10]. "High-resolution" CT systems provide resolution on the order of 100–200 micrometers.

Therefore, alveoli can be seen using newer experimental high-resolution imaging technology [10].

Hounsfield units are based on the radiodensity of distilled water on CT which is zero. Anything whiter than water has positive HU and anything darker than water has negative HU [11]. The Hounsfield unit (HU) or radiodensity of normal lung parenchyma is approximately −900 HU, so it appears blacker than water on CT [12]. Its low density is in large part due to air filling the alveoli. When fluid fills the alveoli, the lung on CT becomes more radiodense or whiter. Emphysema causes the alveoli to fill with more air and so the HU decreases compared to normal lung parenchyma [13]. In contrast lung fibrosis causes increases in the HU of the involved area in the range of −400 to −600 HU [14] (Fig. 4.5).

The term ground glass opacity is used to describe an opacity on CT scan where vessels can be visualized, and the term consolidation is used when an opacity obscures vessels on a non-contrast exam [15]. The image below demonstrates water in three cups. In the first cup, a small amount of water is placed, in the second cup a little more water, and the third



| -950 HU | -850 HU | -600 HU | 0 HU | 1000 HU |
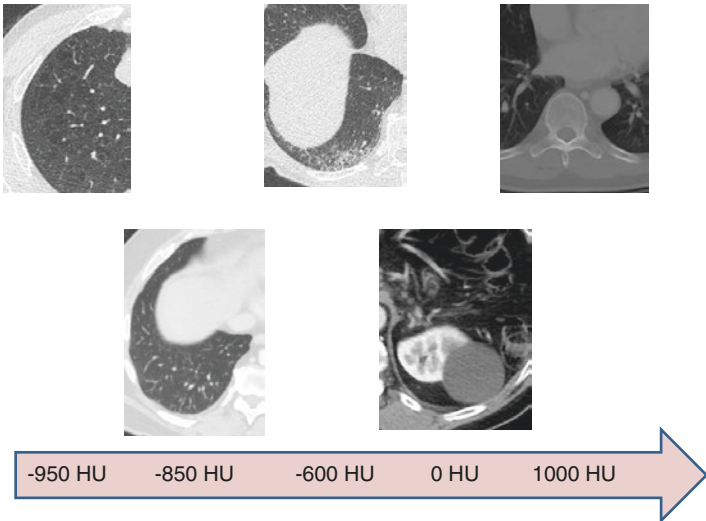
FIG. 4.5  Hounsfield measurements on CT
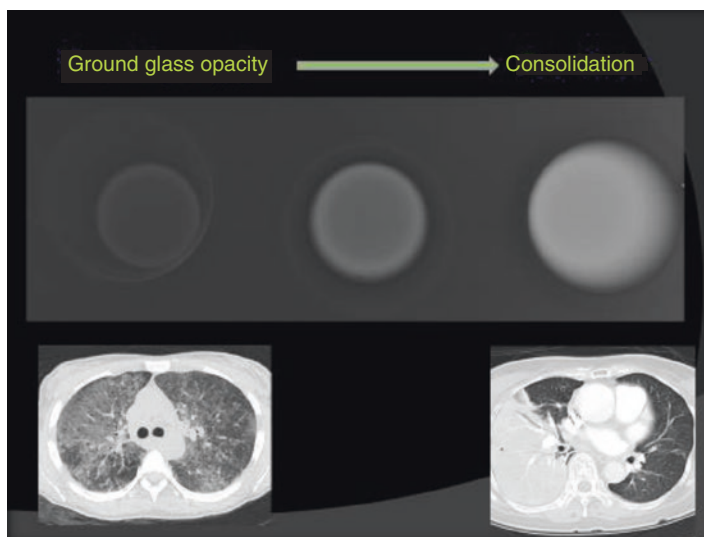
FIG. 4.6 Differentiating ground glass opacity from consolidation in vitro and on cross-sectional imaging

cup is filled with water. Notice how the imaging appearance changes. The cup with less water appears gray and the cup with the most water appears white. In the same way, ground glass opacity appears as a shade of gray, and consolidation is whiter in color (Fig. 4.6). Ground glass opacity can represent a small amount of fluid in the alveoli and consolidation is a larger amount of fluid or cells in the alveoli.

## 4.2.1   Increased Radio Density of Alveoli

Fluid fills the alveoli for a variety of reasons including infection, edema, hemorrhage, and neoplasm. The clinical history and the pattern of filling help to differentiate the various causes. Follow-up imaging is also beneficial because pulmonary edema can resolve in hours, pneumonia and hemorrhage take days, and tumors do not usually spontaneously resolve.

Pulmonary hemorrhage occurs for a variety of reasons, including tumor invasion of an artery, necrotizing infection,

vasculitis, and coagulopathy [16, 17]. The appearance on CT can be ground glass opacities or consolidation depending on the amount of blood (Fig. 4.7). A "crazy-paving" pattern can also be seen with hemorrhage which is ground glass opacity and thickening of the interlobular septa.

Fluid fills the alveoli with severe pulmonary edema when the pulmonary capillary wedge pressure exceeds 25 mmHg. This happens with a catastrophic event to the heart such as a papillary muscle tear or a large cardiac infarct [18]. The distribution of the fluid is typically central giving the so-called "bat wing" appearance (Fig. 4.8). The central location is believed to be due to the pumping effect of respiration
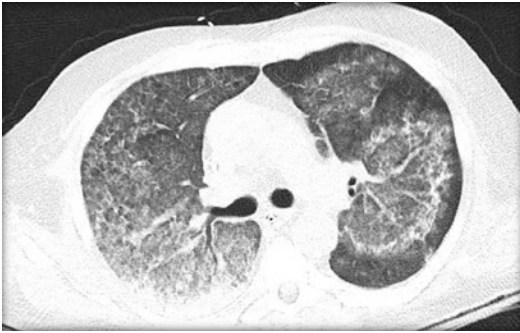


Fig. 4.7 Pulmonary hemorrhage



Fig. 4.8 Severe pulmonary edema with bat wing appearance on CT

which is accentuated in the lung cortex and pushes fluid toward the hilum. Re-expansion pulmonary edema occurs when a large pleural effusion or pneumothorax is corrected vigorously causing fluid in the alveoli. The pathogenesis is believed to be secondary to hypoxia-induced capillary permeability and the release of free radicals [19].

Pneumonia is one of the most common reasons for alveolar opacification. In the case of lobar pneumonia, fluid travels from one alveolus to the other via the pores of Kohn [20] so that at the origin, there is consolidation with all alveoli filled with fluid, but in the periphery, there are fewer alveoli affected giving a more heterogeneous appearance as illustrated in the image below. Central areas of cavitation can be observed with virulent organisms. Air bronchograms which represent unopacified airways confirm that this is an alveolar process but are not specific for pneumonia [21] (Figs. 4.9, 4.10, and 4.11). The most common pathogen causing lobar pneumonia is *Streptococcus pneumoniae* [22]. In contrast to lobar pneumonia which is focal, bronchopneumonia is patchy and bilateral being spread through the bronchi. The most common pathogen for bronchopneumonia is *Staphylococcus aureus* [20, 22].

Presumed pneumonia should be followed up until resolution to exclude the unlikely event that the consolidation
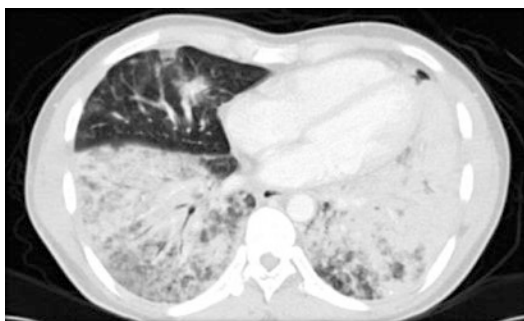


FIG. 4.9 Bilateral lower lobe-predominant bronchopneumonia with air bronchograms. Notice that the consolidation is patchy because the infection is spread through the bronchi
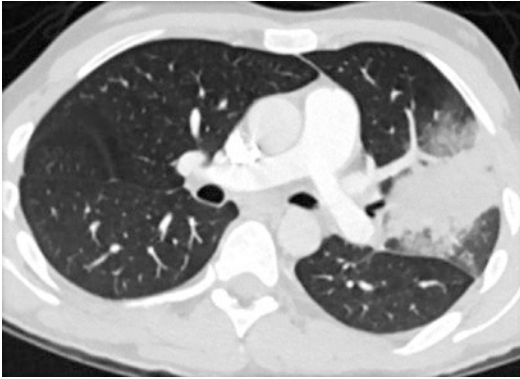
FIG. 4.10 Left upper lobe lobar pneumonia with dense consolidation centrally and ground glass opacity peripherally because the infection has not spread to all peripheral alveoli yet
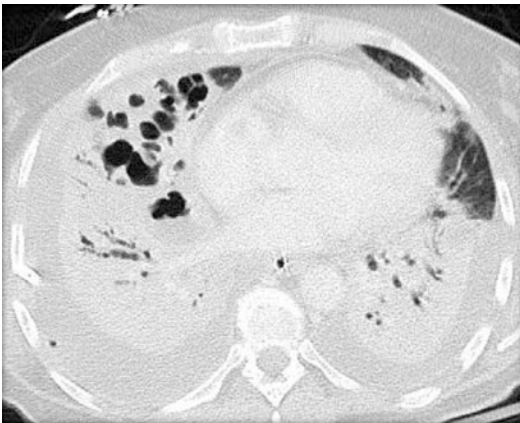


FIG. 4.11 Bilateral bronchopneumonia with cavitation suggesting a virulent organism. Note the bilateral small pleural effusions

represents cancer with tumor cells filling the alveoli instead of neutrophils [23]. In the example below, adenocarcinoma mimicked bronchopneumonia but persisted on follow-up imaging revealing its true identity (Fig. 4.12).
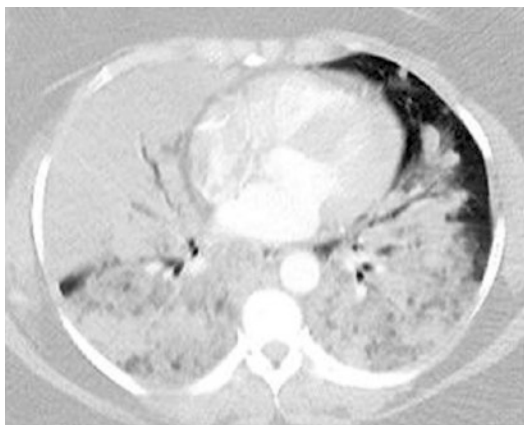
FIG. 4.12 Adenocarcinoma mimicking bronchopneumonia. This image justifies follow-up of presumed pneumonia to demonstrate resolution



FIG. 4.13  Metastatic renal calcifications

Metastatic renal calcification is not common but has a characteristic appearance on CT with dense consolidation associated with sarcoid and renal failure [24] (Fig. 4.13).

Eosinophilic pneumonia and organizing pneumonia can present with consolidation that is typically peripheral but can be bronchovascular. In eosinophilic pneumonia, the alveoli contain eosinophils in the alveoli, and the patients have ele-
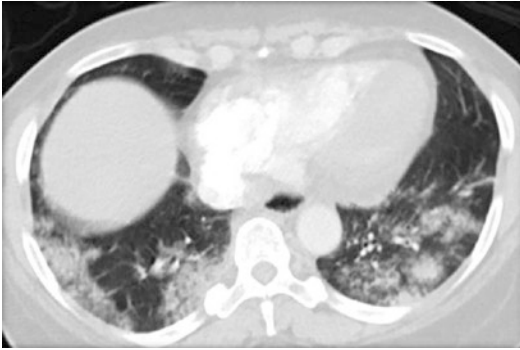
Fig. 4.14  Peripheral consolidation in an asthmatic patient consistent with eosinophilic pneumonia
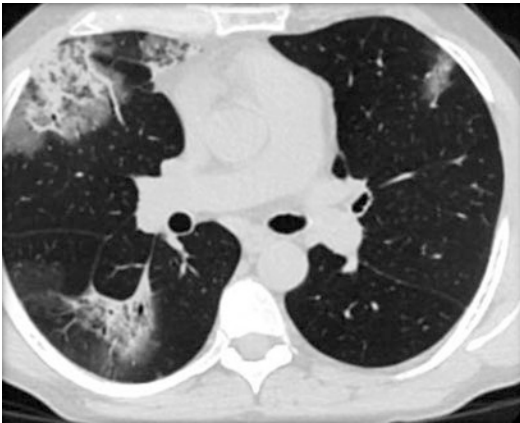


Fig. 4.15  Peripheral consolidation in a patient with positive serologies for connective tissue disease

vated IgE levels (Fig. 4.14). Organizing pneumonia is inflammation of the alveoli and can be seen in association with pneumonia or connective tissue disease or can be idiopathic. A reverse halo sign with peripheral density and central lucency may be present but is not specific for organizing pneumonia (Fig. 4.15).

## 4.2.2   Decreased Radiodensity of Alveoli

When air is trapped within the alveoli, the lung becomes less radiodense or blacker with HU less than −950 [25] (Fig. 4.16). The alveolar distension also increases the size of the secondary pulmonary lobule and ultimately the lung causing flattening of the diaphragms and increased anteroposterior dimension of the hemithorax with splaying of the ribs.

There are three main types of emphysema which are distinguished from each other by their distribution [26] (Fig. 4.17).

Centrilobular emphysema is associated with cigarette smoking and affects the center of the lung initially on cross-sectional imaging [26, 27] (Fig. 4.18). It also affects the upper lobes greater than the lower lobes and puts pressure on both sides of the trachea narrowing its transverse diameter while increasing AP measurements. This appearance has been likened to a saber sheath [28].
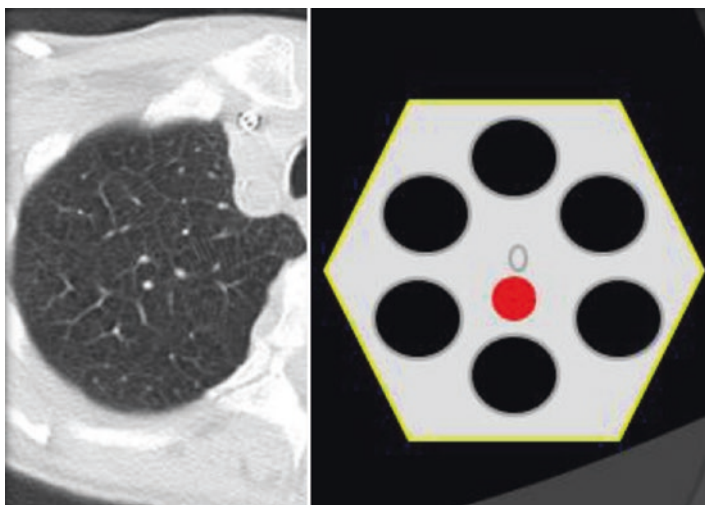


Fig. 4.16 Emphysema increases the size of the secondary pulmonary lobule and decreases HU of the lung tissue
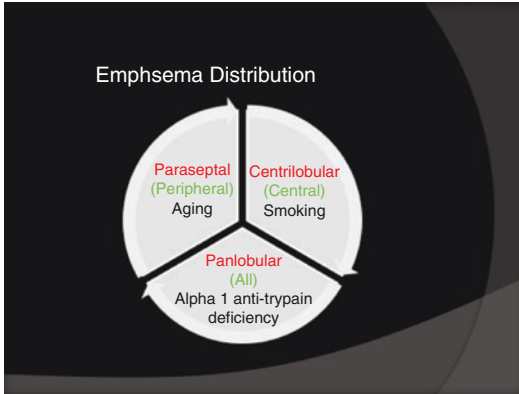
Fig. 4.17 Distribution of emphysema on CT
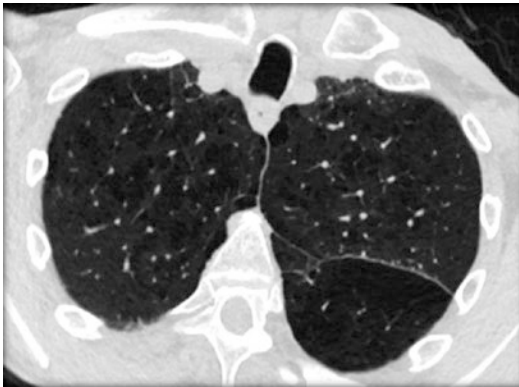


Fig. 4.18 Centrilobular emphysema

Paraseptal emphysema has been traditionally associated with aging but is really related to stiff lung parenchyma which can occur in the elderly. Paraseptal emphysema effects the peripheral SPLs because of tensile forces created

Fig. 4.19  Paraseptal emphysema affecting the peripheral SPL

between the moving ribs and the relatively rigid lung paren-
chyma [26] (Fig. 4.19). Paraseptal emphysema is one layer
thick which differentiates it from honeycombing, a periph-
eral cystic disease which must contain multiple layers of
cysts [29].

Panlobular emphysema is associated with alpha-1 anti-
trypsin deficiency and is a lower lobe-predominant emphy-
sema that is both peripheral and central, hence the name
panlobular [25–27].

Emphysema must be differentiated from cystic lung dis-
eases. In emphysema there is a dot in the center of the lucency
which represents the pulmonary artery. In cystic lung diseases,
the pulmonary lobule is not associated with the lucency.
Tuberous sclerosis is a congenital disease which develops lung
cysts and subcortical tubers in the brain (Fig. 4.20). It is associ-
ated with seizures and adenoma sebaceum [30].
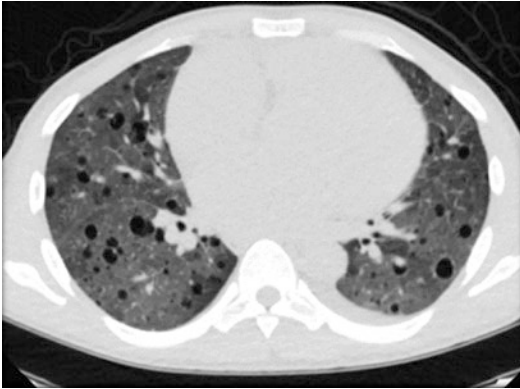
FIG. 4.20 Tuberous sclerosis with pulmonary cysts which must be differentiated from emphysema
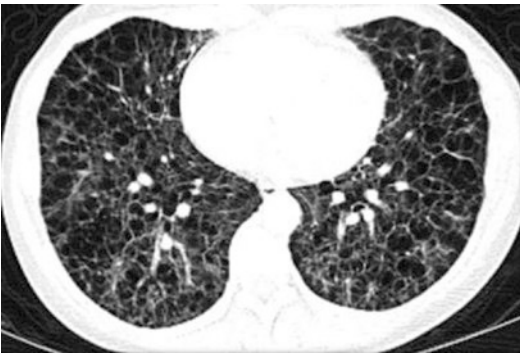


FIG. 4.21 Advanced lymphangioleiomyomatosis with cysts throughout the lung parenchyma

Lymphangioleiomyomatosis is a cystic disease of the lung which affects premenopausal women and causes cysts in the lung (Fig. 4.21). The disease is estrogen dependent and can be treated with antiestrogen medications; oophorectomy but ultimately lung transplant may be necessary [31].

Lymphocytic interstitial pneumonia is one of the rarest of the eight idiopathic interstitial pneumonias and has been seen

in association with HIV and Sjogren's disease. Cysts are seen throughout the lung parenchyma and can increase over time and put patients at risk for pneumothorax [32, 33] (Fig. 4.22).

Langerhans cell histiocytosis is a smoking-related lung disease that causes bizarre cysts and pulmonary nodules with an upper lobe predominance that spares the costophrenic angles [34] (Fig. 4.23).
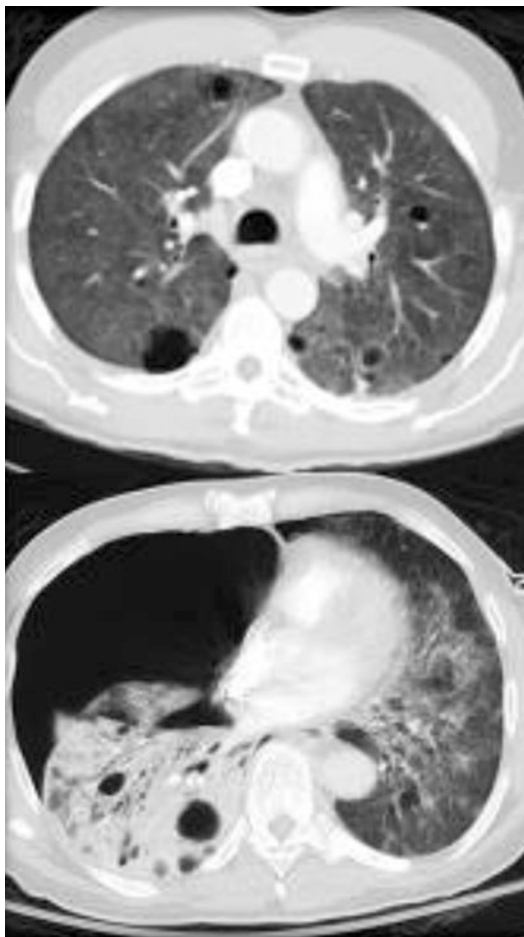


Fɪɢ. 4.22 Lymphocytic interstitial pneumonitis with cysts through-out lung parenchyma putting patient at risk for pneumothorax

So, to reiterate, a single row of peripheral cysts with a central dot is paraseptal emphysema, stacked peripheral cysts are honeycombing, and stacked cysts which are central represent cystic bronchiectasis (Fig. 4.24).



FIG. 4.23 Bizarre cysts and nodules in a patient with Langerhans cell histiocytosis
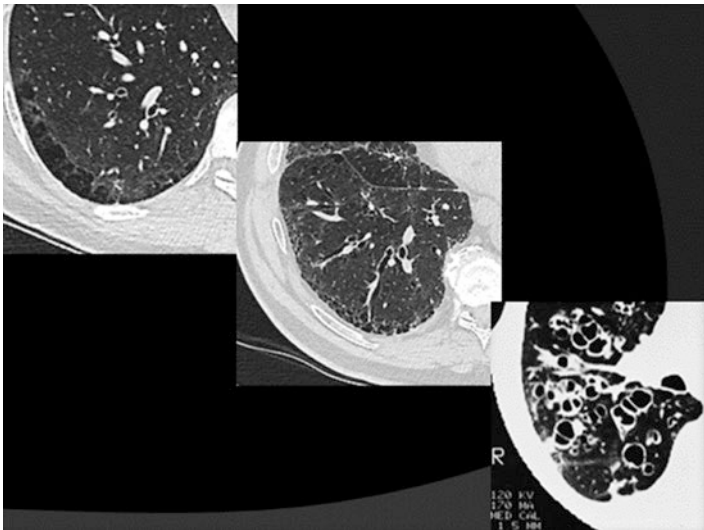


FIG. 4.24 Cystic diseases of the lung parenchyma from left to right: paraseptal emphysema, honeycombing, cystic bronchiectasis

| Diseases increasing HU > −900 | Diseases decreasing HU < −900 |
|---|---|
| Pneumonia<br>  – Lobar<br>  – Bronchopneumonia | Emphysema<br>  – Centrilobular<br>  – Paraseptal<br>  – Panlobular |
| Hemorrhage | Tuberous sclerosis |
| Edema | Lymphangioleiomyomatosis |
| Neoplasm | Lymphocytic interstitial pneumonitis |

## 4.3   The Interlobular Septa

The periphery of the secondary pulmonary lobule is outlined by the interlobular septa which are extensions from the peripheral pleura. The pulmonary veins and lymphatics travel within the interlobular septa. Diseases that affect the pulmonary veins, lymphatics, or connective tissue will cause thickening of the septa which can be identified on CT.

Previously we discussed alveolar edema that occurs with a pulmonary capillary wedge pressure of greater than 25 mmHg. If the pulmonary capillary wedge pressure is elevated between 18 and 25 mmHg, then the veins traveling in the interlobular septa become distended (Fig. 4.25). Typically, there will be associated cardiomegaly and possibly pleural effusions which will support the correct diagnosis. The thickened interlobular septa on CT correlate with "Kerley B lines" on chest X-ray [35].

Any disease that causes obstruction to flow of blood distal to the pulmonary capillaries will cause distension of the pulmonary veins. This would include aortic or mitral valve stenosis/regurgitation, left atrial mass, and pulmonary veno-occlusive disease (PVOD) where there is deposition of collagen within pulmonary veins [36, 37] (Fig. 4.26).

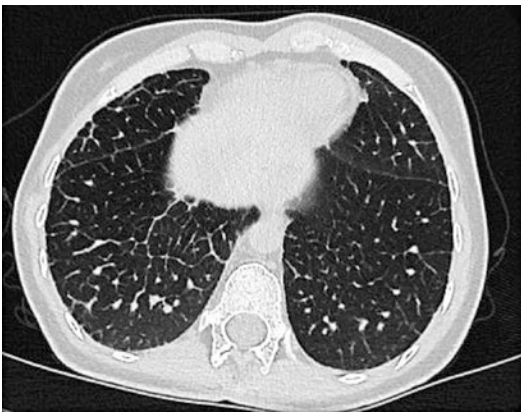FIG. 4.25  Moderate pulmonary edema with thickening of the inter-lobular septa



FIG. 4.26  Pulmonary veno-occlusive disease with interlobular septal thickening

Cancer anywhere in the body can spread to the lymphatics systemically and cause thickening of the interlobular septa which is usually bilateral. Lung cancer can directly invade the lymphatics and cause unilateral distension of the interlobular septa [38] (Figs. 4.27, 4.28, and 4.29).



FIG. 4.27  Bilateral systemic lymphangitic spread of cancer



FIG. 4.28  Lung cancer can cause unilateral lymphangitic spread by direct invasion of adjacent lymphatics

A crazy-paving pattern describes the radiologic pattern of interlobular septal thickening and ground glass opacity (Fig. 4.30). It is most frequently thought of in association with pulmonary alveolar proteinosis, a disease of middle-aged men where surfactant accumulates in the lungs. In reality it is



Fig. 4.29 Unilateral lymphangitic spread of lung cancer by direct extension



Fig. 4.30 Pulmonary alveolar proteinosis: thickened interlobular septa and ground glass opacities causing a "crazy-paving pattern" due to excess surfactant in the lung

more commonly seen with pulmonary edema, hemorrhage, and PCP as these diseases are more common.

In the examples above, the interlobular septa are distended, but the bronchus is unaffected. In the case of pulmonary fibrosis which effects the interlobular septa, the bronchus is distended which helps to differentiate fibrosis from pulmonary edema and lymphangitic spread of cancer (Fig. 4.31).

Fibrosis must be distinguished from atelectasis which can have a similar distribution in the dependent portion of the lung bases on CT. However, atelectasis is not associated with bronchiolectasis (Fig. 4.32). Dependent atelectasis reverses when the patient is positioned prone. Prone CT images should be obtained in patients who are thought to have early lung fibrosis to make sure that they do not have dependent changes.

Osteophytes are common in people over 40 years of age. The constant mechanical irritation of the lung that is caused by the osteophyte leads to lung fibrosis and even honeycombing. Osteophyte-induced fibrosis is a focal fibrosis which does not affect mortality and must be distinguished from the more diffuse fibrosis of idiopathic pulmonary fibrosis with a shortened life expectancy.



Fig. 4.31 Pulmonary fibrosis with thickened interlobular septa and dilated bronchi

Fɪɢ. 4.32  Atelectasis mimicking lung fibrosis

## 4.3.1   *ILD Causes Known and Unknown*

Interstitial lung diseases can be divided into two types: fibrosis that we know the reason for and idiopathic fibrosis whose cause is unknown. Known causes of interstitial lung disease include chronic hypersensitivity pneumonitis, asbestosis, and drug reactions [39]. There are currently eight recognized idiopathic interstitial lung diseases which include usual interstitial pneumonia (UIP), the most common one with the highest mortality. Nonspecific interstitial pneumonitis (NSIP) is associated with connective tissue disease, organizing pneumonia (OP), acute interstitial pneumonia (AIP), respiratory bronchiolitis interstitial lung disease (RB-ILD), desquamative interstitial pneumonitis (DIP), lymphocytic interstitial pneumonitis (LIP), and pleuroparenchymal fibroelastosis (PPFE) [40] (Fig. 4.33).

It is best to consider them in pairs. NSIP and UIP are considered together because they are lower lobe-predominant fibrotic diseases that often are confused with each other. COP and AIP are considered together because they manifest on CT as consolidation. COP can be peripheral or bronchovascular in its distribution. AIP resembles ARDS and is diffuse alveolar disease which is often rapidly fatal. RB-ILD and DIP are smoking-related interstitial diseases and thus

## Interstitial Lung Disease

**Known causes**

**Idiopathic**

- Hypersensitivity pneumonitis
- Asbestosis
- Drug reactions

| UIP | NSIP |
|-----|------|
| COP | AIP |
| RBILD | DIP |
| LIP | PPFE |

FIG. 4.33 Pulmonary fibrosis can be divided into two categories, those that we know the reason for and idiopathic pulmonary fibrosis



FIG. 4.34 Desquamative interstitial pneumonitis with diffuse ground glass opacity

are not truly idiopathic but considered with the others by convention. RB-ILD presents as centrilobular nodules with an upper lobe predominance, and DIP is more extensive ground glass opacity (Fig. 4.34).

The final pair, LIP and PPFE, is very rare. LIP presents with cyst in a bronchovascular distribution and is associated with Sjogren's disease and HIV (Fig. 4.35). PPFE is a very rare disease with apical pleural thickening and restrictive lung disease.
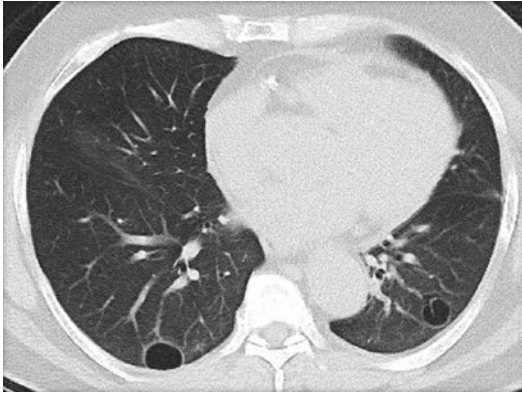
Fɪɢ. 4.35  Lymphocytic interstitial pneumonitis in patient with connective tissue disease

The cause of idiopathic pulmonary fibrosis which is the clinical disease associated with a UIP pattern radiographically and pathologically is unknown. There is an alveolar epithelial cell injury which many believe causes activation of fibroblasts and collagen deposition expanding the extracellular matrix [41, 42]. Others believe the disease is related to atelectasis [43]. Regardless of the pathophysiology of pulmonary fibrosis, the earliest findings radiographically are ground glass opacity and traction bronchiolectasis [44, 45] (Fig. 4.36).

Overtime fibrosis often continues to advance and may develop honeycomb cysts which are stacked pleural-based cysts measuring approximately 1 cm in size and sharing walls with each other. The appearance resembles the stone fences used to separate farms. The fibrosis of UIP is heterogeneous and increases in extent on follow-up imaging [46, 47]. Honeycombing is different from traction bronchiectasis in that the holes are larger (approximately 1 cm in size) and traction bronchiectasis does not typically touch pleural surface (Fig. 4.37).

The American Thoracic Society has provided guidelines for the confident diagnosis of UIP on CT scan which avoids a biopsy in patients who often develop exacerbations following
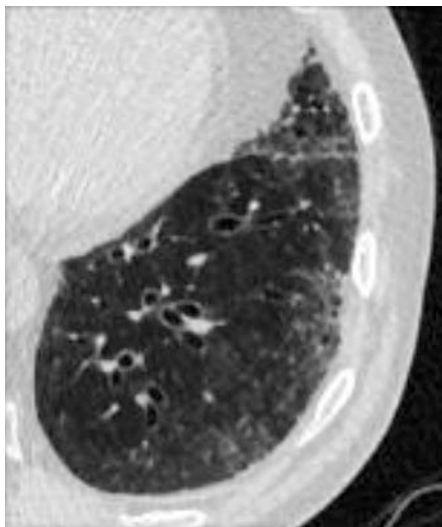
FIG. 4.36 Early UIP pattern with subpleural ground glass opacity and traction bronchiolectasis
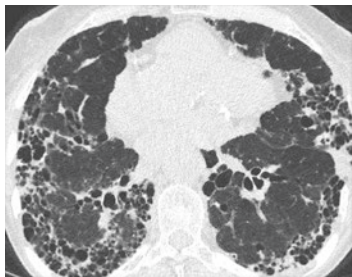


FIG. 4.37 Advanced UIP pattern with honeycomb cysts that touch the pleura and are stacked just like the stone wall touches the land and the stones are stacked

ATS Guidelines for UIP
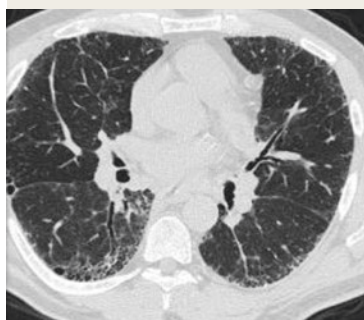
- Subpleural basilar predominant fibrosis
- Reticulations
- Honeycombing
- Absence of features that would suggest and alternative diagnosis

Fig. 4.38  ATS guidelines for the radiologic diagnosis of UIP

anesthesiology. They require the identification of subpleural, basilar-predominant fibrosis with reticulations and honeycombing and absence of features that would suggest an alternative diagnosis [48] (Fig. 4.38).

In order to remember the features that might suggest an alternative diagnosis, we have created a pneumonic. It "CANNOT B" UIP if these features are present. The features include consolidation; if there is consolidation, consider organizing pneumonia or AIP. Air trapping is most commonly seen with chronic hypersensitivity pneumonitis. Nodules can be seen with hypersensitivity pneumonitis and sarcoid. Nonsolid or ground glass opacity is associated with RB-ILD and DIP. O represents cysts as can be seen with LIP. T is for top, fibrosis that is upper lobe predominant includes chronic hypersensitivity pneumonitis (CHP) and stage 4 sarcoidosis (S4). B is for bronchovascular bundles, diseases which are located along bronchovascular bundles including CHP, NSIP, and S4 (Figs. 4.39 and 4.40).

If there is subpleural basilar-predominant fibrosis without honeycombing, the ATS guidelines use the term "possible

Absence of features that would suggest
and alternative diagnosis-CANNOT B UIP

- Consoldation-AIP, COP
- Airtrapping-CHP
- Nodules-CHP, Sarcold
- Nonsolid (ground glass)-RBILD, DIP
- O (cysts)-LIP
- Top-CHP, Sarcoid
- Bronchovascular-CHP, NSIP, Sarcold

Fig. 4.39  Features that go against UIP as the diagnosis

UIP" pattern radiographically. These patients currently may need to have a biopsy for confident diagnosis and are not eligible for treatment with anti-fibrotic medications. A recent white paper published by the Fleischner Society has advocated changing this terminology to "probable UIP" pattern which would avoid biopsy and allow treatment with new anti-fibrotic medications [49] (Fig. 4.41).

Risk factors for UIP overlap with risk factors for lung cancer, and so it is important to look for lung cancer in patients with pulmonary fibrosis (Fig. 4.42).

Lower lobe-predominant fibrosis is usually UIP or NSIP. In order to differentiate these two entities, remember that UIP hugs the periphery of the lung and in NSIP the fibrosis travels along the bronchovascular bundles. There is often peripheral sparing with NSIP, but absence of the finding does not preclude the diagnosis. The real question is why does one idiopathic fibrosis affect the periphery and the other avoid the periphery. The answer to this question will reveal the cause of these idiopathic diseases (Fig. 4.43).

There are two main types of NSIP, cellular and fibrotic. Cellular NSIP has more ground glass opacity and is more likely to respond to steroids (Fig. 4.44).

Fibrotic NSIP has less ground glass and will likely remain fixed if steroids are prescribed. More frequently the pathology reveals a combination of the two (Fig. 4.45).

Consolidation

Air Trapping

Nodules

Nonsolid or Groundglass

Cysts

Top

Bronchovascular
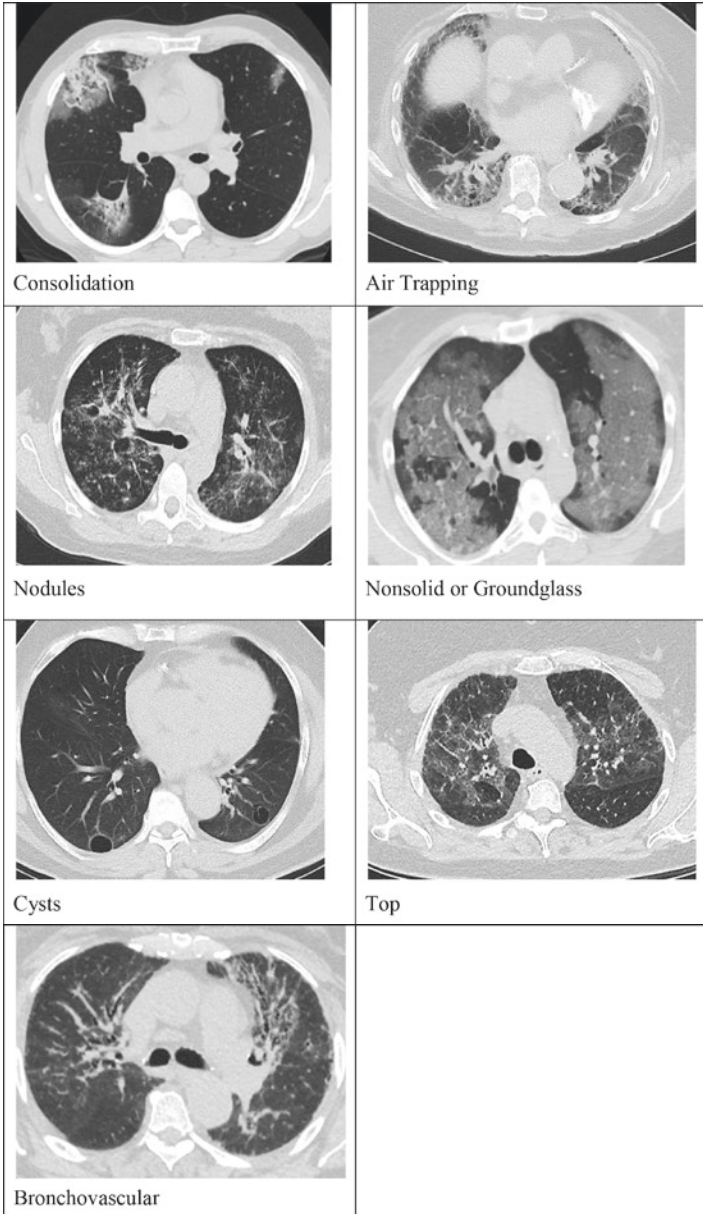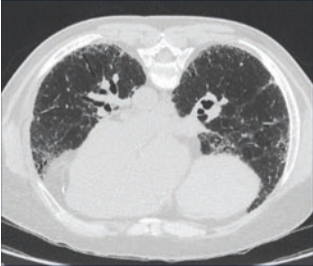
Fig. 4.40  Features that go against UIP as the diagnosis

FIG. 4.41 Subpleural basilar-predominant fibrosis without honeycombing is a "possible UIP" pattern by ATS criteria
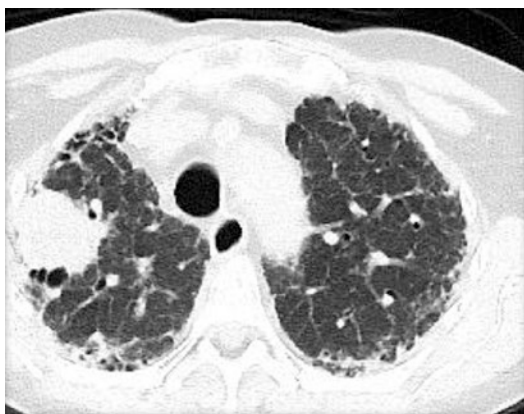


FIG. 4.42  Lung cancer in a patient with pulmonary fibrosis

Patients with connective tissue disease may present with organizing pneumonia early on that resolves and reoccurs as an NSIP pattern. Organizing pneumonia, one of the eight idiopathic interstitial pneumonias, causes shortness of breath and can be confused with bacterial pneumonia; however it does not respond to antibiotics. The most characteristic pattern is
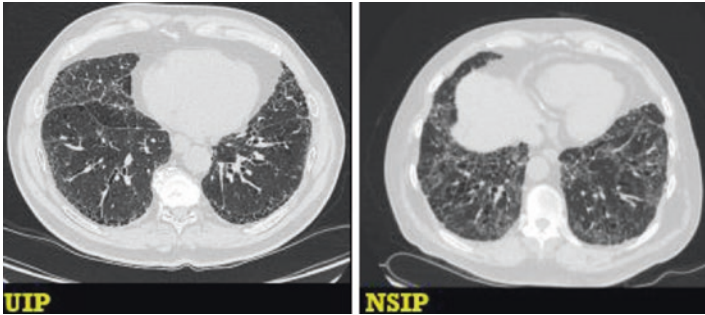
Fɪɢ. 4.43   Differential diagnosis of UIP



Fɪɢ. 4.44   Cellular NSIP
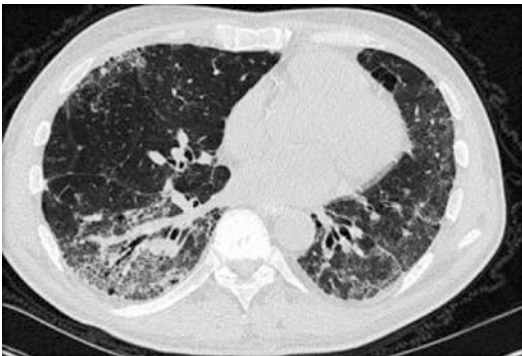


Fɪɢ. 4.45   Fibrotic NSIP

peripheral opacities; however the opacities may also follow the bronchovascular bundles. The atoll sign or reverse halo sign refers to the appearance of organizing pneumonia when the periphery is dense and the center is lucent [50] (Fig. 4.46).

Sometimes organizing pneumonia occurs in combination with an NSIP pattern giving a characteristic lower lobe-predominant fibrosis that appears lacey. It is associated with anti-synthetase syndrome (Fig. 4.47).



Fig. 4.46  Organizing pneumonia with "reverse halo sign"
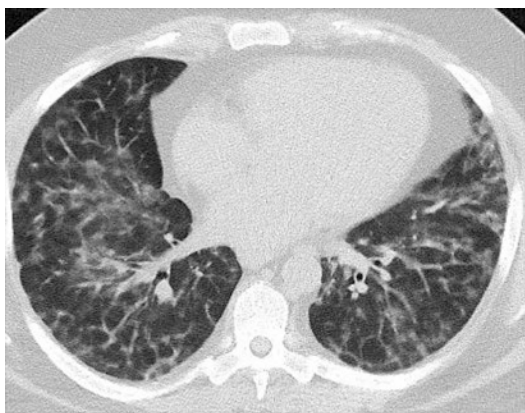


Fig. 4.47  Features of organizing pneumonia and NSIP in a patient with anti-synthetase syndrome

CHP is a not uncommon cause for fibrosis of the lung. It is caused by inhalation of an antigen which irritates the lung parenchyma. Long-term exposure can lead to irreversible fibrosis and even honeycombing. Early recognition of the disease is key to removing the patient from the offending antigen to prevent disease progression. A common form of CHP is bird fancier's disease caused by exposure to the antigen on bird feces. The fibrosis is bronchovascular which makes sense since the antigen is inhaled [51] (Fig. 4.48).

Air trapping is also a key feature of CHP which helps to differentiate it from other types of fibrosis. The air trapping causes a pattern of fibrosis that has been labeled the "headcheese sign" [51] (Fig. 4.49).

In contrast to CHP which tends to affect the anterior aspect of the upper lobe, S4 affects the posterior aspect of the upper lobe pulling the right upper lobe bronchus posterior and increasing the angle between the right upper lobe bronchus and a line drawn between the sternum and vertebrae (Fig. 4.50).
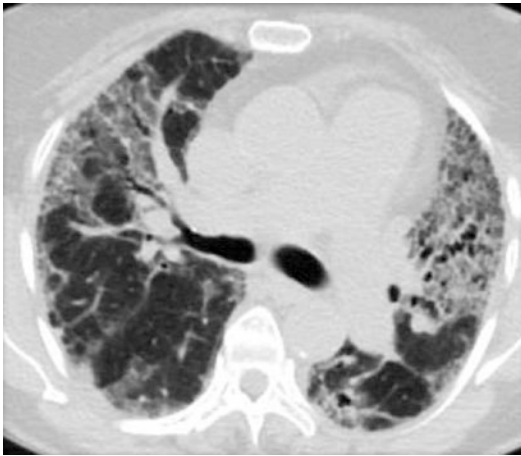


Fig. 4.48 CHP with bronchovascular distribution

Fig. 4.49 Air trapping with CHP
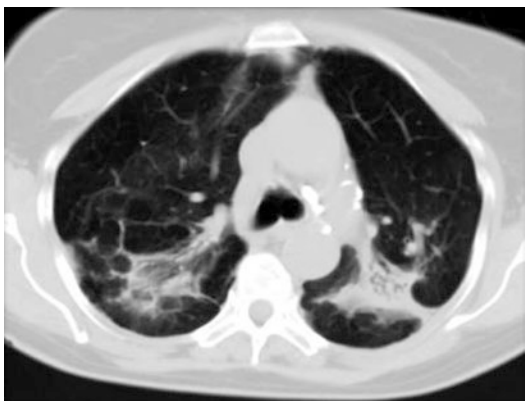


Fig. 4.50 Stage 4 sarcoid distorting right upper lobe bronchus
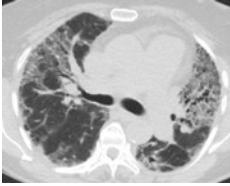
| *Upper lobe-predominant fibrosis: CHP* | *Upper lobe-predominant fibrosis: Sarcoid* |
|---|---|
|  |  |
| • Bronchovascular<br>• Air trapping<br>• Heterogeneous | • Bronchovascular<br>• Heterogeneous<br>• Posterior upper lobe |
| *Lower lobe-predominant fibrosis: UIP* | *Lower lobe-predominant fibrosis: NSIP* |
|  |  |
| • Subpleural<br>• Basilar predominant<br>• Heterogeneous | • Homogeneous<br>• Bronchovascular<br>• Supleural sparing |
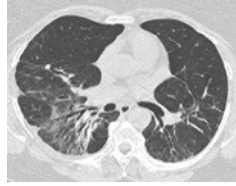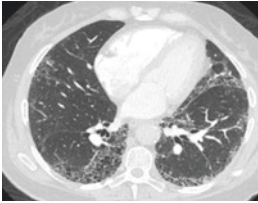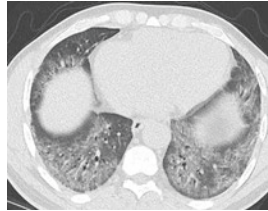
## 4.4   The Pulmonary Artery

Heterogeneous attenuation of the lung parenchyma called "mosaic attenuation" is a not infrequent finding on chest CT scans which can reflect pulmonary artery hypertension

(PAH) [52]. When faced with the pattern of mosaic attenuation, the first thing to do is decide if the vessels in the darker areas are smaller than the vessels in the lighter areas. If they are then the differential diagnosis is PAH or small airways disease. Next perform an expiratory CT scan of the chest, and if the heterogeneity becomes more pronounced, then the cause is air trapping from small airways disease; if not then the pathology is PAH. Sometimes it is unnecessary to perform an expiratory CT because ancillary findings of a large pulmonary artery or thick-walled bronchi help determine the correct diagnosis. If the vessels are normal in the dark area, then the white area represents ground glass opacity, a nonspecific finding which can be seen with infection, edema, or hemorrhage as described earlier (Fig. 4.51).

The main pulmonary artery should be measured on the image where both right and left pulmonary artery are identified. Measure the maximum transverse diameter, and if greater than 3.3 cm, it is 95% specific for PAH [53]. If the ratio of the PA to the aorta is greater than 1, that also supports PAH, and further evaluation should be performed with echocardiogram (Fig. 4.52).
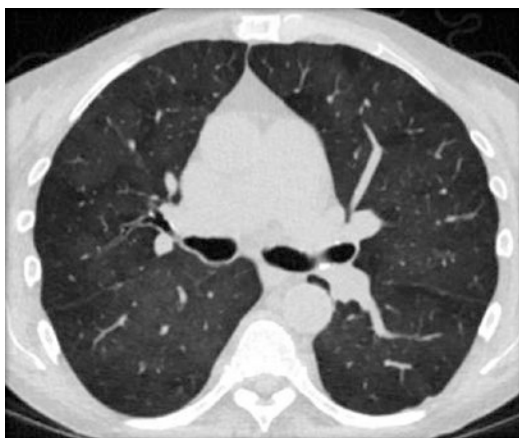


Fig. 4.51 Evaluation of mosaic attenuation: notice that the vessels are smaller in the darker areas, and so the diagnosis is pulmonary artery hypertension or small airways disease

Fɪɢ. 4.52 Pulmonary artery hypertension on chest CT



Fɪɢ. 4.53 Optimal opacification of the pulmonary artery for a PE study with HU above 250

CTA is currently the gold standard for the diagnosis of pulmonary embolism. In order to identify a pulmonary embolism, there needs to be excellent opacification of the pulmonary artery which requires a combination of IV access in the antecubital vein, high flow rates of contrast at 4 cc per second, and timing so that the contrast is in the pulmonary circulation and has not reached the aorta. CT scanners are programmed to begin scanning from the lung bases superiorly when the Hounsfield units of the pulmonary artery reach 100 (Fig. 4.53). This is so that contrast is optimal by the time

scan reaches the pulmonary artery. If there is not enough contrast in the pulmonary artery, an embolus will likely be missed.

Artifacts can mimic pulmonary artery emboli and include mucous in a bronchus. Motion artifact prevents the accurate diagnosis as well. It is important to follow a clot in a vessel back toward the heart to make sure that the clot is in an artery and not a vein. Resist the temptation to call a pulmonary embolism at a branch point of a pulmonary artery or on a single image, it should be seen on multiple slices.

Westermark's sign is peripheral oligemia which can occur with a large central pulmonary embolism as demonstrated on the image below. Notice the paucity of vessels in the right hemithorax in this person with chest pain which led to the correct diagnosis. Additional signs of pulmonary embolism include a Hampton's hump which is a peripheral wedge-shaped density representing infarcted lung that over time decreases in size and ultimately resolves differentiating it from peripheral tumor. Only 15% of emboli lead to infarct due to the dual pulmonary blood supply [54].

Pulmonary emboli can be occlusive or nonocclusive, acute, or chronic. Chronic pulmonary emboli are displaced peripherally within the vessel. When an embolus crosses from one pulmonary artery to another, it is called a saddle embolus (Fig. 4.54).

Saddle pulmonary emboli are typically associated with a large clot burden, and as such they can put increased strain on the right heart. This is demonstrated on CT by observing the interventricular septum which is typically bowed to the right, straighten, or bowed to the left (Fig. 4.55).

Metastatic disease is a systemic process that reaches the lungs via the pulmonary arteries, and as such metastatic pulmonary nodules are typically located at the ends of pulmonary arteries. The nodules are well circumscribed and variable in size with lower lobe predominance (Fig. 4.56).

Miliary TB is systemic spread of infection, and as such it is also located at the end of blood vessels. The nodules of mili-
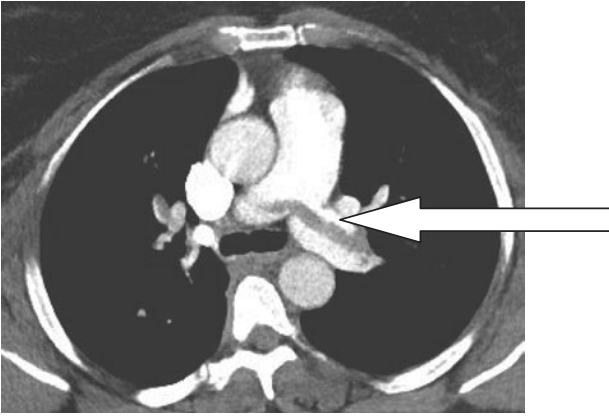
Fɪɢ. 4.54  Saddle pulmonary embolus
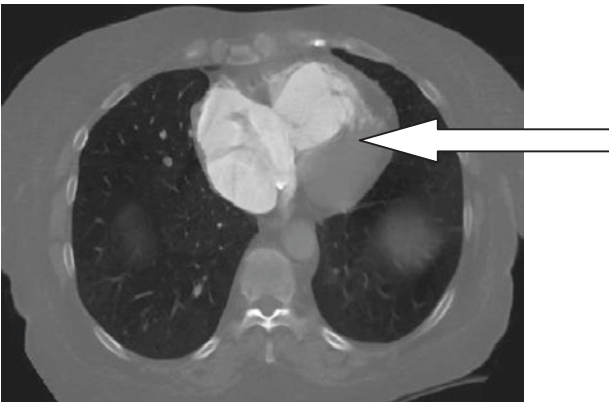


Fɪɢ. 4.55  Right heart strain with bowing of the interventricular sep-
tum to the left

tary TB are very small and were named after millet seed a
kind of bird feed.

Metastatic thyroid cancer can have small nodules and is in
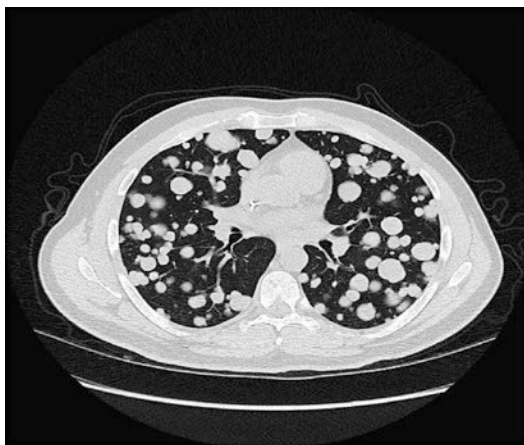the differential diagnosis (Fig. 4.57).

Fig. 4.56  Metastases at the end of blood vessels



Fig. 4.57  Metastatic thyroid nodules are millimeter in size

## References

1. Mata J, Cáceres J, Alegret X, Coscojuela P, De Marcos JA. Imaging of the azygos lobe: normal anatomy and variations. AJR Am J Roentgenol. 1991;156(5):931–7.
2. Seiber W, Karcara N, Pant P. Pulmonary azygos lobe—an anatomical variant. Kathmandu Univ Med J. 2014;46(2):151–2.
3. Miller WS. The lung. Springfield, IL: Thomas; 1947. p. 39–42.

4. Richard Webb W. Thin-section CT of the secondary pulmonary lobule: anatomy and the image—the 2004 Fleischner lecture. Radiology. 2006;239(2):322–38.

5. Weibel ER. Looking into the lung: what can it tell us? AJR Am J Roentgenol. 1979;133:1021–31.

6. Heitzman ER, Markarian B, Berger I, Dailey E. The secondary pulmonary lobule: a practical concept for interpretation of chest radiographs. I. Roentgen anatomy of the normal secondary pulmonary lobule. Radiology. 1969;93:507–12.

7. Osborne DR, Effmann EL, Hedlund LW. Postnatal growth and size of the pulmonary acinus and secondary lobule in man. AJR Am J Roentgenol. 1983;140:449–54.

8. Reid L, Simon G. The peripheral pattern in the normal bronchogram and its relation to peripheral pulmonary anatomy. Thorax. 1958;13:103–9.

9. Ochs M, Nyengaard JR, Jung A, Knudsen L, Voigt M, Wahlers T, Richter J, Gundersen HJG. The number of alveoli in the human lung. Am J Respir Crit Care Med. 2004;169(1):120–4.

10. Itoh H, Murata K, Konishi J, Nishimura K, Kitaichi M, Izumi T. Diffuse lung disease: pathologic basis for the high-resolution computed tomography findings. J Thorac Imaging. 1993;8:176–88.

11. Hounsfield GN. Computed medical imaging. Nobel lecture, December 8, 1979. J Comput Assist Tomogr. 1980;4(5):665–74.

12. Zach J, Newell J, Schroeder J, et al. Quantitative CT of the lungs and airways in healthy non-smoking adults. Invest Radiol. 2012;47(10):596–602.

13. Friedman PJ. Imaging studies in emphysema. Proc Am Thorac Soc. 2008;5(4):494–500.

14. Shin KE, Chung MJ, Jung MP, Choe BK, Lee KS. Quantitative computed tomographic indexes in diffuse interstitial lung disease: correlation with physiologic tests and computed tomography visual scores. J Comput Assist Tomogr. 2011;35(2):266–71.

15. Austin JH, Müller NL, Friedman PJ, et al. Glossary of terms for CT of the lungs: recommendations of the Nomenclature Committee of the Fleischner Society. Radiology. 1996;200:37–1.

16. Marten K, Schnyder P, Schirg E, et al. Pattern-based differential diagnosis in pulmonary vasculitis using volumetric CT. AJR Am J Roentgenol. 2005;184(3):720–33.

17. Ficker JH, Brückl WM, Suc J, Geise A. Haemoptysis: Intensive care management of pulmonary hemorrhage. Internist (Berl). 2017;58(3):218–25.

18. Gluecker T, Capasso P, Schnyder P, Gudinchet F, Schaller M-D, Revelly J-P, Chiolero R, Vock P, Wicky S. Clinical and radiologic features of pulmonary edema. Radiographics. 1999;19(6):1507–31.

19. Baik JH, Ahn MI, Park YA, Park SH. High resolution CT findings of re-expansion pulmonary edema. Korean J Radiol. 2010;11:164–8.

20. Beigelman-Aubry C, Godet C, Caumes E. Lung infections: the radiologist's perspective. Diagn Interv Imaging. 2012;93(6):431–40.

21. Algin O, Gökalp G, Topal U. Signs in chest imaging. Diagn Interv Radiol. 2011;17(1):18–29.

22. Gharib AM, Stern EJ. Radiology of pneumonia. Med Clin North Am. 2001;85(6):1461–91.

23. Patsios D, Roberts HC, Paul NS, Chung T, Herman SJ, Pereira A, Weisbrod G. Pictorial review of the many faces of bronchioloalveolar cell carcinoma. Br J Radiol. 2007;80(960):1015–23.

24. Walter JM, Stanley M, Singer BD. Metastatic pulmonary calcification and end-stage renal disease. Cleve Clin J Med. 2017;84(9):668–9.

25. Gietema HA, Muller NL, Fauerbach PV, Sharma S, Edwards LD, Camp PG, Coxson HO. Quantifying the extent of emphysema: factors associated with radiologists' estimations and quantitative indices of emphysema severity using the eclipse cohort. Acad Radiol. 2011;18:661–71.

26. Smith BM, Austin JH, Newell JD Jr, D'Souza BM, Rozenshtein A, Hoffman EA, Ahmed F, Barr RG. Pulmonary emphysema subtypes on computed tomography: the MESA COPD study. Am J Med. 2014;127(1):94.e7–23.

27. Hogg JC. Pathophysiology of airflow limitation in chronic obstructive pulmonary disease. Lancet. 2004;364:709–21.

28. Tunsupon P, Dhillon SS, Harris K, Alraiyes AH. Saber-sheath trachea in a patient with severe COPD. BMJ Case Rep. 2016;2016. https://doi.org/10.1136/bcr-2016-214648.

29. Hansell DM, Bankier AA, MacMahon H, McLoud TC, Müller NL, Remy J. Fleischner society: glossary of terms for thoracic imaging. Radiology. 2008;246(3):697–722.

30. Baskin HJ Jr. The pathogenesis and imaging of the tuberous sclerosis complex. Pediatr Radiol. 2008;38:936.

31. Ferrans VJ, Yu ZX, Nelson WK, Valencia JC, Tatsuguchi A, Avila NA, et al. Lymphangioleiomyomatosis (LAM): a review of clinical and morphological features. J Nihon Med Sch. 2000;67(5):311–29.

32. Zar HJ. Chronic lung disease in human immunodeficiency virus (HIV) infected children. Pediatr Pulmonol. 2008;43(1):1–10.

33. Tokuyasu H, Watanabe E, Okazaki R, Kawasaki Y, Kikuchi R, Isowa N, et al. Sjögren's syndrome with multiple bullae caused by lymphocytic interstitial pneumonia. Lung. 2007;185(3):187–8.

34. Girschikofsky M, Arico M, Castillo D, et al. Management of adult patients with Langerhans cell histiocytosis: recommendations from an expert panel on behalf of Euro-Histio-Net. Orphanet J Rare Dis. 2013;8:72.

35. Sekar T, Swan KG, Vietrogoski RA. A beeline through Sir Peter James Kerley's life. AJR Am J Roentgenol. 2011;196(4):W375–9.

36. Morgan-Parkers JH. Metastases: mechanisms, pathways, and cascades. Am J Radiol. 1995;164:1075–82.

37. Prakash P, Kaira MK, Sharma A, Shepard JA, Digumarthy SR. FDG PET/CT in assessment of pulmonary lymphangitic carcinomatosis. AJR Am J Roentgenol. 2010;194(1):231–6.

38. Herold CJ, Bankier AA, Fleishmann D. Lung metastases. Eur Radiol. 1996;6:596.

39. Kebbe J, Abdo T. Interstitial lung disease: the diagnostic role of bronchoscopy. J Thorac Dis. 2017;9(Suppl 10):S996–S1010.

40. Travis WD, Costabel U, Hansell DM, King TE Jr, Lynch DA, Nicholson AG, et al. An Official American Thoracic Society/European Respiratory Society statement: update of the international multidisciplinary classification of the idiopathic interstitial pneumonias. Am J Respir Crit Care Med. 2013;188(6):733–48.

41. Bagnato G, Harari S. Cellular interactions in the pathogenesis of interstitial lung diseases. Eur Respir Soc. 2015;24(135):102–14.

42. Urushiyama H, Terasaki Y, Nagasaka S, Terasaki M, Kunugi S, Nagase T, Fukuda Y, Shimizu A. Role of α1 and α2 chains of type IV collagen in early fibrotic lesions of idiopathic interstitial pneumonias and migration of lung fibroblasts. Lab Invest. 2015;95(8):872–85.

43. Todd NW, Atamas SP, Luzina IG, Galvin JR. Permanent alveolar collapse is the predominant mechanism in idiopathic pulmonary fibrosis. Expert Rev Respir Med. 2015;9(4):411–8. https://doi.org/10.1586/17476348.2015.1067609.

44. Salvatore M, Henschke CI, Yip R, Jacobi A, Eber C, Padilla M, Knoll A, Yankelevitz D. JOURNAL CLUB: evidence of interstitial lung disease on low-dose chest CT images: prevalence, patterns, and progression. AJR Am J Roentgenol. 2016;2016(3):487–94.

45. Miller WT, Shah RM. Isolated diffuse ground-glass opacity in thoracic CT: causes and clinical presentations. Chest Imaging. 2005;184(2):613–22.
46. Piciucchi S, Tomassetti S, Ravaglia C, Gurioli C, Gurioli C, Dubini A, Carloni A, Chilosi M, Colby TV, Poletti V. From "traction bronchiectasis" to honeycombing in idiopathic pulmonary fibrosis: a spectrum of bronchiolar remodeling also in radiology? BMC Pulm Med. 2016;16(1):87.
47. Arakawa H, Honma K. Honeycomb lung: history and current concepts. AJR Am J Roentgenol. 2011;196:773–82.
48. Raghu G, Collard HR, et al. An official ATS/ERS/JRS/ALAT statement: idiopathic pulmonary fibrosis: evidence-based guidelines for diagnosis and management. Am J Respir Crit Care Med. 2011;183(6):788–824.
49. Lynch DA, Sverzellati N, Travis WD, Brown KK, Colby TV, Galvin JR, Goldin JG, Hansell DM, Inoue Y, Johkoh T, Nicholson AG, Knight SL, Raoof S, Richeldi L, Ryerson CJ, Ryu JH, Wells AU. Diagnostic criteria for idiopathic pulmonary fibrosis: a Fleischner Society White Paper. Lancet Respir Med. 2018;6:138–53.
50. Montesinos JJ, Laguna MA. Case 1: cryptogenic organizing pneumonia. AJR Am J Roentgenol. 1998;171(3):835. 838–9.
51. Pereira CA, Gimenez A, Kuranishi L, Storrer K. Chronic hypersensitivity pneumonitis. J Asthma Allergy. 2016;9:171–81.
52. Sherrick AD, Swensen SJ, Hartman TE. Mosaic pattern of lung attenuation on CT scans: frequency among patients with pulmonary artery hypertension of different causes. AJR Am J Roentgenol. 1997;169(1):79–82.
53. Alhamad EH, Al-boukai AA, Al-kassimi FA, et al. Prediction of pulmonary hypertension in patients with or without interstitial lung disease: reliability of CT findings. Radiology. 2011;260(3):875–83.
54. Sreenivasan S, Bennett S, Parfitt VJ. Images in cardiovascular medicine. Westermark's and Palla's signs in acute pulmonary embolism. Circulation. 2007;115:e211.

# Chapter 5
# Lung Nodules

- *Is it benign?*
- *Is it lung cancer?*
- *Is it metastatic disease?*
- *Is it pleural disease?*

## 5.1   Non-cancerous Lung Nodules

The most common indication for CT scan of the chest is evaluation of pulmonary nodules. The task is difficult because small nodules can look like blood vessels, and in order to differentiate the two, it is necessary to scroll through the images and note that the nodule is discrete, but a vessel is continuous. Previously chest CT scans used 10 mm collimation so little detail was visualized. Collimation is the thickness of the axial image. Overtime the collimation of CT images has decreased, allowing for increased resolution of nodules. Currently 1 mm images to evaluate the lung parenchyma should be the standard of care. One millimeter collimation generates many

87

more images and requires a greater amount of time for careful review (Figs. 5.1 and 5.2).

Maximum intensity projection (MIP) images are beneficial. MIP images display high attenuation structures preferentially and allow improved visualization of small nodules [1] (Fig. 5.3).

A nodule is defined by the Fleischner Society as "small, approximately spherical, circumscribed focus of abnormal tissue" and the radiologic definition as "round opacity, at least moderately well marginated and no greater than 3 cm in maximum diameter." The term mass is reserved for nodules that measure 3 cm or greater in size. In 2005 the Fleischner
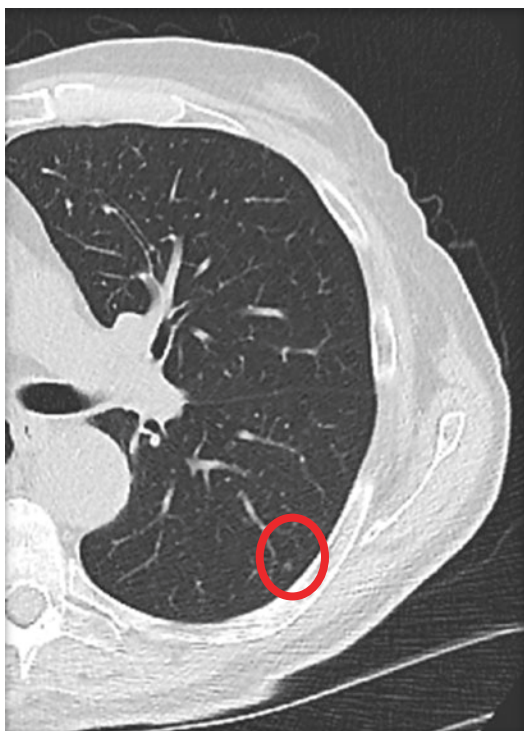


Fig. 5.1  2.5 mm slice thickness (collimation) shows an ill-defined 2 mm nodule in the left lower lobe
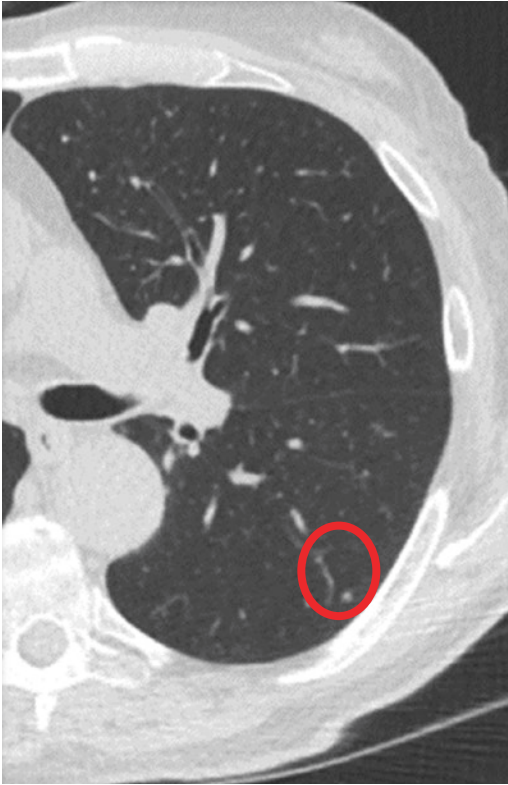
Fɪɢ. 5.2  1 mm slice thickness (collimation) shows the same 2 mm left lower lobe nodule, but now its margins are well defined, allowing for more precise measurement and characterization

Society provided guidelines for the follow-up of solid pulmonary nodules that addressed the size of the nodule and the patient's risk of cancer with the ultimate goal to limit radiation exposure and diagnose cancer early [2]. Central, laminar, or diffuse calcifications support a benign diagnosis and do not require routine follow-up [3] (Fig. 5.4).

Fat density is most consistent with a benign hamartoma [4] (Fig. 5.5).
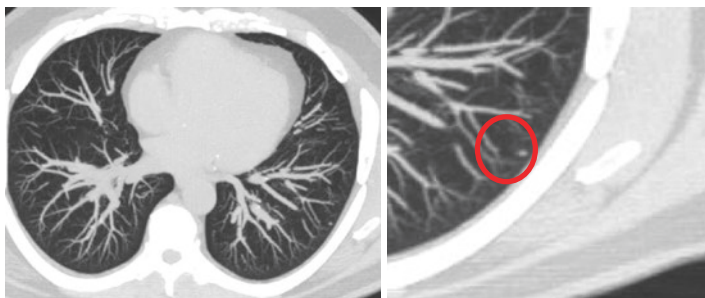
Fig. 5.3 MIP image helps you to clearly distinguish a small nodule from a blood vessel



Fig. 5.4 Central calcification in a calcified granuloma

There are many causes for pulmonary nodules. In patients with sarcoidosis, aspergillomas can form in pre-existing cavities. The hallmarks of aspergillomas are that they should move within the cavity to the dependent portion as the patient is turned. The appearance is very characteristic and additional imaging is rarely required (Fig. 5.6).

Invasive aspergillosis occurs in neutropenic patients and has a classic "halo" of ground glass opacity surrounding the nodule which represents hemorrhage (Fig. 5.7).

FIG. 5.5  Fat in a hamartoma
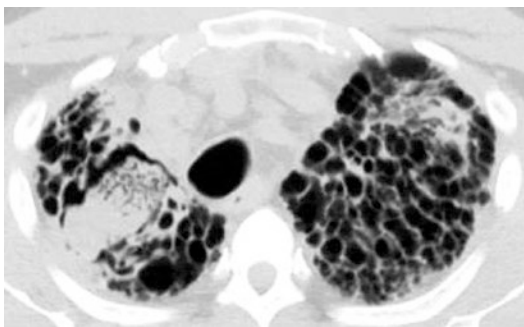


FIG. 5.6  Aspergilloma in patient with sarcoidosis
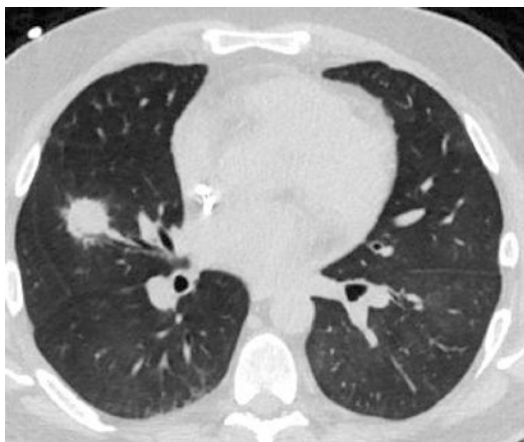
Fɪɢ. 5.7  Invasive aspergillosis with "halo"



Fɪɢ. 5.8  Semi-invasive aspergillosis with cavitating nodules

Semi-invasive aspergillosis is seen as the neutropenic patient regains their immune system and the nodule is cavitary as seen in the figure [5] (Fig. 5.8).

The differential diagnosis for cavitating nodules includes infection or neoplasm. If the cavity wall is extremely thin (<5 mm), infection is more likely. If the cavity is thick-walled
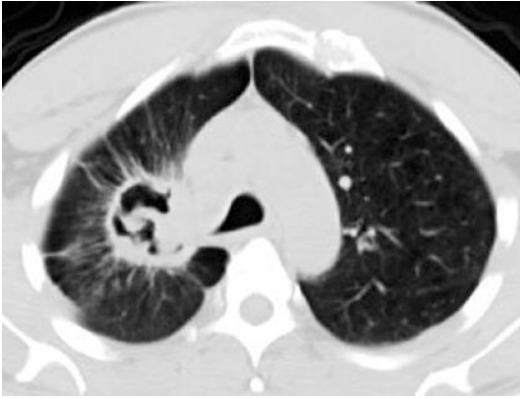
Fɪɢ. 5.9 Cavitary lesion favoring neoplasm because of spiculated margin

(>15 mm), neoplasm is more likely. Between 5 and 10 mm wall thickness is indeterminate (Fig. 5.9).

Aberrant pulmonary vasculature can be mistaken for a pulmonary nodule as occurred on this patient's chest X-ray which ultimately was an anonymous draining vein in a patient with hypogenetic right lung as part of Scimitar syndrome [6] (Fig. 5.10).

Arteriovenous malformations can appear as nodules. The characteristic feeding artery and draining vein are pathognomonic (Fig. 5.11).

Triangular nodules adjacent to fissures are most commonly intraparenchymal lymph nodes. They are triangular in shape because they occupy the corners of hexagonal-shaped secondary pulmonary lobules [7] (Fig. 5.12).

Stage 2 and 3 sarcoid can present with multiple pulmonary nodules in a perilymphatic distribution that studs the pleura and fissures. In Stage 2 the pulmonary nodules are accompanied by lymphadenopathy but not in Stage 3 (Fig. 5.13).

Amyloid can cause multiple randomly distributed pulmonary nodules which can calcify but the size is larger than miliary TB and sarcoid (Fig. 5.14).
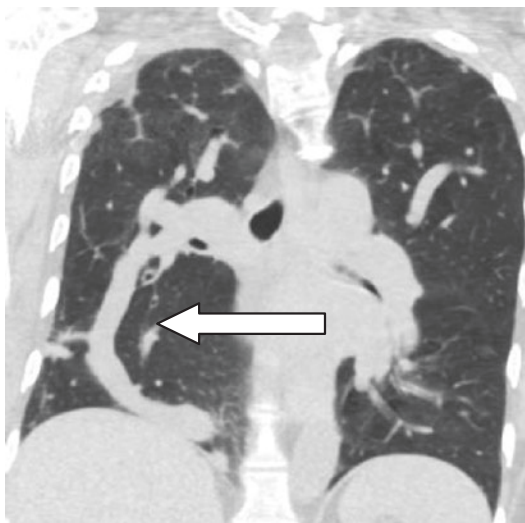
FIG. 5.10 Coronal CT image demonstrates anomalous draining pulmonary vein into the IVC giving an appearance which is likened to a scimitar (arrow)



FIG. 5.11 Arteriovenous malformation
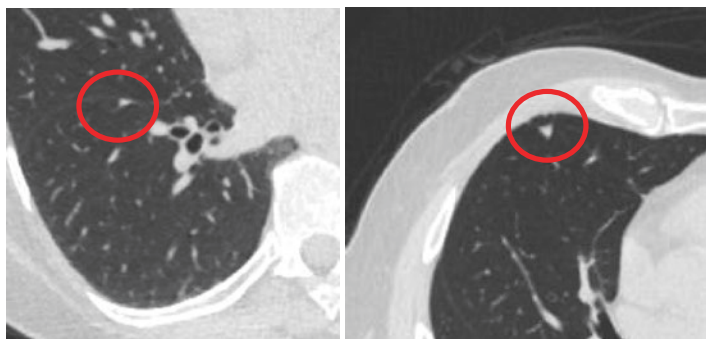
Fɪɢ. 5.12  Triangular intraparenchymal lymph nodes



Fɪɢ. 5.13  Stage 3 sarcoid with multiple pulmonary nodules

When faced with multiple pulmonary nodules, ask if the nodules are well defined or ill defined. If the nodules are ill defined, they are centrilobular nodules and represent fluid in the alveoli as can be seen with hemorrhage, edema, or pneumonia. If the nodules are well defined, ask yourself if they are predominantly peripheral and stud the fissures and pleura and follow the bronchovascular bundles or are they every-
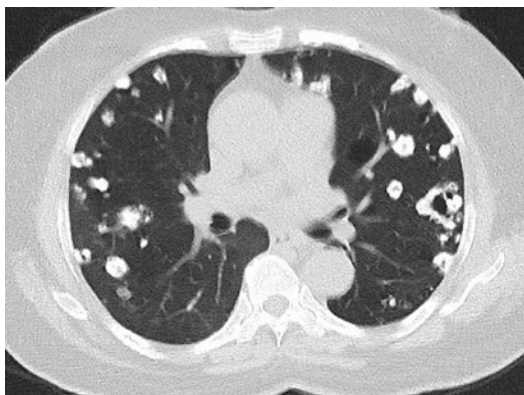
FIG. 5.14  Amyloid nodules in a random distribution
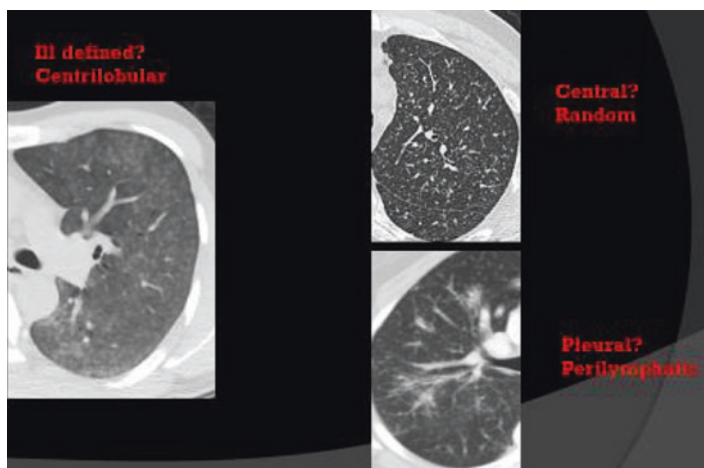


FIG. 5.15  Differentiation of multiple pulmonary nodules on CT

where. If they are everywhere, it is a random distribution as can be seen with metastases or military TB. If they are predominantly pleural based, the best diagnosis is sarcoidosis (Fig. 5.15).

## 5.2   Cancerous Lung Nodules

Nodule spiculations or pleural tail (a dominant spicule extending to the pleura) increases the likelihood of malignancy. Upper lobe nodules are more likely to be lung cancer. Nodule growth rate is important with doubling of size within 100–300 days consistent with malignancy [8] (Fig. 5.16).

Increasing number of pulmonary nodules from 1 to 4 is associated with increased risk of lung cancer, but when greater than 4 nodules, the risk decreases as they are more likely to be granulomatous disease [9].

Newer-generation CT scanners allow for routine identification of nonsolid nodules which would have been invisible on thick section, earlier-generation CT scanners. These nonsolid nodules may represent indolent neoplasm and require longer follow-up than solid nodules. Part-solid pulmonary nodules are nonsolid nodules with a solid component. When the solid component measures greater than 6 mm in size, a biopsy should be considered [10] (Figs. 5.17 and 5.18).
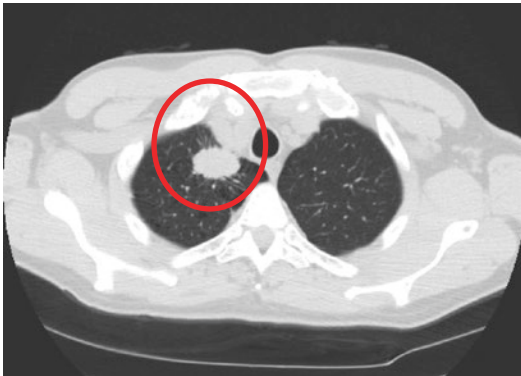


Fɪɢ. 5.ɪ6 Malignant pulmonary nodule with spiculations and a pleural tail
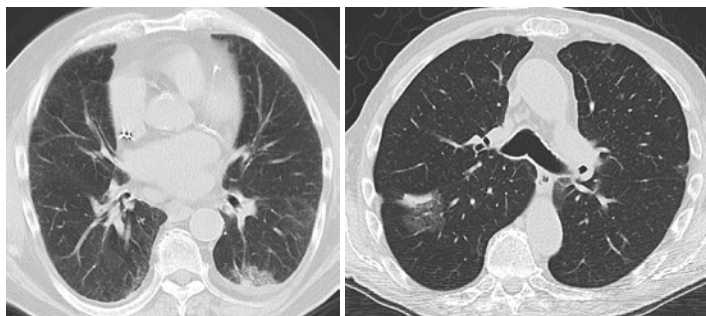
FIG. 5.17  2 Part-solid pulmonary nodules which have potential to be an indolent neoplasm



FIG. 5.18  Part-solid pulmonary nodule with new 6 mm solid component requiring biopsy

Carcinoid tumors of the lung typically originate within the airways and may be associated with adjacent bronchiectasis (Fig. 5.19). Multiple carcinoid tumors of the lung with mosaic attenuation are characteristic of diffuse idiopathic pulmonary neuroendocrine cell hyperplasia (DIPNECH) [11] (Fig. 5.20).

The Fleischner Society guidelines provide us with recommendations for the follow-up of incidentally identified solid and nonsolid pulmonary nodules [10]. Research performed
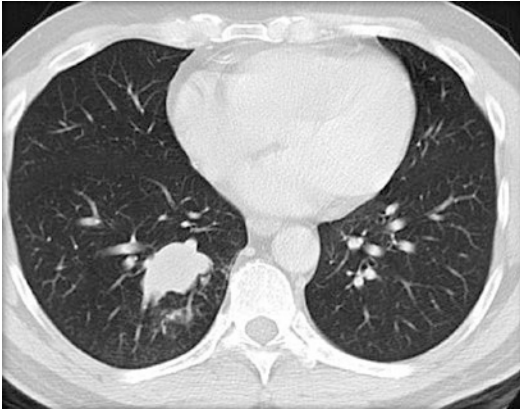
FIG. 5.19  Right lower lobe endobronchial carcinoid tumor
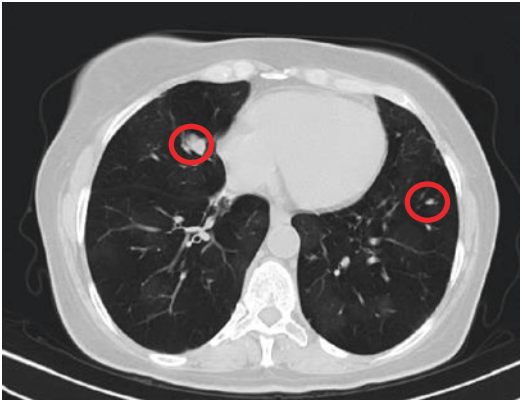


FIG. 5.20  Diffuse idiopathic pulmonary neuroendocrine cell hyperplasia (DIPNECH). Note there are multiple nodules and mosaic attenuation of the lung parenchyma

by Dr. Henschke and the IELCAP investigators have provided the optimal time frame for follow-up of nodules identified during lung cancer screening [12, 13]. Additional guidelines including the Lung-RADS guidelines assign a level of concern based on size and consistency of a nodule
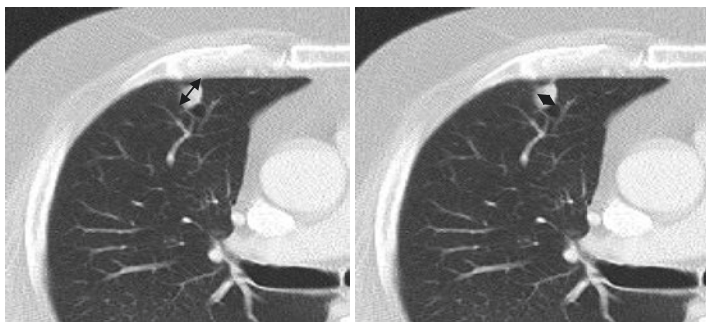
F I G. 5.21 Fleischner guidelines for measuring nodules: largest (5 mm) + perpendicular (3 mm)/2 = 4 mm

and provide recommendations for follow-up in a population of smokers undergoing screening [14]. The three most common guidelines use an average of two measurements to determine follow-up interval of a nodule. The longest dimension plus the perpendicular longest dimension is divided by 2. This system of measurement is beneficial because it compensates for long oval nodules (Fig. 5.21).

It is important to consider the TNM staging guidelines for lung cancer when reviewing a CT scan of the chest for lung cancer. The T in TNM is for tumor. The stage of cancer increases with increasing size of tumor and proximity to vital organs. For example, if 2 masses are the same size and one abuts the chest wall is a stage 3, and the other that invades the mediastinum is a stage 4. Tumors are measured using their largest dimension which is called the RECIST (Response Evaluation Criteria in Solid Tumors) [15] (Fig. 5.22).

The N in TNM is for node. Enlarged (>10 mm in short axis) ipsilateral lymph nodes are N1, mediastinal lymph nodes are N2, and contralateral hilar lymph nodes are N3 (Fig. 5.23).

The M is for metastases. Metastases to the lung such as a malignant pleural effusion or a contralateral nodule are M1a. Distant metastases to adrenals or bones are M1b (Fig. 5.24).

Stages T3b, N3, and M1a and M1b are inoperable (Fig. 5.25).
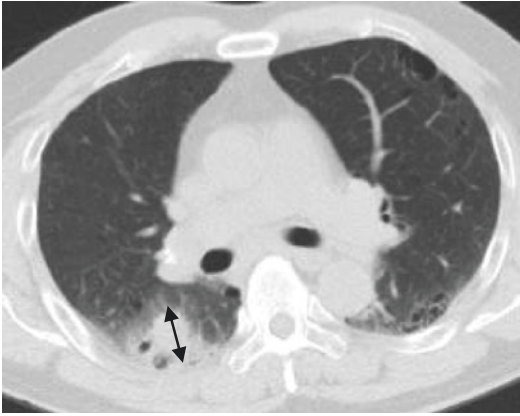
Fig. 5.22 RECIST measurement is the longest dimension of a nodule and is used in TNM staging for lung cancer
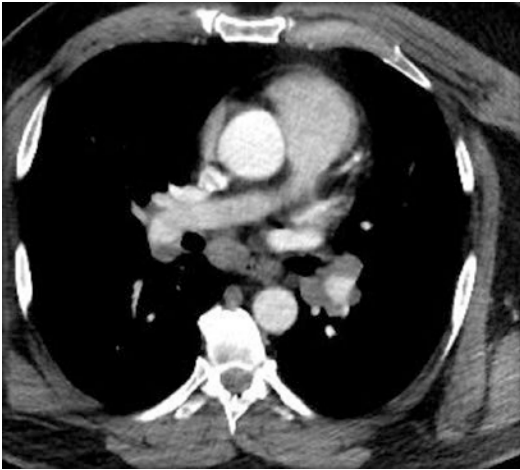


Fig. 5.23 N1 enlarged left hilar lymph nodes in a patient with left lower lobe nodule

Not all patients with lung cancer are candidates for surgery. Radiation provides an excellent option for control of local disease. Newer stereotactic radiation techniques approach lung cancer from all angles so that the center

Fig. 5.24  M1a-trapped lung with malignant effusion. The lung does not expanded despite removal of pleural fluid because of pleural involvement with disease
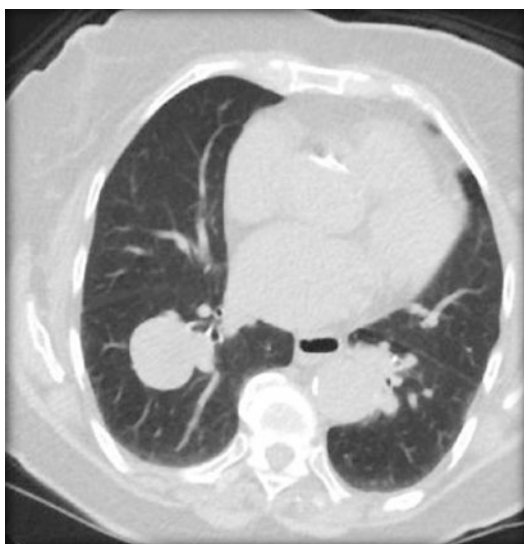


Fig. 5.25  TNM staging demonstrates a 5 cm right lower lobe nodule that is greater than 2 cm from carina (T3). There are no enlarged lymph nodes (N0) or metastases (M0) so stage is Stage 1b and the patient is a surgical candidate
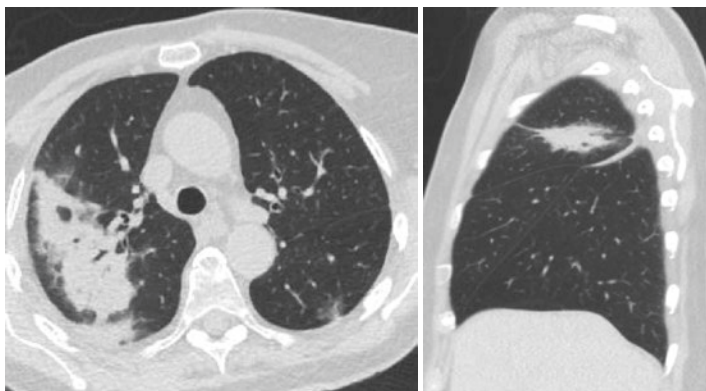
F_IG. 5.26 Axial and sagittal images post stereotactic radiation. There is characteristic consolidation with bronchiectasis in the area that received greater than 20 Gy. Note the relatively straight superior margin of fibrosis

where the tumor is located receives the highest dose and the surrounding tissue is relatively spared. This gives a characteristic appearance on the axial images with consolidation in the areas that received 20 Gy or more radiation. There is bronchiectasis within the consolidation because of the fibrosis [16]. On sagittal view, radiation has a relatively straight line differentiating it from tumor. If tumor recurs, the dilated bronchi may become occluded with tumor (Fig. 5.26).

Be careful about calling a lung nodule cancer without doing a biopsy because even the most ominous looking nodules can resolve on follow-up exam and represent infection or inflammation (Fig. 5.27).

The nodules of Kaposi's sarcoma which occurs in immuno-compromised patients have a characteristic flame shape and are located along the bronchovascular bundle which allows them to be more readily diagnosed radiographically [17] (Fig. 5.28).
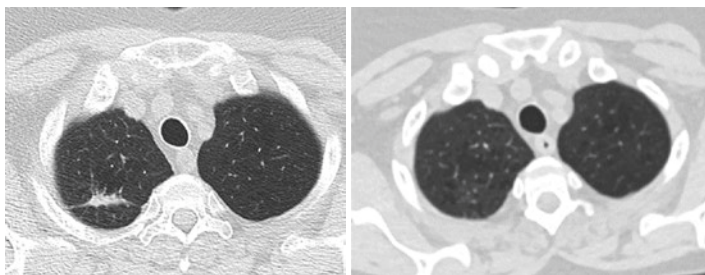
FIG. 5.27 Right upper lobe spiculated nodules with pleural tale looks like lung cancer but resolves on short interval follow-up CT scan of the chest



FIG. 5.28  Flame-shaped nodule of Kaposi's sarcoma

## 5.3   Pleural Nodules and Plaques

Pleural nodules require special consideration. They typically form obtuse margins with the pleura in contrast to pulmonary nodules which form acute angles (Fig. 5.29).

Neural tumors can also present as chest wall masses and pleural tumors and should be in the differential diagnosis of pleural lesions Fig. 5.30).

Nodules which stud the pleura or fissures are suspicious for metastatic disease. Malignant thymoma commonly metastasizes to the pleura.

Fɪɢ. 5.29  Benign fibrous tumor of the pleura. Note the obtuse margin with the chest wall



Fɪɢ. 5.30  A schwannoma presenting as a pleural based mass

Not all nodules that stud the pleura are metastases. Splenosis occurs with trauma to the spleen and small fragments of spleen can be seen along the pleural surface. Splenosis can be confidently diagnosed with a positive

nuclear medicine liver spleen study. Endometriosis can stud the pleura and cause pneumothoraces that correspond temporally to menstrual cycle [18] (Fig. 5.31).

The nodules of Stage 2 and 3 sarcoidosis are perilymphatic and as such they can stud the pleura and fissural surfaces (Fig. 5.32).

Peripheral infections such as actinomyces and nocardia can affect the pleura and chest wall (Fig. 5.33).

Asbestos exposure commonly affects the pleura. On plain film examination, the appearance is likened to a holly leaf. On cross-sectional imaging, the pleural plaques typically begin posterior-lateral in the thorax and are rectangular in shape like a bed (Fig. 5.34). Overtime these plaques may calcify.
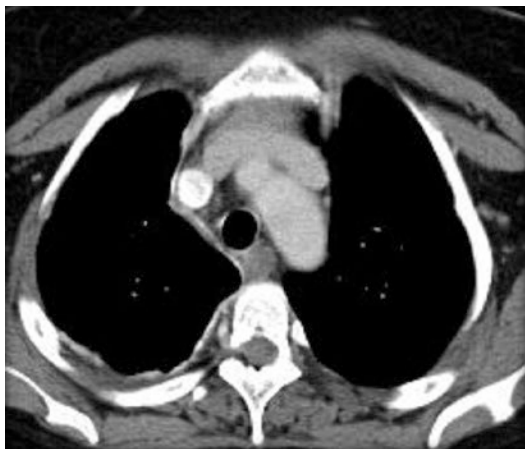


Fig. 5.31 Endometriosis studding the right posterior pleura
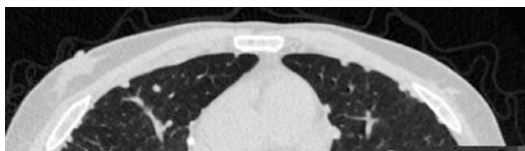


Fig. 5.32 Stage 2 sarcoidosis with perilymphatic nodules along the pleural surface
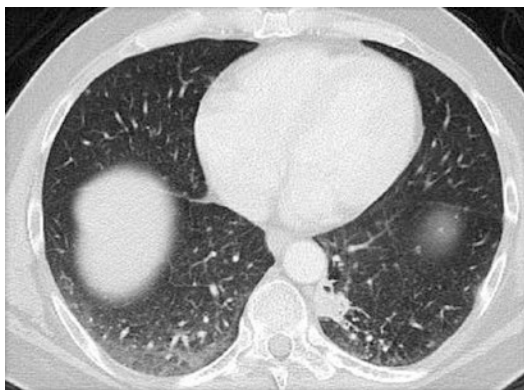
Fɪɢ. 5.33  Nocardia affecting the left posterior chest wall
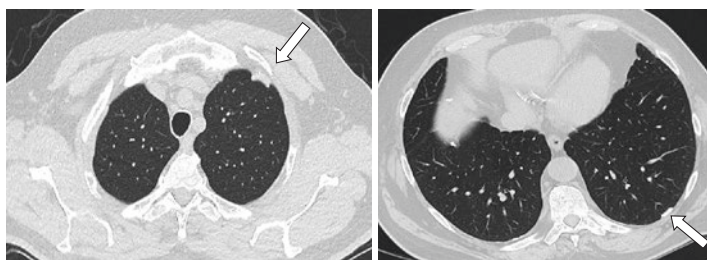


Fɪɢ. 5.34  Asbestos-related pleural disease: non-calcified and calcified pleural plaques (arrows)

Asbestosis is parenchymal involvement by asbestos fibers and can present as a subpleural line that parallels the chest wall approximately 1 cm away or parenchymal bands that are perpendicular to chest wall and 5–10 cm in length. Mesothelioma is a complication of asbestos exposure. It is potentiated by concomitant cigarette smoking. The appearance of mesothelioma on CT is typically confluent nodular thickening of the pleura which is often unilateral in contrast with pleural plaques that are bilateral (Fig. 5.35). Treatment for mesothelioma includes surgery, chemotherapy, and more recently radiation therapy [19].
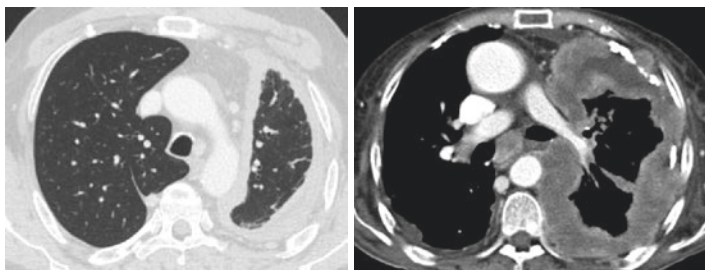
FIG. 5.35  Two separate examples of mesothelioma encasing the lung

# References

1. Dalrymple NC, Prasad SR, Freckleton MW, Chintapalli KN. Introduction to the language of three-dimensional imaging with multidetector CT. Radiographics. 2005;25(5):1409–28.

2. MacMahon H, Austin JHM, Gamsu G, Herold CJ, Jett JR, Naidich DP, Patz EF Jr, Swensen SJ. Guidelines for management of small pulmonary nodules detected on CT scans: a statement from the Fleischner society. Radiology. 2005;237(2):395–400.

3. Erasmus JJ, Connolly JE, McAdams HP, Roggli VL. Solitary pulmonary nodules. I. Morphologic evaluation for differentiation of benign and malignant lesions. Radiographics. 2000;20:43–58.

4. Gaerte SC, Meyer CA, Winer-Muram HT, Tarver RD, Conces DJ. Fat-containing lesions of the chest. Radiographics. 2002;22:S61–78.

5. Franquet T, Müller NL, Giménez A, et al. Spectrum of pulmonary aspergillosis: histologic, clinical, and radiologic findings. Radiographics. 2001;21(4):825–37.

6. Melduni RM, Mookadam F, Mulligan ME. Scimitar syndrome: another one for the radiologists. Radiology. 2006;241(2):629.

7. Shaham D, Vazquez M, Bogot NR, et al. CT features of intrapulmonary lymph nodes confirmed by cytology. Clin Imaging. 2010;34(3):185–90.

8. Li F, Sone S, Abe H, MacMahon H, Doi K. Comparison of thin section CT findings in malignant and benign nodules in CT screening for lung cancer. Radiology. 2004;233(3):793–8.

9. MacMahon H, Naidich DP, Goo JM, Lee KS, Leung ANC, Mayo JR, Mehta AC, Ohno Y, Powell CA, Prokop M, Rubin

GD, Schaefer-Prokop CM, Travis WD, Van Schil PE, Bankier AA. Guidelines for management of incidental pulmonary nodules detected on CT images: from the Fleischner society 2017. Radiology. 2017;284(1):228–43.

10. Naidich DP. Recommendations for the management of subsolid pulmonary nodules detected at CT: a statement from the Fleischner Society. Radiology. 2013;266(1):304–17.

11. Jeung MY, Gasser B, Gangi A, et al. Bronchial carcinoid tumors of the thorax: spectrum of radiologic findings. Radiographics. 2002;22(2):351–65.

12. Henschke CI, McCauley DI, Yankelevitz DF, et al. Early Lung Cancer Action Project: overall design and findings from baseline screening. Lancet. 1999;354:99–105.

13. Henschke CI, Yankelevitz DF, Smith JP, Miettinen OS. Screening for lung cancer: The Early Lung Cancer Action approach. Lung Cancer. 2002;35:143–8.

14. McKee BJ, Regis SM, McKee AB, et al. Performance of ACR lung-RADS in a clinical CT lung screening program. J Am Coll Radiol. 2015;12(3):273–6.

15. Detterbeck FC, et al. The eighth edition lung cancer stage classification. Chest. 2017;151(1):193–203.

16. Knoll M, Salvatore M. The use of isodose levels to interpret radiation induced lung injury: a quantitative analysis of computed tomography changes. Quant Imaging Med Surg. 2016;6(1):35–41.

17. Davis SD, Henschke CI, Chamides BK, et al. Intrathoracic Kaposi sarcoma in AIDS patients: radiographic-pathologic correlation. Radiology. 1987;163(2):495–500.

18. Mortelé KJ, Mortelé B, Silverman SG. CT features of the accessory spleen. AJR Am J Roentgenol. 2004;183(6):1653–7.

19. Roach HD, Davies GJ, Attanoos R, et al. Asbestos: when the dust settles an imaging review of asbestos-related disease. Radiographics. 2002;22. Spec No: S167–84.

# Chapter 6
# The Mediastinum and Pleural

- *Is it anterior?*

- *Is it middle?*

- *Is it posterior?*

- *Is it cardiac?*

- *Is it esophageal?*

- *Is it pleural?*
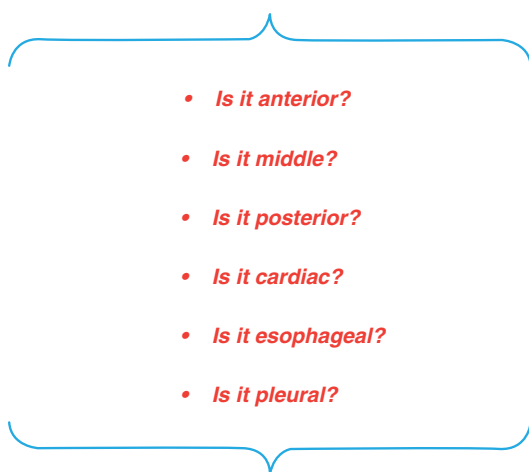
## 6.1 Normal Anatomy and Variants

The mediastinal structures on chest CT which include the thyroid gland, lymph nodes, heart, great vessels, and esophagus should be viewed on mediastinal window settings (Level 40, Window 400). I recommend reviewing each organ individually as you scroll up and down through the organ.

Three vessels typically originate from the arch of the aorta: from right to left, the right brachiocephalic artery, the left carotid artery, and the left subclavian artery (Fig. 6.1).

Common variants of the arch of the aorta are a bovine aortic arch where the right brachiocephalic artery and the left carotid have a common origin [1]. Also the vertebral artery may have a separate origin directly from the arch [2]. A less common variant is an aberrant right subclavian artery which must travel behind trachea and esophagus to go from the left to right side [3] (Fig. 6.2).
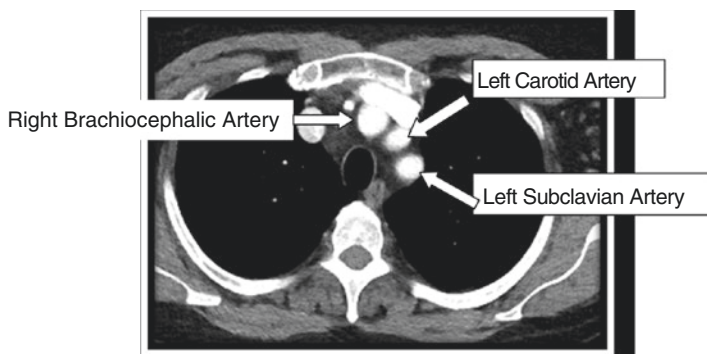


FIG. 6.1  Great vessels as they originate from the arch of the aorta
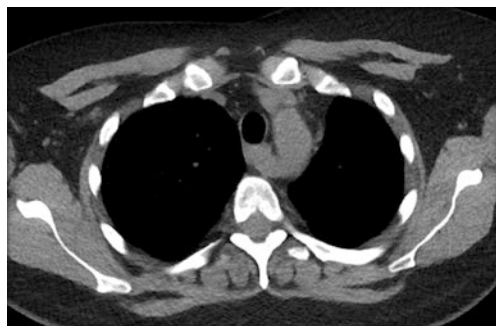


FIG. 6.2  Aberrant right subclavian artery

## 6.2   Lymph Nodes

Next, look for adenopathy by scrolling down through the mediastinum looking at the right side and up looking at the left side. Start with level 1R (right supraclavicular), 2R (high right paratracheal), 4R (low right paratracheal), 10R (right hilar), 7 (subcarinal), 8 (paraesophageal), 10L (left hilar), 5 (aorto-pulmonic window), 4L (low left paratracheal), 6 (pre-aorta), 3 (pre-vascular), 2L (high left paratracheal), and 1L (left supraclavicular). A lymph node is considered enlarged if the short axis is greater than 10 mm (Figs. 6.3, 6.4, 6.5, 6.6, 6.7, 6.8, 6.9, 6.10, 6.11, 6.12, and 6.13).
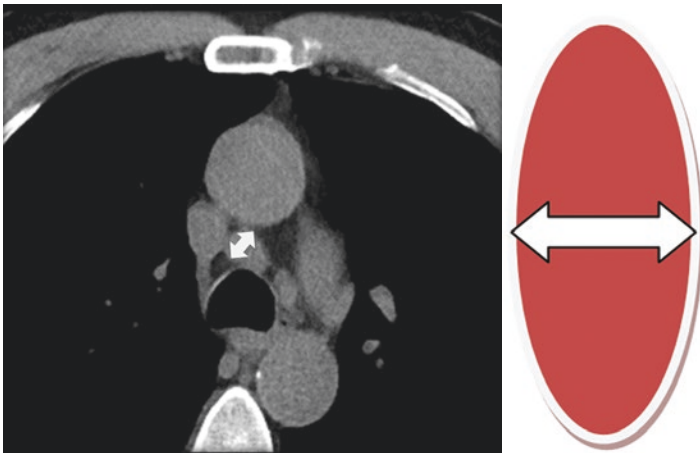


Fɪɢ. 6.3  Measuring lymph nodes by short axis
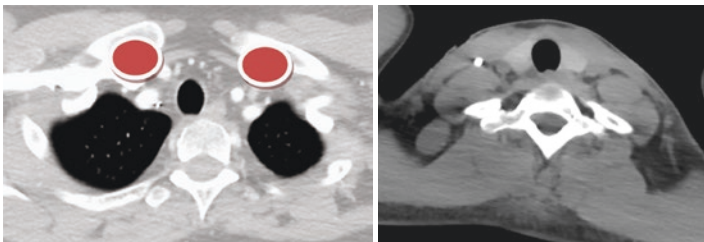


Fɪɢ. 6.4  1R and 1L are supraclavicular lymph nodes. They are very important because when associated with lung cancer, they are always N3 and make the person a nonsurgical candidate
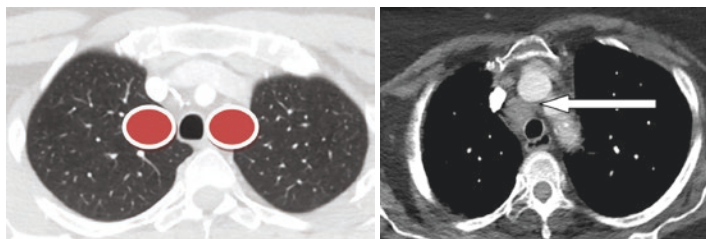
FIG. 6.5  2R and 2L are high paratracheal lymph nodes
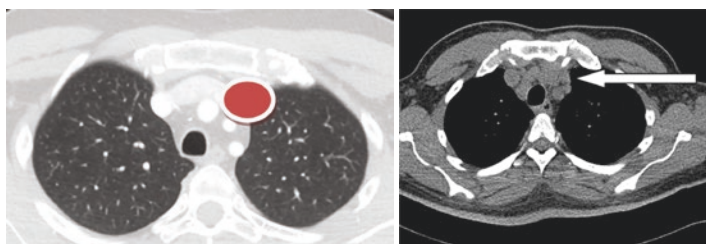


FIG. 6.6  Level 3 lymph nodes are anterior to the great vessels. To remember this, think there are three great vessels, the right brachiocephalic, the left carotid, and the left subclavian and the level 3 lymph node is in front of the them
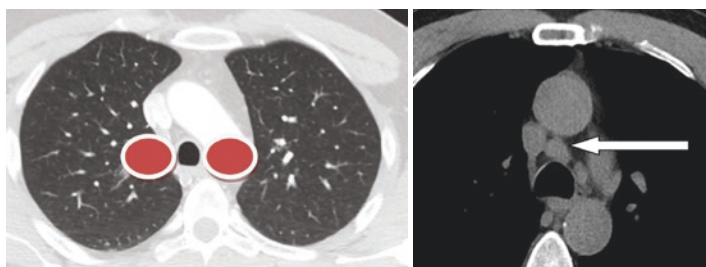


FIG. 6.7  Level 4R and 4L lymph nodes are located on either side of the lower trachea
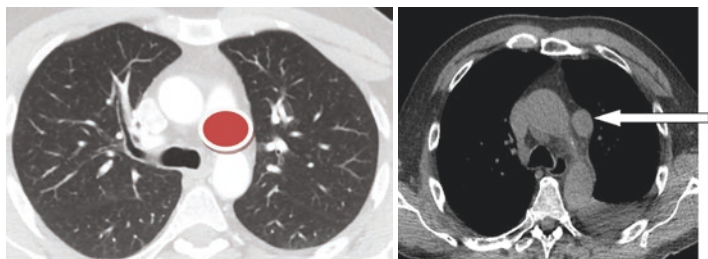
FIG. 6.8  Level 5 lymph nodes are lateral to level 4L lymph nodes and sit in the aorto-pulmonic window which is essentially under the arch of the aorta
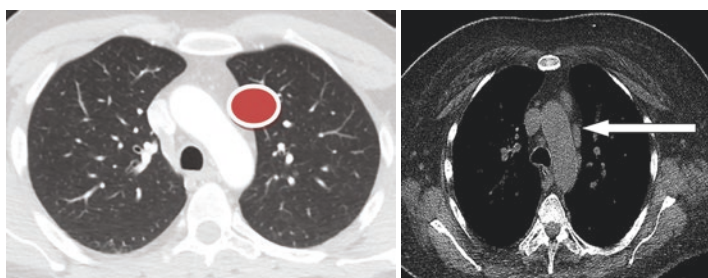


FIG. 6.9  Level 6 lymph nodes are situated in front of the arch of the aorta
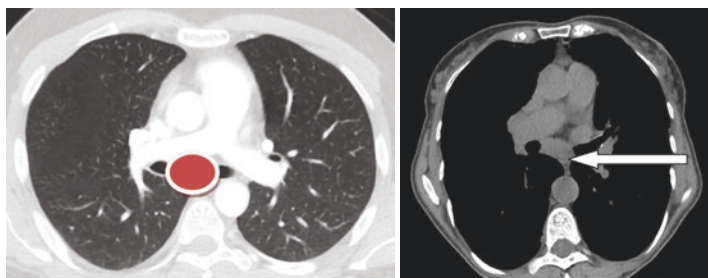


FIG. 6.10  Level 7 lymph nodes are subcarinal lymph nodes and often enlarged with disease
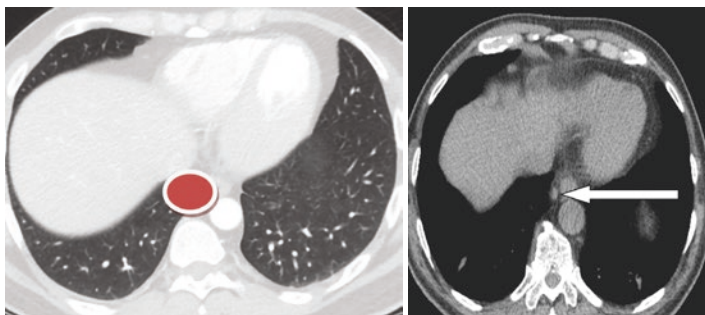
Fig. 6.11 Level 8 lymph nodes are paraesophageal lymph nodes. They are associated with diseases of the esophagus. In order to remember their number, think esophagus … ate … eight!
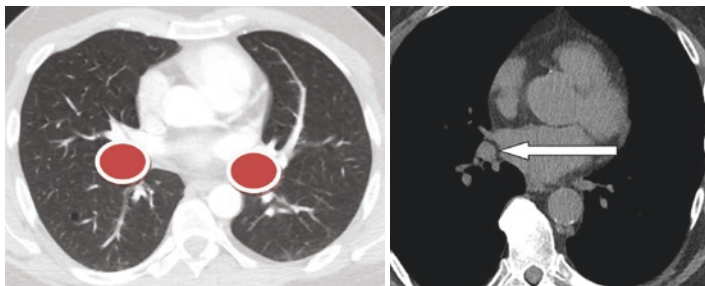


Fig. 6.12 Level 10R and 10L lymph nodes are bilateral hilar lymph nodes
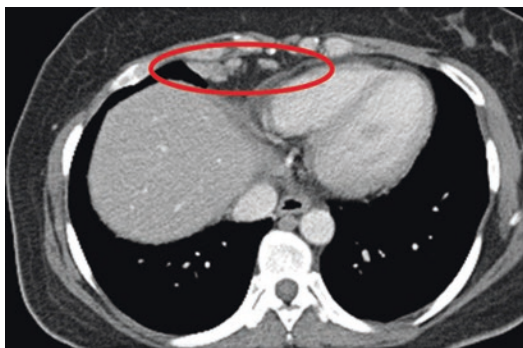


Fig. 6.13 Right cardiophrenic angle lymph nodes are enlarged in patients with liver disease

## 6.3   Anterior Mediastinum

The mediastinum is separated into three compartments. Localizing pathology into a specific compartment allows narrowing of the differential diagnosis. There are many ways to divide the mediastinum, but from a radiology standpoint, it is easiest to consider the anterior mediastinum as everything in front of the heart, the posterior mediastinum as everything from the front of the spine and behind, and the middle mediastinum as everything in between.

The most common diseases of the anterior mediastinum are the 4Ts, thymoma, teratoma, thyroid cancer, and T-cell lymphoma. The first thing to ask when an anterior mediastinal mass is present is does it communicate with the thyroid? If it does, then it is thyroid in origin; if it doesn't, then it is one of the other three. First look at the thyroid glands to see if it is homogenous. The thyroid gland is bright because of its iodine content. Diffuse enlargement of the thyroid gland often represents goiter which can extend behind the sternum or insinuate itself posteriorly between other mediastinal structures [4]. Nodules within the thyroid gland are common. They are typically hypodense on CT but may have associated calcifications. Measure the longest dimension of the nodule when reporting it. Large thyroid nodules often deviate the trachea to the opposite side which helps make the diagnosis on chest X-ray (Fig. 6.14). Ultrasound is the best test for thy-
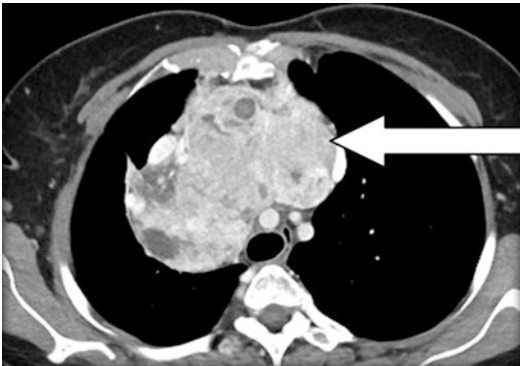


Fig. 6.14  Thyroid mass deviating the trachea to the left of midline

roid nodules; therefore when the nodule measures greater than 1 cm, the patient should be referred for a thyroid ultrasound for further evaluation and possible biopsy.

Thymomas are typically located in the anterior mediastinum and may contain calcifications. Thymoma may be associated with myasthenia gravis [5] (Fig. 6.15).

Teratomas can be distinguished by their fat or calcium content which helps to differentiate it from thymoma and lymphoma [6] (Fig. 6.16).
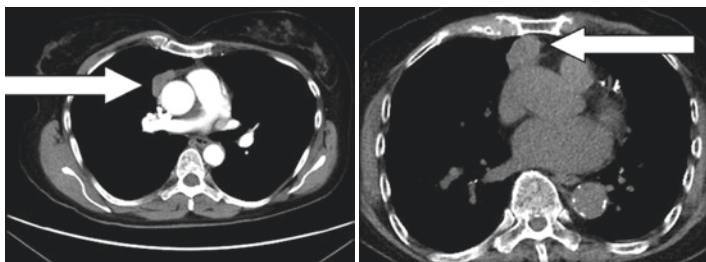


Fɪɢ. 6.15 Two separate examples of well-circumscribed thymomas
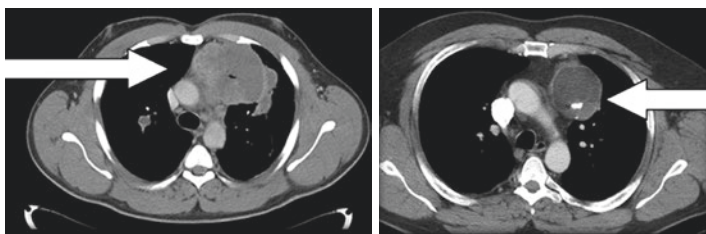


Fɪɢ. 6.16 Two examples of teratomas. Notice the fat and calcium in the lesion

Fɪɢ. 6.17  Lymphoma involving the anterior mediastinum

T-cell lymphoma of the mediastinum is usually a systemic process so it is typically accompanied by lymphadenopathy elsewhere helping to suggest the correct diagnosis [7] (Fig. 6.17).

## 6.4   Middle Mediastinum

Disease of the middle mediastinum is most commonly adenopathy, but congenital duplication cysts and aneurysms can occur in this location as well. Bronchogenic cysts and esophageal duplication cysts occur in the middle mediastinum. Sometimes they are relatively dense making their cystic nature challenging to diagnose, and MR can be helpful in these cases provided the patient does not have a contraindication for MR. Bronchogenic cysts are more common than esophageal duplication cysts [8].
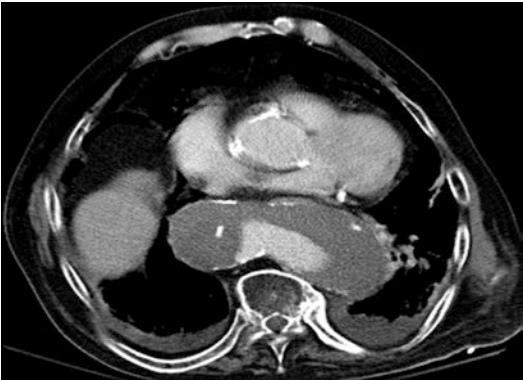
Fig. 6.18 Aneurysm and dissection of the descending thoracic aorta located in the middle mediastinum

Aneurysmal dilatation of the aorta is located in the middle mediastinum (Fig. 6.18).

## 6.5    Posterior Mediastinum

Diseases of the posterior mediastinum often affect the spine itself or may be neurogenic in origin. Extramedullary hematopoiesis occurs in patients with long-standing anemia such as sickle disease. The extra marrow for hematopoiesis can present as a paraspinal mass [9] (Fig. 6.19).

Summary Table: Mediastinal Masses by Distribution

| Anterior | Middle | Posterior |
|----------|--------|-----------|
| – Thymoma | – Lymphadenopathy | – Neurogenic tumor |
| – Thyroid cancer | – Duplication cyst | – Extramedullary hematopoiesis |
| – T-cell lymphoma | – Aneurysm | |
| – Teratoma | | |
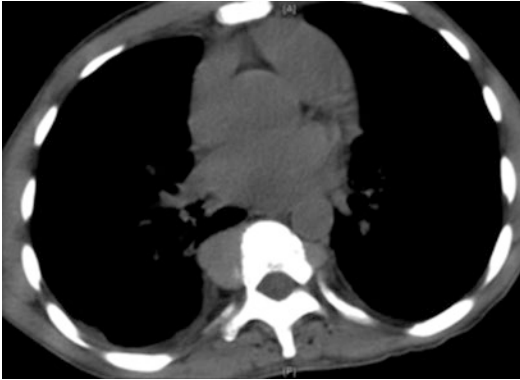
FIG. 6.19 Extramedullary hematopoiesis in a patient with sickle cell disease causing a posterior mediastinal mass

## 6.6   The Heart

The heart sits in the middle of the middle mediastinum. I cannot remember a too small heart but the heart can of course become enlarged. We consider the heart enlarged if it measures greater than 50% of the transverse diameter of the hemithorax. The heart can be enlarged because the chambers are enlarged or because of a pericardial effusion (Fig. 6.20).

A small amount of pericardial fluid is normal and occurs in the dependent part of the heart on CT. Large pericardial effusions can occur when patients have pericarditis and trauma. They can cause tamponade and are an important imaging finding [10] (Fig. 6.21).

Normally the interventricular septum of the heart is bowed toward the right because of increased pressures in the left ventricle compared to the right. However, in the case of pulmonary embolism with large clot burden, the interventricular septum can straighten or move to the left consistent with right heart strain an important prognostic finding on CT [11] (Fig. 6.22).

Fig. 6.20  Right atrium disproportionally enlarged and likely related to tricuspid valve disease
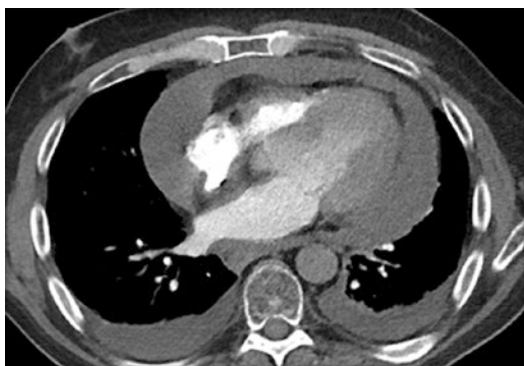


Fig. 6.21  Large pericardial effusion and moderate bilateral pleural effusions. An echocardiogram should be ordered to exclude tamponade

Fɪɢ. 6.22 Straightening of the interventricular septum compatible with right heart strain in a patient with pulmonary emboli

## 6.7   Pleural Effusion and Pneumothorax

Pleural effusions are a common finding on chest CT. They are often seen in patients with pulmonary edema and larger on the right than on the left. When a pleural effusion is present, it means that the capillary wedge pressure is at least 18–25 mmHg and the pulmonary edema is moderate (Fig. 6.23). Pleural effusions associated with pulmonary edema are typically right sided or bilateral. Isolated left pleural effusions raise the possibility of an alternative diagnosis [12].

Pleural effusions may be seen in association with pneumonia and suggest a more complicated course. In case of trauma, a pleural effusion might suggest bleeding into the thorax and rib fractures and organ lacerations should be excluded [13] (Figs. 6.24 and 6.25).

F<small>IG</small>. 6.23 Pleural effusion in patient with moderate pulmonary edema



F<small>IG</small>. 6.24 Hyperdense moderate pleural effusion compatible with a hemothorax. There is associated compressive atelectasis of the right lower lobe

Pleural effusions can be simple or loculated. Simple pleural effusions have a meniscus and layer in the dependent portion of the thorax. Loculated pleural effusions do not remain in dependent portion of the lung. Infected pleural fluid and hemorrhagic pleural effusions can become loculated. Air within pleural fluid suggests a secondary infection. If the air does not go to the nondependent part of the fluid, the fluid is likely septated and will be difficult to drain with a chest tube.
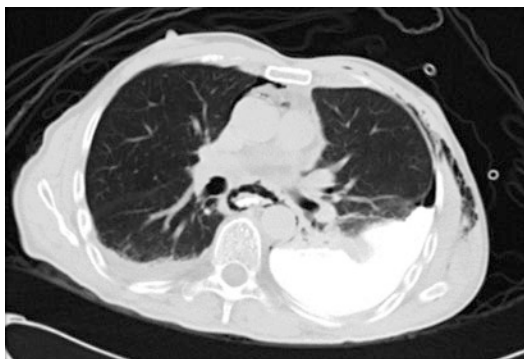
Fig. 6.25 Hyperdense left pleural effusion caused by esophageal tear and direct esophagus to pleural communication. The fluid is hyperdense in this situation because it represents the ingested barium in pleural space confirming the communication



Fig. 6.26 Trapped lung in patient with lung and pleural metastases. Notice how the lung does not expand despite removal of pleural fluid

Loculated pleural effusions can occur in patients with cancer and metastases to the pleura. The lung may not re-expand despite drainage of these pleural effusions and is called "trapped lung." The fluid often re-accumulates requiring long-term chest tube placement and possible pleurodesis [14] (Fig. 6.26).

F<small>IG</small>. 6.27  Catamenial pneumothorax with endometrial implants on the left apical pleura

Patients who have bullous lung disease are at risk for pneumothorax; however, the most common reason for pneumothorax is iatrogenic, and hospitalized patients receive repeat chest X-rays to look for pneumothorax following procedures. Sometimes pneumothorax occurs along with trauma. A rare cause of pneumothorax is a catamenial pneumothorax that occurs in association with menstrual cycle because of endometrial implants on the pleural surface [15] (Fig. 6.27).

Sometimes it becomes necessary to differentiate a large bulla from a pneumothorax. In order to do so, you need to decide if the lucency is surrounding the lung or the reverse. If the lucency surrounds the lung, it is a pneumothorax; if the lung surrounds the lucency, it is a bulla [16] (Fig. 6.28).

## 6.8   Esophagus

Next, the esophagus should be evaluated carefully from top to bottom as it is easy to miss cancer of the esophagus on chest CT which is not the gold standard for its evaluation. In addition to discrete nodules, the esophagus can become cir-
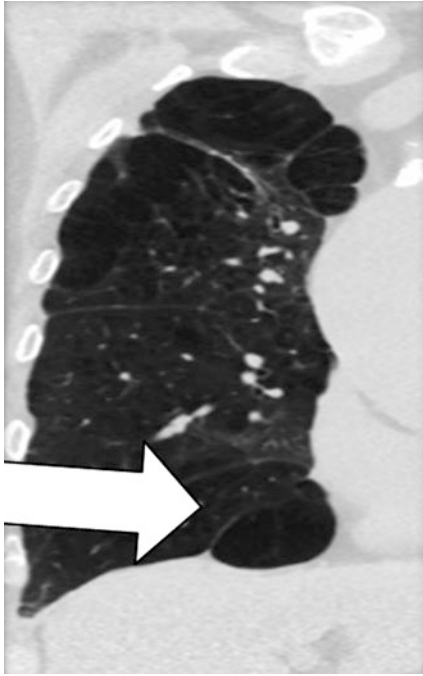
FIG. 6.28 Lower lobe bulla with surrounding lung hugging the bulla

cumferentially thickened by cancer or inflammation and should prompt a referral to gastroenterologist to differentiate and treat. Hiatal hernias are common at the gastroesophageal junction and can be associated with morbidity for the patient. The entire esophagus may become dilated in older people because of dysmotility and called a presbyesophagus. Esophageal dilatation is associated with achalasia and scleroderma as well (Fig. 6.29).

Outpouching of the esophagus (diverticulum) can cause dysphagia and aspiration pneumonia. A common esophageal

F̦ɪɢ. 6.29  Dilated esophagus in a patient with scleroderma
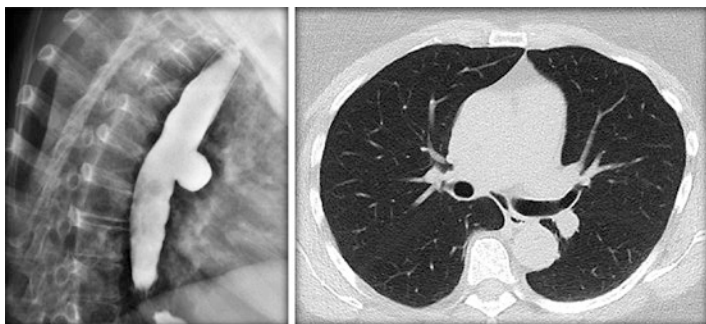


F̦ɪɢ. 6.30  Esophagram and non-contrast CT scan of the chest demonstrating an anterolateral esophageal diverticulum

diverticulum is a Zenker's diverticulum located just above the cricopharyngeal muscle [17] (Fig. 6.30).

The esophagus can become diffusely thickened with esophagitis. Gastroesophageal reflux can lead to Barrett's esophagus placing the patient at increased risk for esophageal cancer [18] (Fig. 6.31).
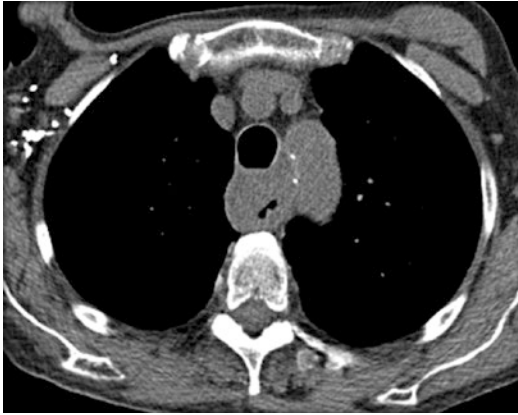
Fig. 6.31 Thickening of the wall of the esophagus at the level off the arch of the aorta due to esophageal cancer

## References

1. Layton KF, Kallmes DF, Cloft HJ, et al. Bovine aortic arch variant in humans: clarification of a common misnomer. AJNR Am J Neuroradiol. 2006;27(7):1541–2.
2. Einstein EH, Song LH, Villela NLA, et al. Anomalous origin of the left vertebral artery from the aortic arch. AORTA J. 2016;4(2):64–7.
3. Donnelly LF, Fleck RJ, Pacharn P, et al. Aberrant subclavian arteries: cross-sectional imaging findings in infants and children referred for evaluation of extrinsic airway compression. AJR Am J Roentgenol. 2002;178(5):1269–74.
4. Hurley DL, Gharib H. Evaluation and management of multinodular goiter. Otolaryngol Clin North Am. 1996;29(4):527–40.
5. Santana L, Givica A, Camacho C, et al. Best cases from the AFIP: thymoma. Radiographics. 2002;22 Spec No:S95–S102.
6. Ueno T, Tanaka YO, Nagata M, et al. Spectrum of germ cell tumors: from head to toe. Radiographics. 2004;24(2):387–404.
7. Shields TW. General thoracic surgery. Philadelphia, PA: Lippincott Williams & Wilkins; 2009; ISBN: 0781779820.
8. Juanpere S, Cañete N, Ortuño P, et al. A diagnostic approach to the mediastinal masses. Insights Imaging. 2013;4(1):29–52.

 9. Choi H, David CL, Katz RL, et al. Case 69: extramedullary hematopoiesis. Radiology. 2004;231(1):52–6.
10. Zamorano JL, Bax JJ, Rademakers FE. The ESC textbook of cardiovascular imaging. London: Springer; 2010; ISBN: 1848824203.
11. Kang DK, Thilo C, Schoepf UJ, et al. CT signs of right ventricular dysfunction: prognostic role in acute pulmonary embolism. JACC Cardiovasc Imaging. 2011;4(8):841–9.
12. Gluecker T, Capasso P, Schnyder P, et al. Clinical and radiologic features of pulmonary edema. Radiographics. 1999;19(6):1507–31.
13. Kaewlai R, Avery LL, Asrani AV, et al. Multidetector CT of blunt thoracic trauma. Radiographics. 2008;28(6):1555–70.
14. Khan H, Fernandez-Perez ER, Caples SM. Post-thoracentesis trapped lung. J Postgrad Med. 2007;53(2):119–20.
15. Marshall MB, Ahmed Z, Kucharczuk JC, et al. Catamenial pneumothorax: optimal hormonal and surgical management. Eur J Cardiothorac Surg. 2005;27(4):662–6.
16. Hansell DM, Bankier AA, Macmahon H, et al. Fleischner Society: glossary of terms for thoracic imaging. Radiology. 2008;246(3):697–722.
17. Siddiq MA, Sood S, Strachan D. Pharyngeal pouch (Zenker's diverticulum). Postgrad Med J. 2001;77(910):506–11.
18. Van der Veen AH, Dees J, Blankensteijn JD, et al. Adenocarcinoma in Barrett's oesophagus: an overrated risk. Gut. 1989;30(1):14–8.

# Chapter 7
# The Upper Abdomen

*Is each organ homogeneous?*

*Is there ascites?*

*Are there abnormal calcifications?*

## 7.1    Abdominal Organs on Chest CT

The upper abdomen to the level of the adrenal glands is routinely included on CT scans of the chest. The organs are usually suboptimally evaluated because contrast is not commonly used for chest CT scans; however one must look carefully to make sure that pathology is not missed. The abdominal structures on chest CT which include the liver, spleen, gallbladder, pancreas, adrenals, kidneys, and bowel should be viewed on mediastinal window settings (Level 40, Window 400). I recommend reviewing each organ individually as you scroll up and down through the organ (Fig. 7.1).
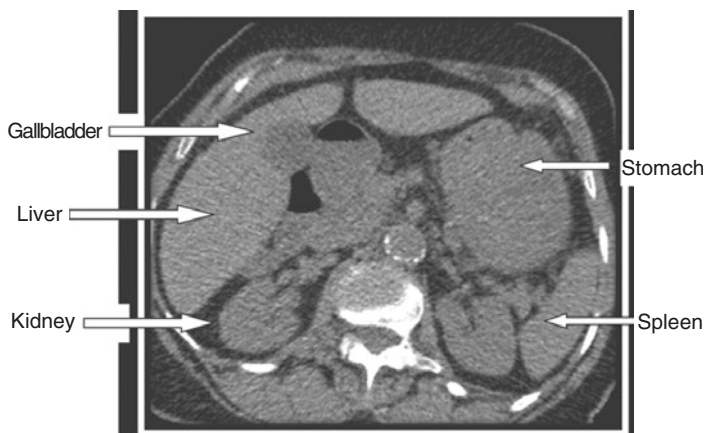
FIG. 7.1 Overview of the abdomen

## 7.2    Liver

Diseases can affect the liver focally or diffusely. Diffuse disease of the liver can cause the attenuation to either increase or decrease [1, 2]. The most common reason for diffuse decrease of liver attenuation is hepatic steatosis [3]. The average Hounsfield units are less than 40 with this disease [4]. It is important because it is a risk factor for subsequent liver cancer [5]. The liver is hypodense compared to the spleen in hepatic steatosis (Fig. 7.2).

The liver is typically hyperdense when compared to the spleen but can become more than normal dense (HU> 75) [6]. The differential diagnosis for a hyperdense liver includes hemochromatosis, a genetic disease with excess iron deposition in the liver requiring phlebotomy [7]. Hemosiderosis causes a hyperdense liver too and is seen in patients with diseases that require frequent transfusions [8]. Amiodarone toxicity has been reported to cause a hyperdense liver and hyperdense lung consolidation [9, 10].

Cirrhosis is a diffuse disease of the liver that causes a nodular contour of the periphery of the organ which ultimately shrinks in size over time (Figs. 7.3 and 7.4). Associated findings of liver cirrhosis are splenomegaly, varices, ascites, and right cardiophrenic angle lymph nodes [11]. It is impor-

Fig. 7.2  Hepatic steatosis
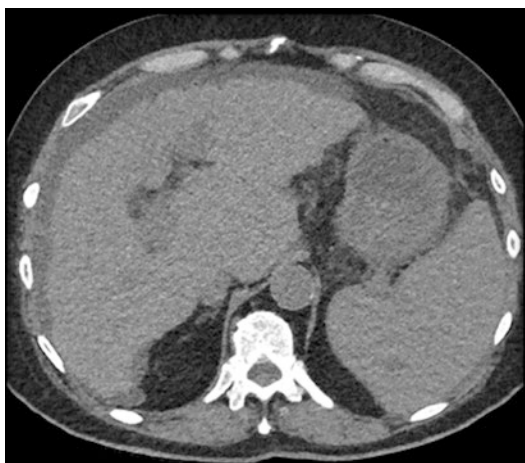


Fig. 7.3  Liver cirrhosis, ascites, and splenomegaly

tant to screen for liver cancer in patients with cirrhosis because they are at increased risk.

Focal lesions of the liver can be benign or malignant [12]. Cysts are a common benign lesion of the liver and are diagnosed when a well-circumscribed hypodense lesion measures less than 20 HU [13]. They can be incidental or seen in asso-

Fig. 7.4  Caudate enlargement with cirrhosis



Fig. 7.5  Complex cystic lesion of the liver requiring MR or contrast abdominal CT for further characterization

ciation with polycystic kidney disease [14]. Liver hemangiomas have a characteristic pattern of enhancement on contrast CT, MR, and tagged RBC studies [12]. Complex cystic lesions of the liver should be further evaluated with dedicated abdominal imaging (Fig. 7.5).

Liver lesions can represent hepatocellular carcinoma or more frequently metastatic [15] (Figs. 7.6 and 7.7).

F<small>IG</small>. 7.6  Solitary liver lesion representing hepatocellular carcinoma



F<small>IG</small>. 7.7  Metastatic disease to the liver

## 7.3   Gallbladder

The gallbladder is a nonessential organ but can cause trouble when it becomes obstructed or if cancer develops. Gallstones are common and usually contain calcium and appear hyperdense on CT, but sometimes they contain cholesterol and appear hypodense (Fig. 7.8). Thickening of the gallbladder
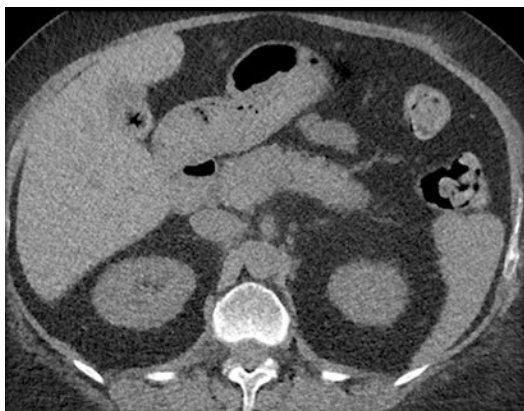
Fig. 7.8  Cholesterol gallstone



Fig. 7.9  Porcelain gallbladder with calcification of the gallbladder wall

wall may represent infection or inflammation, but cancer cannot be excluded. Emphysematous cholecystitis which can be life threatening should be suggested when air is seen within the gallbladder wall [16].

A porcelain gallbladder is peripheral calcification of the wall of the gall bladder and has been associated with an increased risk of cancer of the gallbladder [17] (Fig. 7.9).
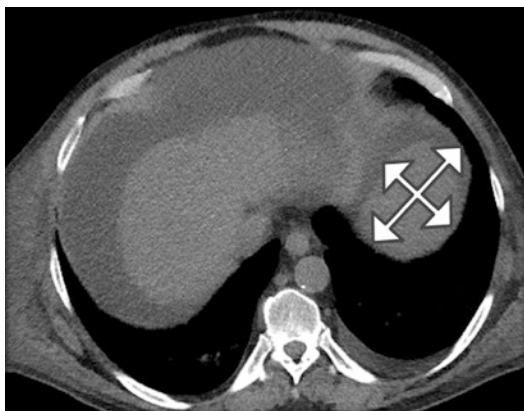
Fig. 7.10  Measuring the spleen. It is considered enlarged if measures greater than 12 by 5 cm

## 7.4  Spleen

The spleen is located in the left upper quadrant of the abdomen. It becomes enlarged when there is portal hypertension or lymphoma infiltrates the gland. A large spleen is one that measures greater than 12 cm by 5 cm with 5 cm or greater waist being the more reliable measurement (Figs. 7.10 and 7.11). Wedge-shaped hypodense lesion is seen with infarcts. Patients with sickle cell disease suffer from many splenic infarcts and ultimately may develop small calcified spleens [18] (Fig. 7.12).

## 7.5  Pancreas

The pancreas is identified with its tail in the splenic hilum. Follow it to the right where the head of the pancreas ends in a sharp "V" called the uncinate process [19] (Figs. 7.13 and 7.14). It is normal for the pancreas to atrophy with age and become fatty involuted making it more difficult to identify [20]. Swelling of the pancreas with phlegmonous changes of

FIG. 7.11  The spleen larger than the liver in patient with polycythe-
mia vera
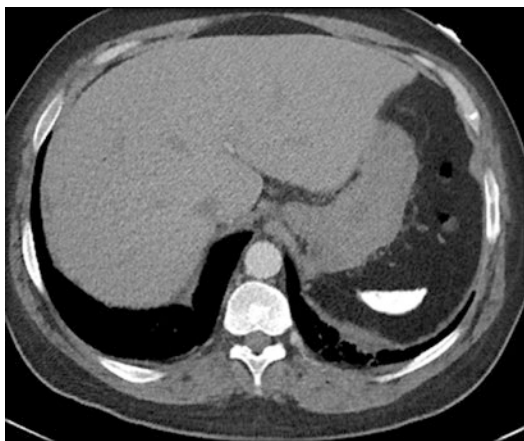


FIG. 7.12  Small calcified spleen in patient with sickle cell disease

the surrounding fat is seen with acute pancreatitis [21].
Course calcifications of the gland are seen in association with
chronic alcoholism [22]. Masses of the pancreas often obstruct
the pancreatic duct and cause downstream dilatation.

FIG. 7.13 Normal pancreas with "V-shaped" uncinate process



FIG. 7.14 Hypodense lesion of the pancreas requiring further imaging with dedicated pancreatic protocol CT or abdominal MR

## 7.6 Adrenals

The adrenal glands are the reason that chest CT scans extend below the diaphragm. It is in order to look for metastases from lung cancer. The adrenal gland sits on top of the kidney,

Fɪɢ. 7.15  Normal right adrenal gland looks like an inverted Y

but because the kidney tilts forward, it appears to be anterior to the kidney [23]. The adrenals typically resemble inverted "Ys" (Fig. 7.15). Nonspecific thickening of the limbs of an adrenal gland can occur or more focal nodules. Fortunately, the more common type of nodule to the adrenal gland is a low-density adrenal adenoma measuring less than 20 HU. Metastatic disease to adrenal gland presents as a solid nodule measuring greater than 20 HU [24]. Primary neoplasms of the adrenal gland can occur but are less frequent.

## 7.7   Kidneys

Kidneys can become diffusely enlarged when there is engorgement from venous obstruction. More commonly they undergo compensatory unilateral enlargement when there is compromise to the contralateral kidney. The kidneys become atrophic when there is long-standing renal insufficiency. Hydronephrosis can be identified on CT, but the cause will not necessarily be known as the ureter is incompletely evaluated. Nonobstructive renal stones are frequently seen within the renal parenchyma [25]. Renal hypodensities are present in most people over 50 years old; if they measure less than 20

Fig. 7.16 Renal cyst measuring less than 20 HU



Fig. 7.17 Renal cell carcinoma measuring greater than 20 HU and enhancing with contrast

HU, they are likely to be renal cysts. Some dense renal cysts are secondary to hemorrhage, but neoplasm cannot be excluded, and further evaluation with dedicated abdominal imaging is warranted [26] (Figs. 7.16 and 7.17).

## 7.8    Bowel

The bowels are suboptimally evaluated on chest CT because of the absence of oral contrast. Nonetheless, we see the bowels and should review them for pathology. The stomach may be collapsed or filled with food on CT. The walls are likely to appear thicker when the stomach is collapsed. Diffuse thickening of the wall of the stomach can be seen with gastritis. Focal thickening raises the possibility of a neoplasm including a GIST tumor [27, 28] (Figs. 7.18 and 7.19).

The duodenum and small bowel are identified in part and can be dilated or collapsed. Portions of the colon can be distinguished from small bowel by the presence of stool. Outpouchings of the colon without inflammation are diverticuli. If there is associated inflammation, then the diagnosis is diverticulitis [29]. The omentum is normally not well seen on CT unless there is pathology (Fig. 7.20).



Fig. 7.18 Thickening of the gastric antrum caused by primary gastric cancer. There is associated ascites

Fig. 7.19 Focal thickening of the lesser curvature of the stomach in a patient with gastric cancer



Fig. 7.20 Omental thickening called caking due to metastatic ovarian cancer

# References

1. Boll DT, Merkle EM. Diffuse liver disease: strategies for hepatic CT and MR imaging. Radiographics. 2009;29(6):1591–614.

2. Yeom SK, Lee CH, Cha SH, Park CM. Prediction of liver cirrhosis, using diagnostic imaging tools. World J Hepatol. 2015;7(17):2069–79.

3. Jacobs JE, Birnbaum BA, Shapiro MA, et al. Diagnostic criteria for fatty infiltration of the liver on contrast-enhanced helical CT. AJR Am J Roentgenol. 1998;171(3):659–64.

4. Schwenzer NF, Springer F, Schraml C, Stefan N, Machann J, Schick F. Non-invasive assessment and quantification of liver steatosis by ultrasound, computed tomography and magnetic resonance. J Hepatol. 2009;51(3):433–45.

5. Baffy G. Hepatocellular carcinoma in non-alcoholic fatty liver disease: epidemiology, pathogenesis, and prevention. J Clin Transl Hepatol. 2013;1(2):131–7.

6. Kodama Y, Ng CS, Wu TT, Ayers GD, Curley SA, Abdalla EK, Vauthey JN, Charnsangavej C. Comparison of CT methods for determining the fat content of the liver. AJR Am J Roentgenol. 2007;188:1307–12.

7. Grosse SD, Gurrin LC, Bertalli NA, Allen KJ. Clinical penetrance in hereditary hemochromatosis: estimates of the cumulative incidence of severe liver disease among HFE C282Y homozygotes. Genet Med. 2017. https://doi.org/10.1038/gim.2017.121.

8. deJongh AD, van Beers EJ, de Vooght KMK, Schutgens REG. Screening for hemosiderosis in patients receiving multiple red blood cell transfusions. Eur J Haematol. 2017;98(5):478–84.

9. Kim BB, Kim DM, Choi DH, et al. Amiodarone toxicity showing high liver density on CT scan with normal liver function and plasma amiodarone levels in a long-term amiodarone user. Int J Cardiol. 2014;172(2):494–5.

10. Wolkove N, Baltzan M. Amiodarone pulmonary toxicity. Can Respir J. 2009;16(2):43–8.

11. Gupta AA, Kim DC, Krinsky GA, et al. CT and MRI of cirrhosis and its mimics. AJR Am J Roentgenol. 2004;183(6):1595–601.

12. Jang HJ, Yu H, Kim TK. Imaging of focal liver lesions. Semin Roentgenol. 2009;44(4):266–82.

13. Mortelé KJ, Ros PR. Cystic focal liver lesions in the adult: differential CT and MR imaging features. Radiographics. 2001;21(4):895–910.

14. Butscher A, Phan O, Bonny O. Extra-renal manifestations of the autosomal dominant polycystic kidney disease. Rev Med Suisse. 2017;13(551):450–6.

15. Assy N, Nasser G, Djibre A, Beniashvili Z, Elias S, Zidan J. Characteristics of common solid liver lesions and recommendations for diagnostic workup. World J Gastroenterol. 2009;15(26):3217–27.

16. Grand D, Horton KM, Fishman EK. CT of the gallbladder: spectrum of disease. AJR Am J Roentgenol. 2004;183(1):163–70.

17. Revzin MV, Scoutt L, Smitaman E, Israel GM. The gallbladder: uncommon gallbladder conditions and unusual presentations of the common gallbladder pathological processes. Abdom Imaging. 2015;40(2):385–99.

18. Karlo CA, Stolzmann P, Do RK, Alkadhi H. Computed tomography of the spleen: how to interpret the hypodense lesion. Insights Imaging. 2013;4(1):65–76.

19. Martin DF. Computed tomography of the normal pancreatic uncinate process. Clin Radiol. 1988;39(2):195–6.

20. Sato T, Ito K, Tamada T, et al. Age-related changes in normal adult pancreas: MR imaging evaluation. Eur J Radiol. 2012;81(9):2093–8.

21. Foster BR, Jensen KK, Bakis G, Shaaban AM, Coakley FV. Revised Atlanta classification for acute pancreatitis: a pictorial essay. Radiographics. 2016;36(3):675–87.

22. Lesniak RJ, Hohenwalter MD, Taylor AJ. Spectrum of causes of pancreatic calcifications. Am J Radiol. 2002;178:79–86.

23. Montagne JP, Kressel HY, Korobkin M, Moss AA. Computed tomography of the normal adrenal glands. AJR Am J Roentgenol. 1978;130(5):963–6.

24. Schieda N, Siegelman ES. Update on CT and MRI of adrenal nodules. AJR Am J Roentgenol. 2017;208:1206–17.

25. Furlan A, Federle MP, Yealy DM, Averch TD, Pealer K. Nonobstructing renal stones on unenhanced CT: a real cause for renal colic? AJR Am J Roentgenol. 2008;190(2):W125–7.

26. Kay FU, Pedrosa I. Imaging of solid renal masses. Radiol Clin North Am. 2017;55(2):243–58.

27. Virmani V, Khandelwal A, Sethi V, Fraser-Hill M, Fasih N, Kielar A. Neoplastic stomach lesions and their mimickers: spectrum of imaging manifestations. Cancer Imaging. 2012;12(1):269–78.

28. Kim HC, Lee JM, Kim KW, et al. Gastrointestinal stromal tumors of the stomach: CT findings and prediction of malignancy. AJR Am J Roentgenol. 2004;183(4):893–8.

29. Humes D, Simpson J, Spiller RC. Colonic diverticular disease. BMJ Clin Evid. 2007;2007:0405.

# Chapter 8
# The Soft Tissues

Is the breast ok?

Are the axillary lymph nodes ok?

Is there a sebaceous cyst?
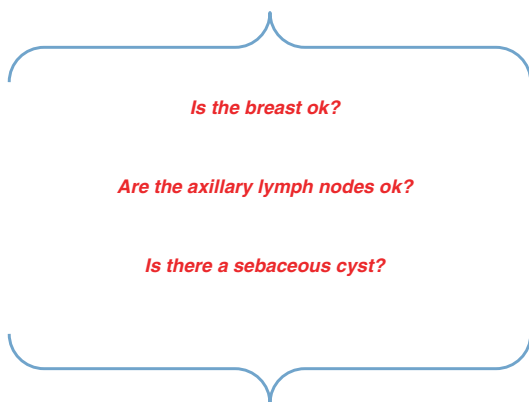
## 8.1   Breast on CT

The visualized soft tissues on chest CT include the breast tissue, muscles, and subcutaneous tissue and should be viewed on mediastinal window settings on axial images (Level 40, Window 400). I recommend beginning with the right side and scrolling from superior to inferior and then left side inferior to superior.

Women are having fewer mammograms currently. The indications for chest CT are increasing as lung cancer screening

147

received approval for reimbursement by Medicare [1]. Therefore, the only opportunity we may have to diagnose breast cancer early is on a CT scan of the chest. It is imperative that the scanned breast be included on the images provided to the radiologist for interpretation and they are often not included so that the field of view for evaluating the lung parenchyma is not compromised. A viable solution is to include the entire breast on soft tissue windows only and allow lung windows to be optimized for evaluation of the lung.

Recently many states have demanded that the density of a woman's breast be recorded on the mammogram report because women with dense breast parenchyma are at increased risk for breast cancer because they have more breast parenchyma and cancer can hide in dense breast tissue. It is required by many states to offer women with dense breast parenchyma a breast ultrasound exam which can identify mammographically occult cancers. It follows that if we can see the breast tissue on CT scan, we should comment on the breast density as well.

Breast density is defined as Grade 1 if 0–25% breast parenchyma, Grade 2 if 26–50% breast parenchyma, Grade 3 if 51–75% breast parenchyma, and Grade 4 if 76–100% breast parenchyma. Grades 3 and 4 are offered a breast ultrasound. Inter-reader agreement for breast density grade on CT is high ($k$ = .79) and should be included on chest CT reports [2, 3] (Fig. 8.1).

Breast nodules are a common finding on chest CT scans. When a breast nodule is identified, we should consider four things: location, associated findings, size, and Hounsfield units. Note if the nodule is above or below the nipple or medial or lateral to the nipple to determine which quadrant of the breast the nodule is located in (Fig. 8.2).

Next consider associated findings which include skin thickening, architectural distortion and course calcifications, nipple retraction, or necrosis (Fig. 8.3).

Next, the longest dimension of the nodule should be considered (Fig. 8.4).

Grade 1 (0-25% Breast Parenchyma)    Grade 2 (26-50% Breast parenchyma)

Grade 3 (51-75% Breast Parenchyma)    Grade 4 (76-100% breast parenchyma)
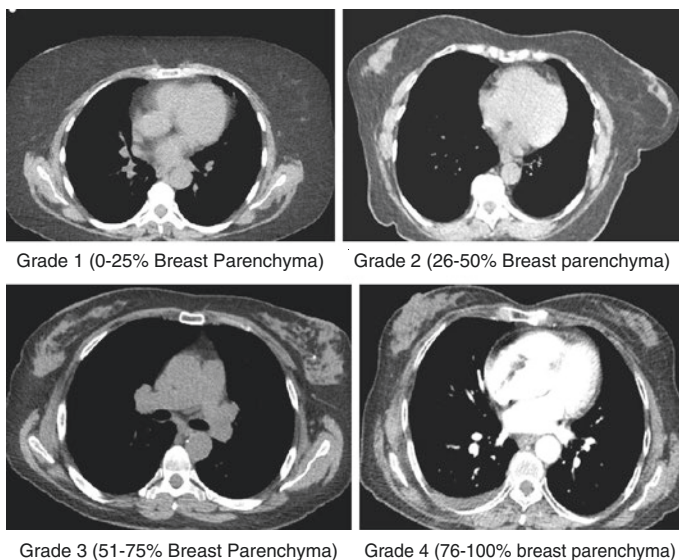
Fɪɢ. 8.1  Breast density on chest CT
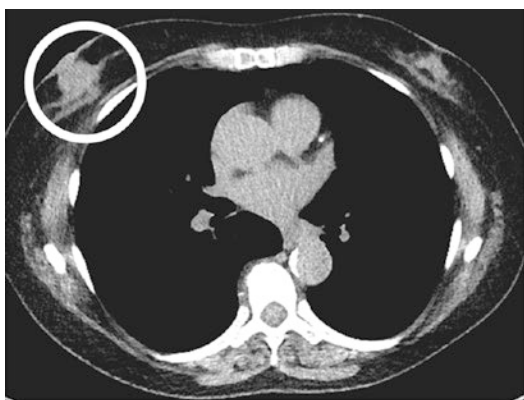


Fɪɢ. 8.2 Right breast retroareolar nodule. The breast density grade is 2
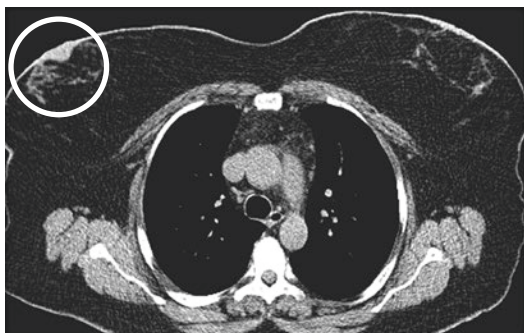
FIG. 8.3  Right nipple inversion. The breast density is Grade 1



FIG. 8.4  Left breast upper inner quadrant nodule measuring 1 cm in size with no associated findings. The breast parenchyma is a Grade 2

It is also valuable to measure the Hounsfield units of the breast nodule to determine if it is more likely cystic or solid. Measurements less than 20 HU are more likely to represent intraparenchymal cysts [4]. Metastatic disease can present as a breast nodule (Fig. 8.5).

It is common for men to develop breast tissue and is associated with liver cirrhosis and medications. Usually it is symmetric but may present asymmetrically as well making the diagnosis more challenging as breast cancer can occur in men [5] (Figs. 8.6 and 8.7).
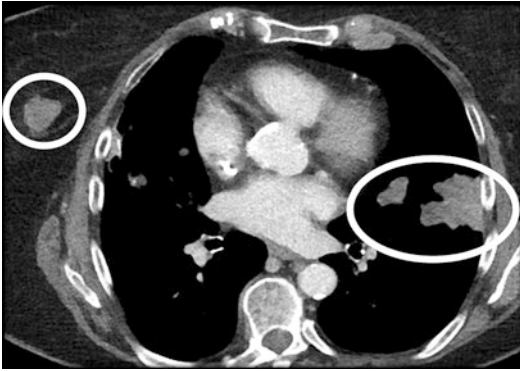
Fig. 8.5 Right breast upper inner quadrant nodule measuring 15 mm in size and 40 HU. There is an associated finding which is a left lung mass. The nodule represented metastatic disease from the lung



Fig. 8.6 Symmetric gynecomastia

It is important to emphasize that chest CT scan should not be used for the definitive diagnosis of breast cancer at this time. Its current role is to identify asymptomatic breast disease and alert the patient to get a mammogram for definitive diagnosis.

Prior breast surgery can be identified on chest CT (Fig. 8.8).
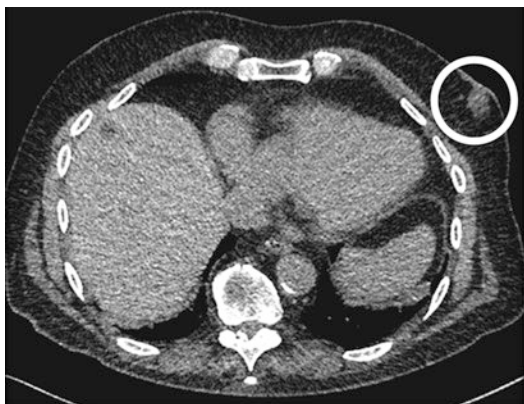
FIG. 8.7  Left breast upper outer quadrant nodule measuring 1.2 cm in size and 35 HU representing male breast cancer



FIG. 8.8  Patient with right mastectomy and breast prosthesis

## 8.2    Subcutaneous Tissue

In addition to breast tissue, the subcutaneous tissue can be evaluated for subcutaneous emphysema which can occur following procedures or in association with pneumothorax or
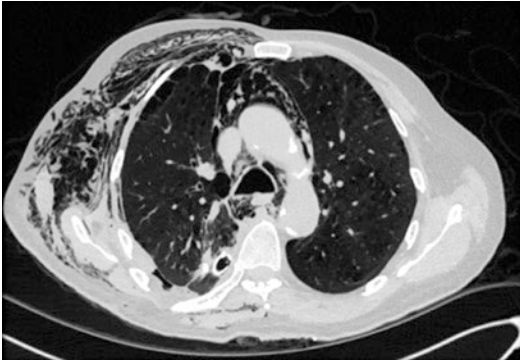
Fig. 8.9  Subcutaneous emphysema of the right chest wall in patient with pneumothorax and pneumomediastinum
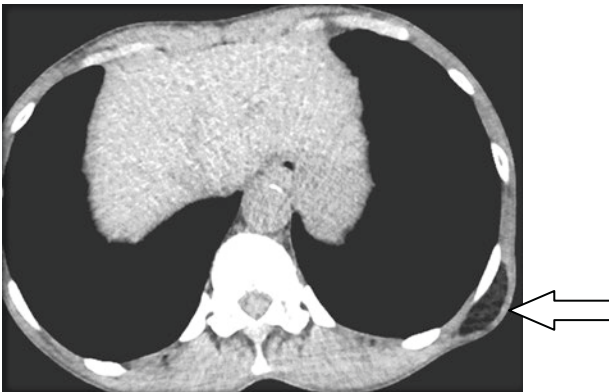


Fig. 8.10  Breast density on chest CT

pneumomediastinum [6] (Fig. 8.9). Phlegmonous changes or stranding of the soft tissues can be seen in association with trauma and can help localize additional organ injury.

Intramuscular lipomas are fatty tumors that are common and should be differentiated from more worrisome pathology. The figure demonstrates a left flank intramuscular lipoma (Fig. 8.10).

Chest wall masses are identified while looking at the subcutaneous tissues or ribs. Chest wall abnormalities can be caused by tumors such as neurogenic tumors or bone tumors.
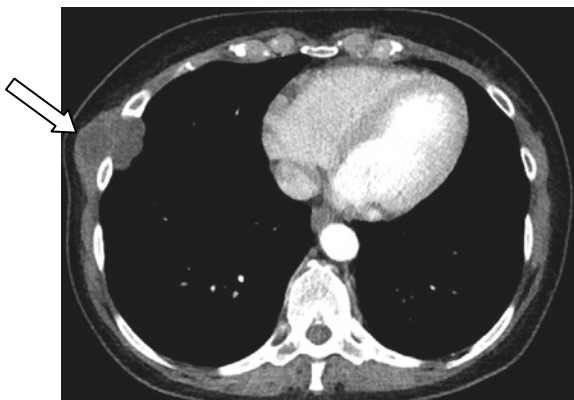
FIG. 8.11 Molded ribs as in the case of cystic hygroma, a slow-growing benign neoplasm

Infections in the lung can extend through the chest wall, most notably actinomycosis and nocardia infections [7]. Hematomas following trauma can also present as chest wall masses, and the history will be helpful. Evaluation of adjacent ribs is helpful in distinguishing benign from malignant disease. Destroyed ribs are associated with aggressive tumors, while molded ribs are associated with slow-growing benign neoplasms (Fig. 8.11).

# References

1. www.Medicare.gov
2. Salvatore M, Margolies L, Kale M, Wisnivesky J, Kotkin S, Henschke CI, Yankelevitz DF. Breast density: comparison of chest CT with mammography. Radiology. 2014;270(1):67–73.
3. Margolies L, Salvatore M, Eber C, Jacobi A, Lee IJ, Liang M, Tang W, Xu D, Zhao S, Kale M, Wisnivesky J, Henschke CI, Yankelevitz D. The general radiologist's role in breast cancer risk assessment: breast density measurement on chest CT. Clin Imaging. 2015;39(6):979–82.
4. Margolies LR, Salvatore M, Yip R, Tam K, Bertolini A, Henschke C, Yankelevitz D. The chest radiologist's role in invasive breast cancer detection. Clin Imaging. 2017;50:13–9.

5.  Sonnenblick EB, Salvatore M, Szabo J, Lee KA, Margolies LR. Incremental role of mammography in the evaluation of gynecomastia in men who have undergone chest CT. AJR Am J Roentgenol. 2016;207(2):234–40.
6.  Murayama S, Gibo S. Spontaneous pneumomediastinum and Macklin effect: overview and appearance on computed tomography. World J Radiol. 2014;6(11):850–4.
7.  Valour F, Sénéchal A, Dupieux C, et al. Actinomycosis: etiology, clinical features, diagnosis, treatment, and management. Infect Drug Resist. 2014;7:183–97. https://doi.org/10.2147/IDR.S39601.

# Chapter 9
# The Osseous Structures

*Is it lytic?*

*Is it sclerotic?*

*Is it broken?*
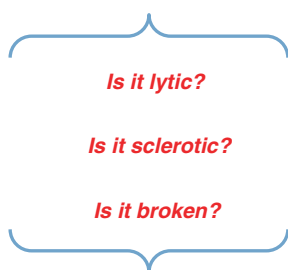
## 9.1    Spine

The visualized osseous structures on chest CT which include the spine, ribs, sternum, scapula, and humerus should be examined on bone window settings (Level 600, Window 3000). Begin with the spine and scroll from superior to inferior slowing down to identify the lamina and pedicle of each vertebrae (Fig. 9.1). Metastatic disease has a propensity for the pedicles.

Further evaluate the spine on sagittal projection where it is easier to diagnose a compression fracture with its loss of height or a spondylolisthesis which is a slippage of one vertebra on top of the other (Figs. 9.2 and 9.3). The spondylolisthesis is named by the direction of the more superior vertebrae.
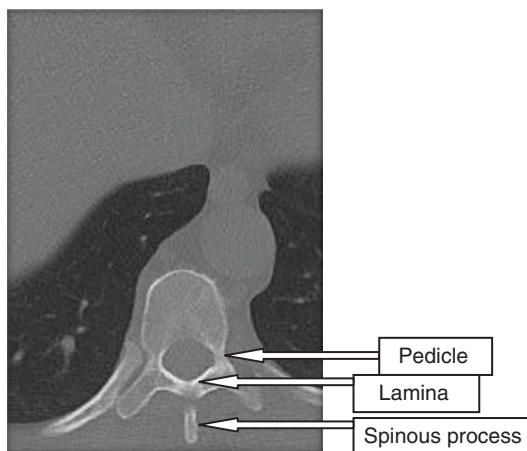
F<small>IG</small>. 9.1  Axial image of vertebrae

Slippage is graded from 1 to 4 and based on percentage of vertebra that is exposed with grade 1 being the mildest with 1–25% of vertebrae advanced anteriorly or posteriorly [1].

Spinal metastases can be lytic or sclerotic. Spinal hemangiomas are common lucent lesions with speckled internal appearance (Figs. 9.4 and 9.5).

Look for neural tumors while scrolling through the spine (Fig. 9.6).

## 9.2    Ribs

Next look at the right ribs, as you scroll down look at the anterior right ribs, and count them as you go. Scroll up looking at the posterior right ribs and count them as well. Do the same for the left ribs so that you do not miss a subtle rib fracture or bone lesion (Fig. 9.7).

Fig. 9.2 Normal thoracic spine on sagittal projection with uniform height of vertebrae and normal alignment

Rib fractures are often incidentally noted on chest CT; however sometimes unsuspected rib fractures are the cause of a patient's pain and shortness of breath (Fig. 9.8).

Lucent or low-density bone lesions can be benign or malignant. Signs of benignity include well-circumscribed margins and intact cortex (Fig. 9.9).

Fig. 9.3 Sagittal image of the thoracic spine with multiple vertebral body compression fractures. Note the air within the disc space called vacuum disc phenomenon

Fɪɢ. 9.4 Sclerotic metastases to the spine from prostate cancer
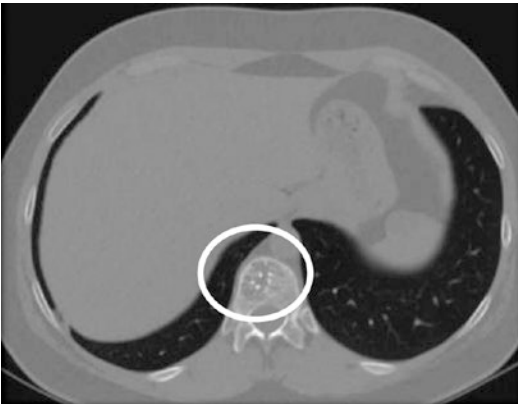


Fɪɢ. 9.5 A vertebral body hemangioma is a common benign tumor with a characteristic speckled appearance
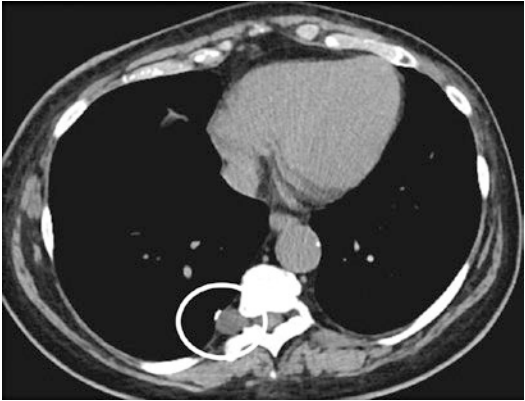
FIG. 9.6  Neurofibroma of the thoracic spine
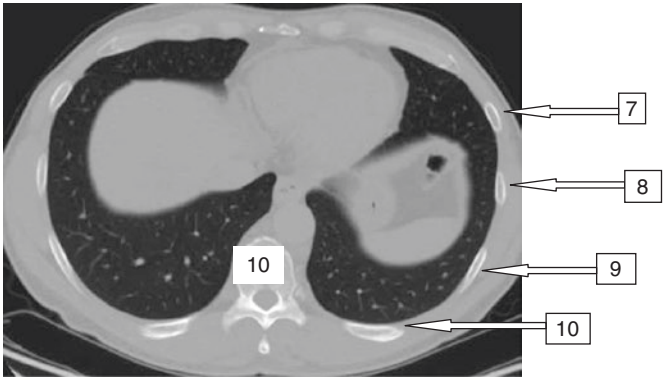


FIG. 9.7  Ribs are counted by first identifying the vertebrae and then decreasing the count as you go anteriorly

FIG. 9.8 Non-displaced left rib fracture
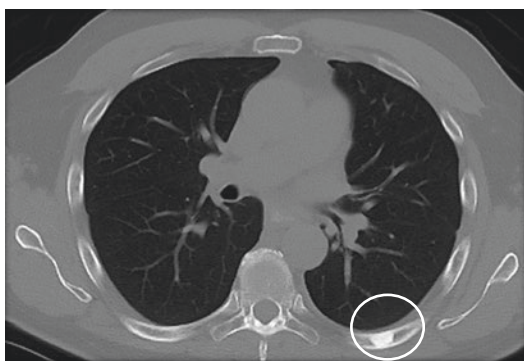


FIG. 9.9 Benign bone island of the left rib

## 9.3    Sternum

Next scroll through the sternum and continue by looking at each shoulder separately (Fig. 9.10).

Sclerotic lesions of the bones are common and usually represent benign bone islands. They are sclerotic and hyperdense foci with "thorny" radiations that blend with surrounding trabeculae [2]. The differential diagnosis could include sclerotic metastases, and a nuclear medicine bone scan may be needed to differentiate (Fig. 9.11).
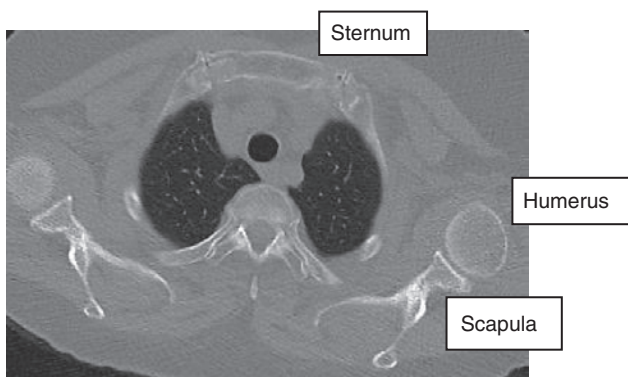


Fɪɢ. 9.10  Sternum and bilateral shoulder joints
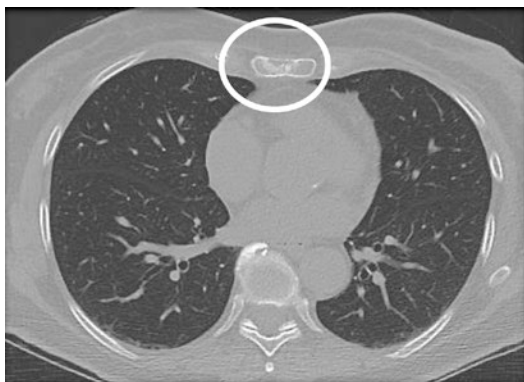


Fɪɢ. 9.11  Sternal metastases

Fig. 9.12 Sternal fracture



Sternal fractures are typically iatrogenic following coronary artery bypass surgery but should not be overlooked especially in patient's status post motor vehicle trauma (Fig. 9.12).

Two of the most commonly encountered chest wall deformities are pectus excavatum and pectus carinatum. Pectus excavatum is more common [3]. In pectus excavatum the sternum is displaced posteriorly, thus narrowing the AP dimension of the thoracic cavity with resultant pressure on right atrium. The Haller index is a reflection of the degree of deformity. It measures the transverse diameter of the hemithorax divided by the narrowest AP diameter on the same image. Normal is 2.5 (Fig. 9.13).

Pectus carinatum is the opposite of excavatum with the sternum displaced anteriorly which increases the AP diameter of the thorax. There are two types described: chondrogladiolar is protrusion of the middle and lower sternum and chondro-manubrial is protrusion of the manubrium and upper sternum also called Currarino-Silverman syndrome [4] (Fig. 9.14).
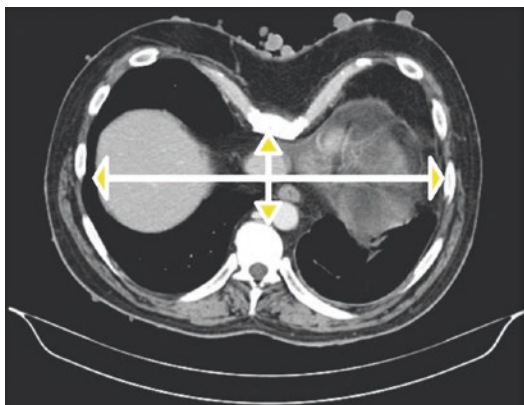
Fɪɢ. 9.13  Pectus excavatum with Haller index of 2.5
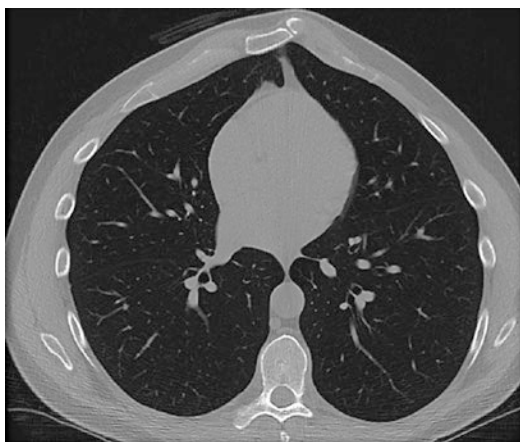


Fɪɢ. 9.14  Pectus carinatum is the opposite of excavatum with the sternum displaced anteriorly which increases the AP diameter of the thorax

## 9.4    Shoulders

The scapula, humeri, and clavicles may be partially imaged on a CT scan of the chest and should be reviewed to identify fractures and lytic and sclerotic lesions (Fig. 9.15).
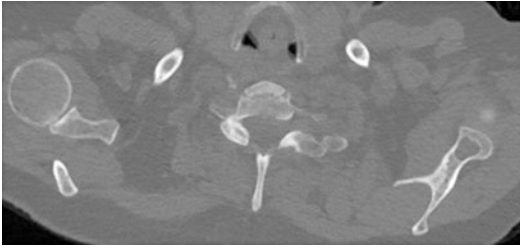
FIG. 9.15  Benign lytic lesion of the left scapula

# References

1. Lovell WW, Winter RB, Morrissy RT, et al. Lovell & Winter's pediatric orthopaedics. Philadelphia, PA: Lippincott Williams & Wilkins; 2006.
2. Greenspan A. Bone island (enostosis): current concept — a review. Skeletal Radiol. 1995;24(2):111–5.
3. Restrepo CS, Martinez S, Lemos DF, et al. Imaging appearances of the sternum and sternoclavicular joints. Radiographics. 2009;29(3):839–59.
4. Jeung MY, Gangi A, Gasser B, et al. Imaging of chest wall disorders. Radiographics. 1999;19(3):617–37.

# Concluding Remarks

Now you have the tools necessary to use chest CT to help patients. After careful review of the CT scan, we are left with a list of pertinent positives and negatives. Careful analysis of these findings with consideration of the patient's presenting symptoms allows for as narrow as possible differential diagnosis and optimal recommendations for patient management. The following worksheet may be helpful to complete when evaluating a CT scan of the chest as it summarizes the findings (Table A1).

169

TABLE A1  Overview of key findings on chest CT

| Review | Positive findings |
|---|---|
| 1. Dose | |
| 2. Scout | |
| 3. Airways | |
| 4. Lung parenchyma | |
| 5. Lung nodules | |
| 6. Mediastinum | |
| 7. Upper abdomen | |
| 8. Soft tissue | |
| 9. Osseous structures | |
| 10. Pertinent positives | |
| 11. Pertinent negatives | |
| 12. Recommendations | |

# Index